Development And Computational Studies Of Multi-Channel Adsorbent Hollow Fibre For The Removal Of Volatile Organic Compounds

Alsharif, Aesam

Award date:
2017

Awarding institution:
University of Bath

DEVELOPMENT AND COMPUTATIONAL STUDIES OF MULTI-CHANNEL ADSORBENT HOLLOW FIBRE FOR THE REMOVAL OF VOLATILE ORGANIC COMPOUNDS

Aesam Alsharif

A thesis submitted for the degree of Doctor of Philosophy

University of Bath

Department of Chemical Engineering

July 2017

Declaration of Authorship

I certify that I have read and understood the entry in the Programme Handbook for the Department of Chemical Engineering on Cheating and Plagiarism and that all material in this thesis is my own work, except where I have indicated with appropriate references or acknowledgements. I agree that, in line with Regulation 15.3(e), if requested I will submit an electronic copy of this work for submission to a Plagiarism Detection Service for quality assurance purposes.

Name: Aesam Alsharif

Signature:

Date:

Abstract

Escalating energy and environmental issues are driving researchers and industries throughout the world to study gas separation. Being common toxic gases, volatile organic compounds (VOCs) must be removed from the atmosphere. When compared to the conventional adsorption process, e.g. packed bed to separate VOC, the adsorbent hollow fibre has exhibited advantages in low pressure drop, easy operation and lower capital cost with high adsorption performance. This research investigates the optimisation and development of single and multi-channel adsorbent hollow fibres to improve the mechanical properties, flexibility, adsorbent loading and enhance adsorption capacity. These fibres are made up of an adsorbent (13X zeolite, HiSiv 1000 zeolite powder and HiSiv 3000 zeolite powder) held together with a polymer (polyethersulfone) binder through wet/wet spinning followed by a phase inversion process. Single adsorbent hollow fibres were optimised by changing the ratio of adsorbent to the polymer, the viscosity of polymer/adsorbent/solvent mixtures, the pre-treatment temperature and by adding a pore former. This optimal recipe of polymer/adsorbent/solvent mixtures was then used to fabricate tri-lobe and hexagonal multi-channel adsorbent hollow fibre. The adsorption performance and mechanical properties of these multi-channel fibres were compared to those of the single adsorbent hollow fibres. Dynamic adsorption challenges were carried out using n-butane as the VOC model gas to provide breakthrough curves using a flame ionisation detector (FID) hydrocarbon analyser. Scanning electron microscopy (SEM) was used to characterise the surface and porous structures of the different adsorbent hollow fibres formation. Adsorption isotherm experiments were also used to measure the surface area of adsorbent hollow fibres. In order to understand the transport mechanism of gases through adsorbent hollow fibres, single and multi-channel fibres were modelled using a computational fluid dynamic (CFD) using COMSOL software 5.2, thus enabling the prediction of breakthrough time and mass transfer for the new geometries of adsorbent hollow fibre.

Acknowledgement

I would like to express my sincerest gratitude to both my supervisors, Professor Semali Perera and Dr Y. M. John Chew. Their support and guidance have been invaluable to me over the course of my PhD. Dr Olivier Camus also very kindly provided help and advice on setting up most of the experiments in the Lab. I am grateful to a number of technical staff at the University; particularly Paul Frith, John Bishop, Fernando Acosta and Alex Cuipa.

I gratefully acknowledge the funding received towards my PhD from the Interior ministry of Saudi Arabia.

I wish to thank my parents for their love and encouragement, without whom I would never have done so many opportunities. I would like to thank my wife Dr Reem Alotaibi for standing beside me throughout my PhD and writing this thesis. Finally, my brothers, my sisters and my sons (Saif, Qussi, Yazan and Battal) deserve my thanks for all their love, support and understanding during my PhD.

Nomenclature

Roman and Greek

P	Total pressure	Pa
P^*	Vapour pressure	Pa
v	Volume of gas adsorbed	m^3
v_m	Volume of monolayer of gas adsorbed	m^3
c	Constant	---
θ	Number of sites which are covered by adsorbate	---
K	Equilibrium constant between adsorption and desorption	m^3/mol
p	Partial pressure for adsorbate species	Pa
x	The amount of adsorbate	g
m	Adsorbent mass	g
n	Empirical constant	---
C_0	The inlet gas concentration	mol/m^3
C	The outlet gas concentration	mol/m^3
t	Time	h
t_b	Breakthrough time	h
t_{eq}	Equilibrium time	h
t_s	Stoichiometric time	h
L_s	Saturation length	cm
L_{eq}	Adsorbed length	cm
MW	Molecular weight	g/mol
$\boldsymbol{R}$	Gas constant	m^3 Pa /K mol
Q	Volumetric flow rate	m^3/s
T	Temperature	K

ζ	Shape factor	---
Re	Reynolds number	---
u	Superficial velocity	m/s
ρ	Gas density	kg/m^3
d	Particle diameter	m
μ	Gas viscosity	Pa.s
ΔP	Pressure drop	Pa
L	Bed length	m
r_i	Inner radius	m
ε	Porosity	---
d_p	Particle diameter	m
φ_p	Sphericity of the particles	---
E	Tensile module	N/m^2
σ	Stress	N/m^2
σ_Y	Stress at yield	N/m^2
ε	Strain	---
ε_Y	Strain at yield	---
h_m	Height difference between liquid levels on manometer	m
ρ_m	Density of water	kg/m^3
g	Acceleration due to gravity	m/s^2
$\mathbf{u}$	Velocity vector	m/s
R	Fluid phase concentration source term	mol/m^3 s
D	Diffusion coefficient	m^2/s
r_{ads}	Rate of adsorption	mol/m^3 s
r_{des}	Rate of desorption	mol/m^3 s

ρ_b	Bulk density	kg/m^3
S	Source term	mol/m^3 s
k_a	Adsorption rate coefficient	1/s
k_d	Desorption rate coefficient	m^3/mol s
τ_F	Tortuosity factor	---
k_p	Constant which equal to k_a/k_d	mol/m^3
D_D	Dispersion tensor	m^2/s
θ	Volume fraction	---
D_F	Effective diffusion	m^2/s
r_o	Outer radius	m
Q_{sat}	Adsorption capacity	mol/m^2
D_{eff}	Effective diffusivity	m^2/s

Acronyms

VOCs	Volatile Organic Compounds
NMP	1-methyl-2pyrrolidone
FID	Flame Ionisation Detector
SEM	Scanning Electron Microscopy
CFD	Computational Fluid Dynamic CFD
NMVOCS	Non-Methane Volatile Organic Compounds
HCs	Hydrocarbons
TSA	Temperature-Swing Adsorption
PSA	Pressure- Swing Adsorption
TPSA	Temperature-Pressure Swing Adsorption
BET	Brunauer, Emmett and Teller
MTZ	Mass Transfer Zone

MTZ_{length}	Length of Mass Transfer Zone
$MTZ_{velocity}$	Velocity of Mass Transfer Zone
PESF	Polyethersulfone
SAHF	Single Bore Adsorbent Hollow Fibre
TAHF	Tri-lobe Three Bore Adsorbent Hollow Fibre
HAHF	Hexagonal Seven Bore Adsorbent Hollow Fibre
PDEs	Partial Differential Equations
FEM	Finite Element Method

Table of Contents

List of Figures

List of Tables

Chapter 1: Introduction

There are several sources of volatile organic compounds (VOCs) such as paint, oil refining processes, and emissions from vehicles. Major sources of man-made VOCs are petroleum-based. In nature, VOCs can be emitted from fossil fuel, volcanoes, bacteria and vegetation. Benzene, n-butane and acetone are examples of VOCs. VOCs and nitrogen oxides (NO_x) react in the presence of the sun to form ground level ozone. The emissions of these toxic gases have impact human health, the environment, building materials and vegetation. In 2015, the UK was estimated to have 0.8 million tonnes of VOCs in the atmosphere emanating from various sources. Figure 1.1 shows the emission of non-methane VOCs in the UK. The UK, together with other members of the European Union, aims to reduce VOCs to 40% of 1990 levels by 2030 (Department for Environment, 2014).

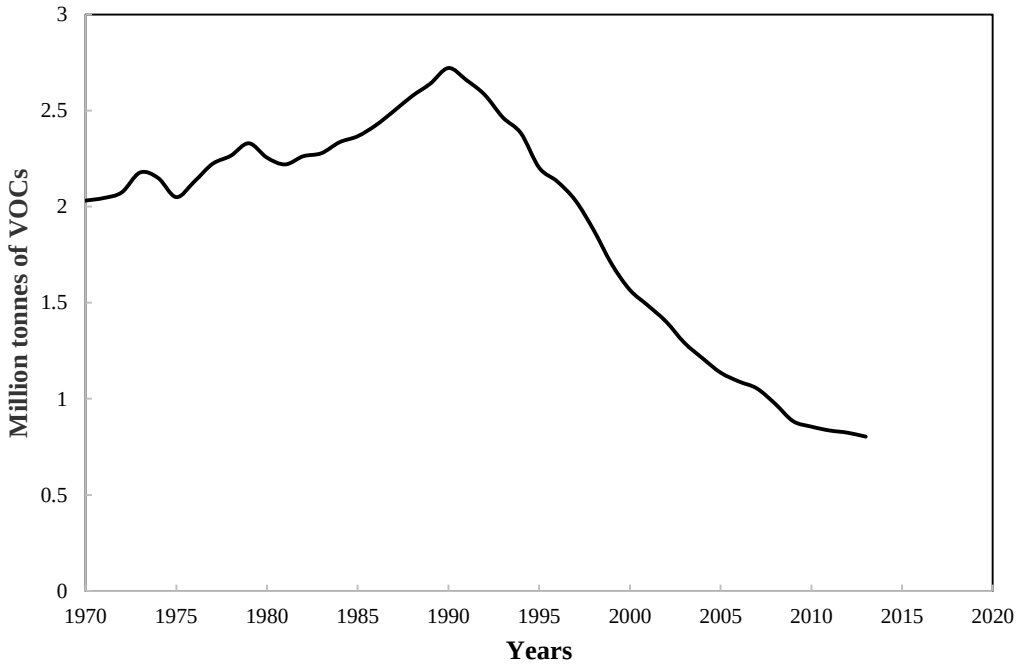

Figure 1.1. Trend in UK non-methane volatile organic compounds emissions (Department for Environment, 2014).

There are various methods to remove and recover VOCs from process streams such as adsorption, absorption, condensation and incineration. Many of industries have used adsorption processes for the recovery and removal of VOCs, which presents several advantages such as the ability to reuse adsorbents cost effectively and with minimum

waste. Temperature-swing adsorption (TSA), Pressure swing adsorption (PSA) and thermal-pressure swing adsorption (TPSA) using activated carbon have been among the adopted adsorption processes used. However, the use of activated carbon in these adsorption process does have some disadvantages including pore blocking, increased fire risk and issues connected with the regeneration process (Zhao *et al.*, 1998). To overcome the problems caused by using activated carbon for VOC removal, much consideration has been given to the use of hydrophobic zeolite and high sieve adsorbent materials instead.

Usually, all adsorbent particles used for gas separation are microporous or macroporous for packed bed. In some cases, such particles can offer fast mass transfer and lead to sharp breakthrough curves due to the phenomenon of lower mass transfer resistance. However, the small size of the adsorbent particles can cause an increase in pressure drop, which would lead to a reduction in the effectiveness of the adsorbent particles, bed lifting, and the different distributions of fluid flow and to extra pumping costs (Feng *et al.*, 1998). To prevent such an increase in pressure, the adsorbent particles need to be between 1 and 2 mm.

Hollow fibres and monoliths are examples of low pressure drop structured packing which are now widely used in gas adsorption processes (Rezaei and Webley, 2010). A monolith is composed of structured fabricated material with parallel channels and different of cross-sectional shapes. It can be made from different types of materials including ceramics, activated carbon, metals and plastic, depending on the type of process in which it will be used. Monoliths made from activated carbon are used to recover VOCs from the air (Williams, 2001). Monoliths, as structured adsorbents, offer a number of advantages such as higher surface areas, high mass transfer rates with low resistance and low pressure drops. However, although the decrease of monolith walls can optimise the adsorption kinetics, it can also lead to a decrease in the adsorbent loading per unit volume, thus affecting its mechanical properties (Rezaei and Webley, 2010).

Pan and McMinis used hollow fibre membranes for liquid and gas separations. It was found that a hollow fibre structure holding very small adsorbent particles offers minimum resistance to a fluid flow with pores (Pan and McMinis, 1992). When compared with granular and bead structured adsorbents, hollow fibre presents several

advantages, such as a significant low pressure drop due to the gas flow passing through the hollow fibre without any barrier, a lower mass transfer resistance due to the use of very small adsorbent particles and higher contact between the gas and the adsorbent particles with minimum dead-spicing due to the presence of a channel for the gas to pass through and the shape of the hollow fibres (Tai, 2007).

This research focuses on the optimisation and development of a high efficient novel adsorbent hollow fibre for gas adsorption and separation. These hollow fibres are made of adsorbent and a polymer. 13X zeolite has been chosen as adsorbent due to offers high adsorption capacity for VOC recovery (Díaz *et al.*, 2004). High silica HiSiv 1000 zeolite powder and HiSiv 3000 zeolite powder have also been used as adsorbents as a result of competitive adsorption of VOC in the presence of moisture was a challenge. The high temperature polymer is a polyethersulfone (PESF) which has good thermal and physical properties. The phase inversion method was used to prepare the adsorbent hollow fibres. It is acknowledged that there are many parameters that can affect the performance and structure of the fibres, such as the concentration of polymer/adsorbent/solvent mixture, the ratio of the polymer to the adsorbent, additives, the gas flow rate, and the pre-treatment temperature. Each has been studied and discussed with a view to maximising the adsorption performance of single adsorbent hollow fibres. The optimum recipe for the polymer/adsorbent/solvent mixture was employed to develop a highly novel multi-channel adsorbent hollow fibres and the number of channels created using two specially designed spinnerets (tri-lobe and hexagonal) by the University of Bath. The efficiency of the adsorbent hollow fibres in removing VOCs was tested using a hydrocarbon analyser with a flame ionisation detector (FID). The breakthrough curves of n-butane on the adsorbent hollow fibres were observed, and the equilibrium loadings of all adsorbent hollow fibres were measured. The nitrogen adsorption/desorption isotherm of adsorbent hollow fibres and pressure drop of the gas through the fibres were also investigated. The data obtained from these experiments was used for the development and validation of the mathematical models.

Computational fluid dynamics (CFD) were coupled with experimental data to elucidate the transport mechanisms in single and multi-channel hollow fibres using the computational fluid dynamic software COMSOL Multiphysics. The goal of CFD

modelling is to understand and predict the transport phenomena of various geometries of adsorbent hollow fibres and then use experiments to verify the CFD modelling.

1.1 Aims and objectives

The overall aim of the research is to develop, optimise and model single and multi-channel adsorbent hollow fibre structures with a low pressure drop, high adsorption performance, high adsorbent loading and good mechanical properties, for the recovery or removal of volatile compounds from the process stream.

Novel areas of this research include:

- The study concentrates on the development and optimisation of a multi-channel highly adsorbent loaded hollow fibre structure for efficient VOC adsorption. The creation of highly adsorbent loaded multichannel fibres with an impermeable outer skin is novel and has not been achieved before.

- The manufacture of optimised fibres has been challenging. Optimisation has been carried out by incorporation of novel additives (pore formers) into the green fibre during the spinning process and then removing these additives by heat treatment. Licowax C micropowder PM is an example of these additives.

- Single channel is fragile and difficult to handle in industrial applications. Therefore, with an optimised recipe, multi-channel fibres have been fabricated to improve mechanical strength and to enhance the adsorbent weight in a given volume, resulting in reduced voidage and improved adsorption capacity. The intention of increasing the adsorbent weight of the fibre is to compete with the current state of the art packed bed systems.

- The hydrophilic 13X Zeolite and hydrophobic adsorbent high silica zeolite (HiSiv 1000 and HiSiv 3000), were selected as the model adsorbents in this study. High temperature polymer polyethersulfone (PESF) was selected as the test polymer and the model adsorbate is butane.

- The adsorbent hollow fibres have been characterised using dynamic adsorption breakthrough studies and adsorption isotherms. The morphology of the fibres have been studied using scanning electron micrographs, mechanical strength

studies and pore size distribution using porosimetry.) The data obtained from these experiments has been used for model development and validation of the model.

- Computational fluid dynamic (CFD) has been coupled with experimental data to elucidate the transport mechanisms in single and multi-channel hollow fibres using computational fluid dynamic software, COMSOL Multiphysics. The goal of CFD modelling is to understand and predict the transport phenomena of various geometries of adsorbent hollow fibres and then use experiments to verify the CFD modelling. To the best of my knowledge this research will be done for the first time and therefore is novel.

The specific objectives are to:

1. Optimise the single adsorbent hollow fibre structure to achieve the fast adsorption kinetics, greatest adsorption capacity and lowest mass transfer resistance by changing the composition of adsorbent/polymer/solvent mixture, bore fluid composition and pre-treatment temperature.

2. Develop and design the tri-lobe three channel adsorbent hollow fibres with a high adsorption capacity, good mechanical properties and high adsorbent loading in the hollow fibre structure.

3. Develop and design the hexagonal seven channel adsorbent hollow fibres with low mass transfer resistance and good mechanical properties.

4. Characterisation and comparison of all adsorbent hollow fibre structure by using SEM, nitrogen adoption isotherm experiments, mechanical studies and adsorption breakthrough experiments.

5. Couple experiments with CFD modelling to analyse and understand the behaviour of gas molecules through the lumen and porous medium and investigate the efficiency of new geometric adsorbent hollow fibres.

1.2 Structure of the thesis

Chapter 2 provides background information on this research and presents a detailed literature review of studies on volatile organic compounds (VOCs), methods to control VOCs emission, the types of polymers and adsorbents which can be used, structured adsorbents and hollow fibres. It also presents a review of the theories which are relevant to this study, including theories relating to breakthrough curves, pressure drops, adsorption and mass transfers. Chapter 3 describes the materials and types of spinneret which can be used in this research. It also explains the preparation, characterisation and testing of adsorbent hollow fibres. Chapter 4 describes the optimisation process of single adsorbent hollow fibres for removal of n-butane. It also presents information regarding the morphology, mechanical properties, surface areas and breakthrough curves of single adsorbent hollow fibres. Chapter 5 focuses on the development of multi-channel adsorbent hollow fibres to improve adsorption performance and their mechanical properties by fabricating adsorbent hollow fibres with three and seven bores. These are then compared with single adsorbent hollow fibres. Chapter 6 presents the results which will be used in the modelling of single and multi-channel adsorbent hollow fibres using CFD COMSOL Multiphysics. It also explores the possibility of using this simulation to predict the effect of several parameters such as gas diffusivity, effective diffusivity and adsorption rate coefficient. Chapter 7 outlines the overall conclusion of the project and makes recommendations for follow-up research.

Chapter 2: Literature Review

This research concerns the development and use of a multi-channel adsorbent hollow fibre to remove VOCs. This thesis is divided into two parts: the experimental part and the modelling part. Experiments were carried out to optimise the recipe of adsorbent hollow fibres, to develop multi-channel adsorbent hollow fibres, study their adsorption efficiency for VOC recovery and compare their mechanical strength and results with the performance of single adsorbent hollow fibres under mild operating conditions. Four models were created and used to understand the transport mechanism and analyse the behaviour of gas as it passes through the adsorbent hollow fibres.

2.1 Volatile organic compounds (VOCs)

Volatile organic compounds (VOCs) are compounds of carbon which exclude carbon monoxide (CO), carbon dioxide (CO_2), ammonium carbonates ($(NH_4)_2CO_3$), carbonates (CO_3^{-2}) and carbonic acid (H_2CO_3). In general, they are solid or liquid chemicals that have a high vapour pressure at ordinary room temperature (between 20°C and 25°C) resulting in a low boiling point, such as methane (CH_4) which has a boiling point of up to -161°C at an atmospheric pressure of one atm (Wypych, 2001). Therefore, VOC molecules are easily evaporated from the surface of these compounds into the atmosphere. VOCs comprise various types of chemical compounds. Hydrocarbons, oxygenates and some of halogens are examples of these compounds. VOCs have a range of impacts on the environment: they contribute to global warming acid rain fall and the destruction of the ozone layer. Also, human health and vegetation are affected by VOC emissions. There are two main sources of VOC emissions: natural and man-made. Plants are responsible for natural emissions which represent approximately 90% of the emissions found on earth. Man-made emissions usually increase in cities and industrial areas (Khan and Kr Ghoshal, 2000). Table 2.1 shows data relating to the health impacts of VOCs found in workplaces. Most man-made VOC components resulting in emissions are found in paints, solvents and vehicle fuel (Sarkar and Mulchandani, 2015).

Table 2.1: Health issues caused by VOC exposure in the workplace (Sarkar and Mulchandani, 2015).

VOC	Health issues
Acetone	An eye irritant. Causes headaches and dizziness.
Methanol	May cause drowsiness. Respiratory irritant.
Toluene	Causes central nervous system depression and fatigue.
Ethanol	An eye irritant. Causes headaches, fatigue.
Ethylbenzene	An eye and skin irritant.
Formaldehyde	Potential occupational carcinogen.

The United Nations Economic Commission for Europe (UNECE) Gothenburg Protocol concerning the Control of Emissions of Volatile Organic Compounds was revised in 2012. In 2020, it demanded that the European Union (EU) reduce its emissions of volatile organic compounds by 28%. VOC emissions can damage ecosystems through, for instance, ground level ozone where the chemical reaction (Equation 2.1) involving non-methane volatile organic compounds (NMVOCs) produce the polluting gas ozone (O_3). This toxic gas can influence crops, forests and plants and warm the atmosphere (Department for Environment, 2014).

$$NO + VOC + O_2 + Sunlight \rightarrow NO_2 + O_3 \qquad (2.1)$$

The National Emission Ceilings Directive (NECD) is used to monitor the emissions of toxic gases throughout the EU annually and report the data back to the European Commission and to various Conventions. The Gothenburg Protocol set emission reduction targets in the long term (Department for Environment, 2014).

2.2 Methods for controlling VOC emissions

A mix of both economic and environmental advantages can determine the choice of VOC control processes. Two approaches have been applied to control VOC from process streams so far: recovery and destructive (Khan and Kr Ghoshal, 2000). Figure 2.1 shows the methods used in both approaches. Usually, the choice of separation method is dependent upon the amount and concentration of the sample, volumetric flow rate, cost, the desired purity of the sample and the equipment available (Watson, 1999).

In destruction approach, VOCs are destroyed by several methods of oxidation such as bio-filtration, catalytic and thermal. Disadvantages of destruction especially catalytic

incinerators include catalyst poising is probable, initial cost usually is high, particle of catalyst must be removed and catalysts cannot be regenerated (Khan and Kr Ghoshal, 2000).

Recovery technology has the advantage of saving on cost and the amount of energy required. A key benefit of recovery methods is the ability to reuse adsorbents with minimum waste compared to destruction methods. Recently, the adsorption as recovery method has been considered as the most attractive method to use for separation of VOC due to the ability of regeneration of adsorption units which can provide an economical advantage (Dou *et al.*, 2011; Huang *et al.*, 2011; Subrenat and Le Cloirec, 2006; Kuboňová *et al.*, 2013). As a consequence of some VOCs are valuable products which have an active economic role in industrialised countries, this research focuses on the use of recovery technology (adsorption).

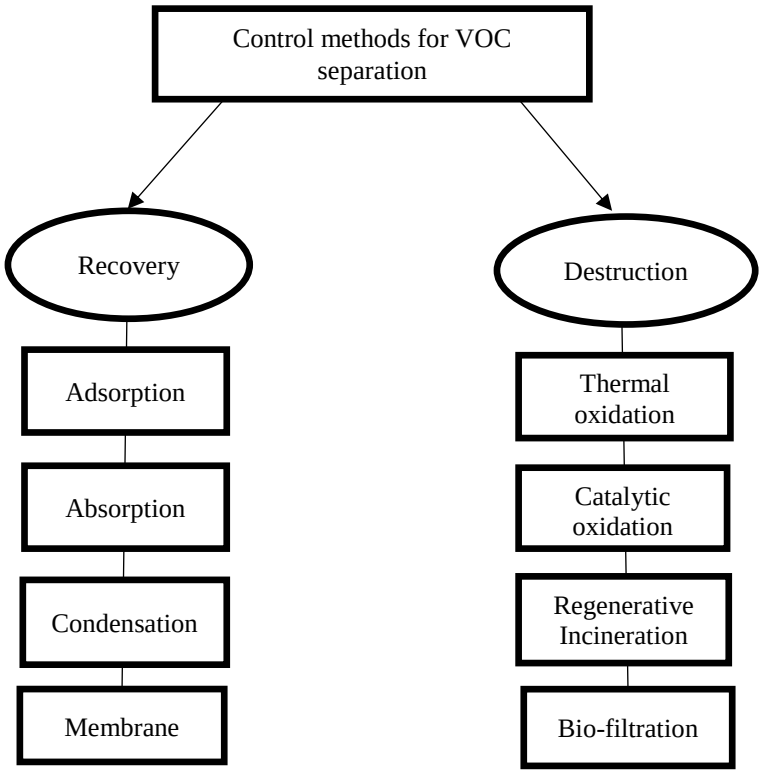

Figure 2.1. Methods used to remove VOCs (Gupta and Verma, 2002; Ozturk and Yilmaz, 2006; Sarkar and Mulchandani, 2015; Subrenat and Le Cloirec, 2006; Dwivedi *et al.*, 2004; Khan and Kr Ghoshal, 2000).

2.3 Adsorption

Adsorption process technology was established as a key separation tool over twenty years ago and was used in the chemical and oil industries for removal of polluted gases

from gas streams (Yang, 2013). In this technique molecules or particles of gas accumulate at the surface of a solid or liquid. There are two types of adsorption processes: physical and chemical. The Van der Waals force is the attraction existing between atoms and molecules which is used in physical adsorption while chemical adsorption acts upon the chemical forces between atoms and molecules. Physical adsorption is more widely used in gas separation process than chemical adsorption (Henley *et al.*, 2011). A major advantage of physical adsorption is that it does not require activation energy and takes place at ordinary room temperature (between 20°C and 25°C). Another advantage is the ability to regenerate with high selectivity and efficiency.

There are several factors which influence the extent of adsorption, among them the nature of the adsorbent and adsorbate, the experimental conditions and the activation of the adsorbent. The kinetic theory for adsorption can be divided into three steps (Henley *et al.*, 2011):

1. Adsorbate transport by bulk flow (convection) and dispersion on the adsorbent surface.

2. Adsorbate transport from bulk flow to the external surface (interface) of adsorbent.

3. Adsorbate transport to the internal surface of adsorbent by diffusion.

There is significant interest in the use of physical adsorption to recover VOC from gas streams which make it convenient to regenerate the gas (Yang, 1986). A considerable amount of literature has been published on gas separation for VOC removal (Dou *et al.*, 2011; Huang *et al.*, 2011; Kim and Ahn, 2012; Song *et al.*, 2005; Subrenat and Le Cloirec, 2006). These studies have revealed that the adsorption technique can remove low concentrations of VOCs (>100 ppm), regenerate the adsorption units at low pressure and gain high adsorption capacity, which make it a more cost-effective technique when compared with other techniques. However, it was found that the pores of the adsorbent can be blocked by the large particles in gas streams. Adsorbents such as zeolite, activated carbon and silica gel can be used depending on the type of gas involved and the application.

2.3.1 Adsorption equilibria

To achieve adsorption equilibria, there are three factors that can affect adsorbent capacity: temperature (T), adsorbate concentration in the gas or liquid phase (P) and adsorbate concentration in the solid phase (C_s). Plotting Cs against P and maintaining T as a constant value provides an adsorption isotherm which is one of the most commonly used to study the adsorption process. Different models have been used, such as the Brunauer, Emmett and Teller (BET) isotherm and the Langmuir and Freundlich isotherm. The assumption underlying these models is that there is just one adsorbate in the bulk phase. Hence, they are less accurate when modelling the application (Henley *et al.*, 2011).

BET Isotherms have suggested five isotherm graphs based on Equation 2.2.

$$\frac{P}{v(P^* - P)} = \frac{1}{v_m c} + \frac{c-1}{v_m c}\left(\frac{P}{P^*}\right) \qquad (2.2)$$

where

P is the total pressure while $P^*$is the vapour pressure of the adsorbate; v and v_m are the volume of gas adsorbed and the volume of the monolayer of gas adsorbed at 0°C and 1 atm respectively and c is a constant.

Figure 2.2 shows the BET types of isotherms. Type I describes the monolayer of adsorbed gas formation when $P/P^*<1$ and $c<1$. This type occurs in microporous adsorbents where pores are occupied at low gauge pressure. In type II, the intermediate flat indicates multilayer formation on the surface of the adsorbent below the saturation pressure and critical temperature. These two types of adsorption isotherms are usually used in separation processes which provide favourable adsorption, with a high uptake even at low pressures. Types I and II are the most common isotherms in separation processes. In type III, there is no flattish portion in the curve which corresponds to no more layer formation at the surface of the adsorbent until the pressure reaches the saturation point. This type appears in macroporous adsorbents or non-porous adsorbents where the interconnection between the adsorbate and the adsorbent is weak. Both type IV and V are explained by type II and III respectively, when the gases get condensed in the capillary pores of the adsorbent at pressures below the saturation pressure, but with added hysteresis (Henley *et al.*, 2011).

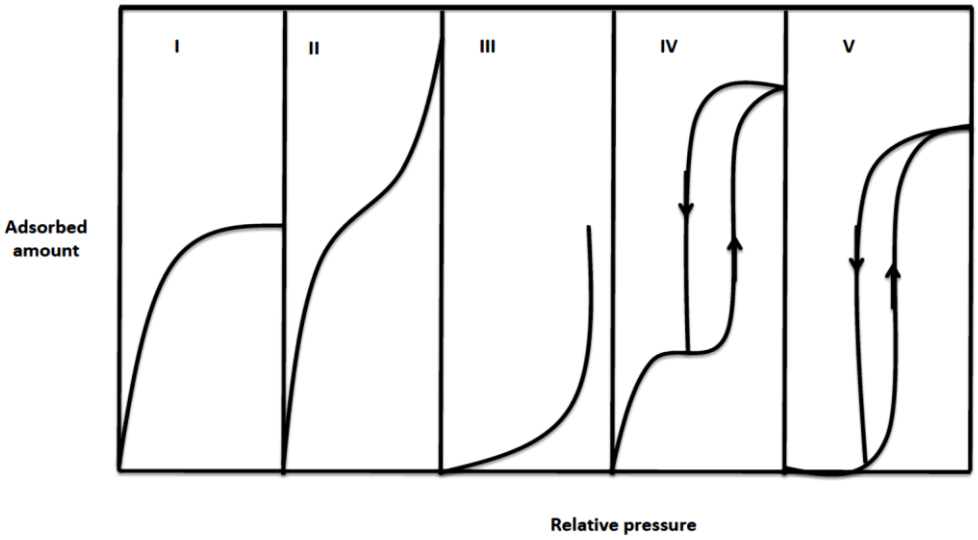

Figure 2.2. Schematic Diagram of the gas physisorption isotherms (Henley *et al.*, 2011).

The Langmuir and the Freundlich isotherm are also used as models to predict the equilibrium distribution. Langmuir Adsorption is a semi-empirical isotherm which is based on the fact that all adsorbent sites are equivalent to adsorbed molecules. This assumption is valid when the concentration of adsorbate is very high in the bulk phase. It is assumed that there is only a monolayer formation on the surface of the adsorbent at the maximum adsorption. The number of sites which are covered by adsorbate is θ. The rate of adsorption (r_{ads}) is obtained by Equation (2.3).

$$r_{ads} = k_a\, p\, (1 - \theta) \qquad (2.3)$$

where

k_a = the adsorption rate coefficient.

p = partial pressure for adsorbate species.

$(1 - \theta)$= the number of sites which are not covered yet by the adsorbate molecules.

And the rate of desorption (r_{des}) is given by the Equation (2.4).

$$r_{des} = k_d\, \theta \qquad (2.4)$$

where

k_d = the desorption rate coefficient.

When the dynamic equilibrium is reached the Langmuir equation shown in Equation 2.5 which describes the relationship between the pressure and the active sites of the surface. Basically, this equation is based on adsorption and desorption equilibrium (Henley *et al.*, 2011).

$$\theta = \frac{K\,p}{1 + K\,p} \qquad (2.5)$$

where

K = the equilibrium constant between adsorption and desorption (k_a/k_d).

The Freundlich isotherm is an empirical equation which describes the difference in the adsorption isotherm of the amount of gas adsorbed by a unit mass of adsorbent with pressure.

At low pressure, extent of adsorption is relational to pressure:

$$\frac{x}{m}\ \alpha\ p^1$$

where

x = the amount of adsorbate

m= adsorbent mass

Whereas at high pressure, extent of adsorption is independent of pressure:

$$\frac{x}{m}\ \alpha\ p^0$$

Therefore, at intermediate value of pressure, adsorption is relational to pressure raised to power *1/n*. Here n is a constant whose value depends on the type of adsorbent and gas component whose value is greater than one. The Freundlich adsorption equation is presented in Equation 2.6 below:

$$\frac{x}{m} = Kp^{\frac{1}{n}} \qquad (2.6)$$

Figure 2.3 shows the favourable (Type I in the BET and Freundlich, n<1), strongly favourable (Langmuir), linear (Freundlich, n=1) and unfavourable (Freundlich, n>1) isotherm shapes. These isotherm shapes are used to determine the adsorption

characteristics. In most separation processes, type I isotherms perform better than type III, because of high loading occurring at low adsorbate concentration. Irreversible adsorption can take place and is shown in an isotherm as a straight horizontal line, representing the fact that the amount adsorbed is independent of concentration.

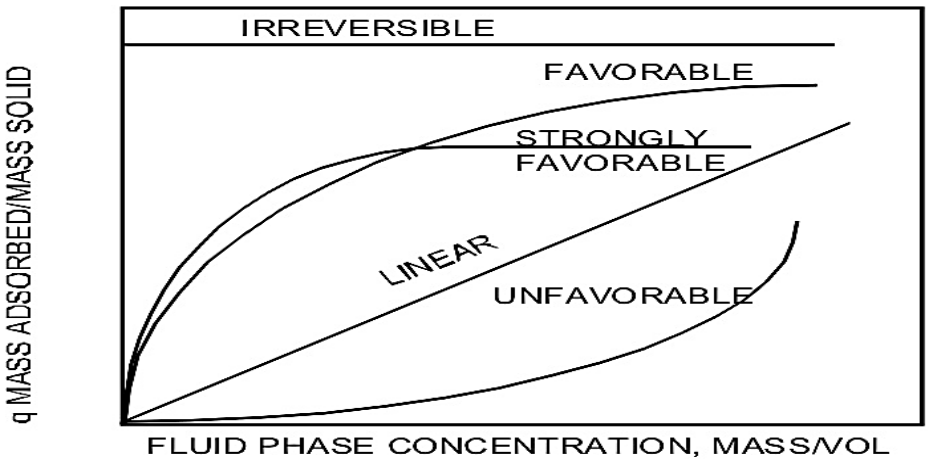

Figure 2.3. Some general isotherm shapes (Vivek Kumar, 2012).

2.3.2 Adsorption breakthrough curves

In an adsorbent filled column, process stream containing toxic gases that can be adsorbed by the adsorbent is passed through the adsorbent column from the top to the bottom. These toxic gases will adsorb onto the adsorbent at the inlet until the adsorption rate approaches equilibrium. When the top section has reached an equilibrium, there are no more toxic gases to be adsorbed or removed from the process stream. The mass transfer zone (MTZ) is the section where the adsorption process occurs. The progress of MTZ and corresponding breakthrough curves is shown in Figure 2.4.

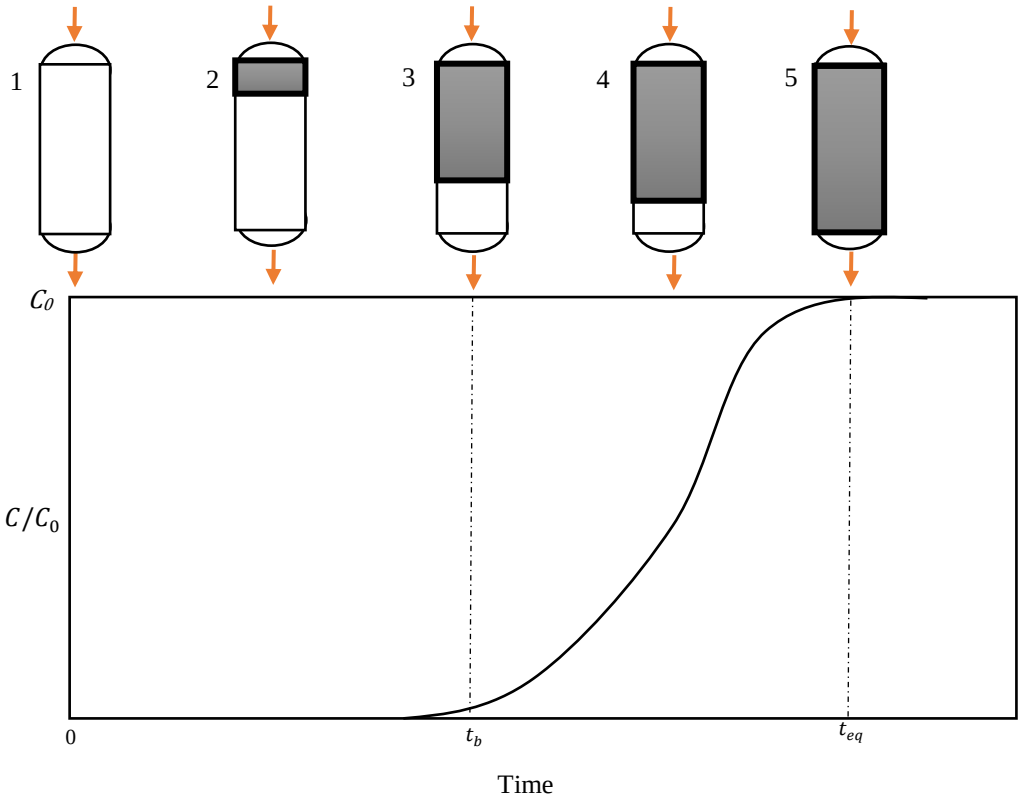

Figure 2.4. The movement of the mass transfer zone in column bed adapted from (Henley *et al.*, 2011).

The breakthrough curve is widely used to describe the concentration profile through an adsorption process by plotting the outlet concentration of adsorbate in the bulk fluid (C), normalised to the inlet concentration (C_0), as a function of time (t). As can be seen in Figure 2.5, the breakthrough curve has a distinguishing curve which is S-shaped. The breakthrough curve can be used to assign two important points which are breakthrough time (t_b) and equilibrium time (t_{eq}). The breakthrough and equilibrium time is normally taken when the concentration profile reaches 0.05 and 0.95 respectively.

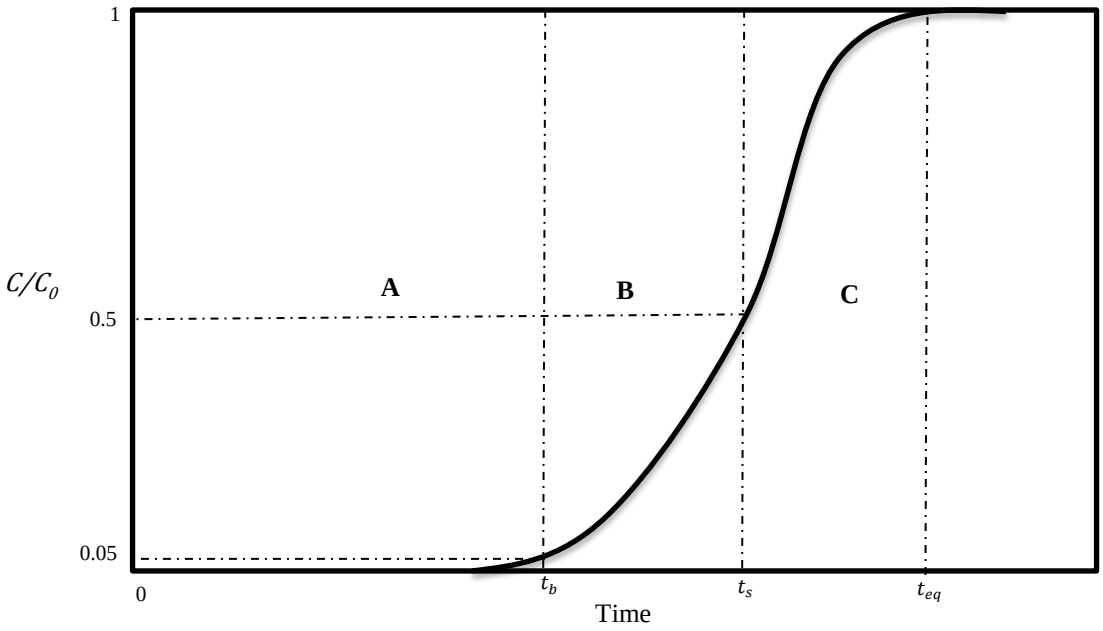

Figure 2.5. Schematic representation of breakthrough curve of column bed.

For the purposes of this study, the adsorption breakthrough curve is provided by using the dynamic adsorption experiment. The adsorbate is n-butane which has a molecular weight equal to 58.12 g/mol. 13X zeolite is employed as an adsorbent. Equilibrium loading, MTZ length and MTZ velocity are properties of the adsorption unit. These parameters were calculated from Figure 2.5. Equation 2.7 is used to calculate the equilibrium loading, which is the amount of adsorbate in the adsorbent at the saturation state. The area of A, B and C is equal to the first term on the right side of this equation whereas the area of C is equal to the second term on the same side (Brenner, 2013).

$$\text{Equilibrium loading} = \frac{MW * Q * P * C_0}{10^6 * \boldsymbol{R} * T} * t_{eq} - \frac{MW * Q * P * C_0}{10^6 * R * T} * \int_0^{t_{eq}} \frac{C}{C_0} dt \qquad (2.7)$$

where

MW = the molecular weight of n-butane

Q = the flow rate (m^3 /min)

P = the pressure (atm)

C_0= the initial concentration (ppm)

$\boldsymbol{R}$ = gas constant (atm L/mol K)

T= the temperature (293 K)

t_{eq}= the equilibrium time (min)

The breakthrough loading can be calculated using Equation 2.8.

$$\text{Breakthrough loading} = \frac{MW * Q * t_b * C_0}{Dry\ mass\ of\ adsorbent * v} \quad (2.8)$$

where

t_b= the breakthrough time (min)

$$v = \frac{n * \boldsymbol{R} * T}{P}$$

where

v= volume of gas (L/mol) and n= number of moles

In order to calculate the length of the mass transfer zone, the identification of equilibrium time (t_{eq}), stoichiometric time (t_S) and breakthrough time (t_b) is important. At stoichiometric time (t_s), the outlet concentration (C) rises from zero to the value which is close to an initial concentration (C_0) while the equilibrium time (t_{eq}) is when C is equivalent to C_0.

First, the stoichiometric time (t_s) can be calculated using Equation 2.9 (Seader and Henley, 2011).

$$t_s = \int_0^{t_{eq}} 1 - \frac{C}{C_0} dt \quad (2.9)$$

The length of unused bed (LUB) is defined as the length of the bed without uniform adsorption. This length can be calculated from the breakthrough curve and is defined by Equation 2.10.

$$LUB = L\left[\frac{(t_s - t_b}{t_s}\right] \quad (2.10)$$

where

L = the length of column bed (cm)

The mass transfer zone length (MTZ_{length}) and mass transfer zone velocity ($MTZ_{velocity}$) can be determined from the B and C areas (Brenner, 2013).

First, the shape factor (ξ) can be calculated using Equation 2.11.

$$\xi = \frac{Area\ of\ B(\frac{g}{m^3}\ min)}{Area\ of\ B\left(\frac{g}{m^3}\ min\right) + Area\ of\ C(\frac{g}{m^3}\ min)} \qquad (2.11)$$

The MTZ_{length} is then calculated from Equation 2.12.

$$MTZ_{length} = \frac{LUB}{\xi} \qquad (2.12)$$

The $MTZ_{velocity}$ can then be estimated using Equation 2.13.

$$MTZ_{velocity} = \frac{MTZ_{length}}{(t_{eq} - t_b)} \qquad (2.13)$$

Several factors can have an impact on the length and velocity of the mass transfer zone (Schweitzer, 1988):

1. The size of adsorbent particles: the small size of particles offers a higher surface area, higher adsorption capacity and sharper MTZ when compared with large particles.
2. Temperature: if the temperature is increased, the physical adsorption capacity is decreased, diffusion rates is increased and the MTZ will be shorter. Regarding to gas adsorption, this means that a shorter MTZ is less important than increased movement velocity.
3. Concentration of adsorbate: the velocity of the MTZ movement will increase with increased concentration and, so, the time will decrease.
4. Velocity of gas: the velocity of gas can change the flow regime of gas from a laminar to a turbulent flow. In turbulent flow, the rate controlling step is pore diffusion, in laminar it is bulk diffusion.
5. The presence of other adsorbates: this causes lower adsorption capacity and increases the velocity of MTZ movement and its length.

6. Adsorbent bed length: to gain a high adsorption capacity and use the longest bed possible, the adsorbent bed length must be nearly three times longer than MTZ_{length}.

2.4 Types of adsorbents

Number of commercial adsorbents are used for VOC recovery with a high surface area (high adsorption capacity) and high thermal and chemical stability. Easy regeneration and low cost are other advantageous properties of adsorbents (Yang, 1986). Table 2.2 shows the types and properties of several adsorbent materials used for several applications.

Table 2.2: Widely used commercial adsorbents

Adsorbent	Properties
Activated Carbon	-Has Non-polar surface leads to weak bond that means low energy requirement. -Large surface area (300-2500 m^2/g). -Pore size = 10-25 Å
Activated Alumina	-Has the highest affinity for water. -Surface area (250-350 m^2/g) -Low micropore volume.
Silica Gel	-Has Polar surface used in drying application. -Higher capacity for water. -Surface area (300-850 m^2/g) and pore volume (22-150 Å) depending upon the its type.
Molecular Sieve Carbon	-Has Non-polar surface used in wet gas separation. -Good adsorption capacity -Pore size (4-9 Å).
Zeolites	-Has surface area (500-800 m^2/g). -Used for high temperature applications especially for removal of VOCs. -The ability of adsorption is very strong.

In this study, three types of adsorbent have been used, namely 13X zeolite, HiSiv1000 and HiSiv 3000. Zeolites are hydrated crystalline aluminosilicate having a pore size between 2.5 and 10 Å. In general, the specific surface area of zeolites and the stability to temperature are high. The pore size of the channels, the reasonably low cost and the internal framework structure of zeolites offer advantages in the area of gas separation (Akhtar *et al.*, 2014). Up to 194 unique zeolite frameworks have been classified by the International Zeolite Association (IZA).

The chemical formula for zeolite minerals is:

$$M_{\frac{x}{m}}[(AlO_2)_x(SiO_2)_y]zH_2O \qquad (2.14)$$

Where AlO_2 is alumina and SiO_2 is silica while x and y refer to the ratio between silica to alumina. M is the ion balancing the charge of the aluminosilicate ion such as Na^+, K^+, Li^+, Ag^+ with valence m. z is the number of water molecules. If the zeolite contains no alumina, it will be a silicate mineral. Most zeolites carry negative charges from the internal frameworks. The presence of additional framework cations balances with these negative charges leading to great internal electrical field gradients. Therefore, the interaction between zeolites and other molecules with large electric quadruple is very strong and can thus ease the separation of these molecules (Akhtar *et al.*, 2014). The removal of water molecules by vacuum and heating can improve the adsorption capacity of zeolites.

The Si/Al ratio affects the properties and stability of zeolite which can transit it from being a hydrophilic to a hydrophobic. For example, a low Si/Al ratio (1-1.5) can produce hydrophilic zeolites (e.g. 13X, 5A) with high cation concentration and 4, 6 and 8 rings. However, hydrophobic zeolites (e.g. ZSM-5) have high Si/Al ratio (10-100) with low cation concentration and 5 rings. Moreover, there is some ability to exchange the cations in zeolite with other metals which leads to a change in the effective aperture sizes. For example, the swap Na+ cations in type 4 zeolite with K+ can transit to type 3A zeolite (Flanigen *et al.*, 1991). Different skeletal structures have been classified by IZA, such as zeolite X, zeolite A and ZSM-5, as shown in Figure 2.6. Zeolites are commonly used for recovery for most toxic gases such as carbon dioxide, ammonia, methanol and VOC (Kim and Ahn, 2012; Akhtar *et al.*, 2014; Díaz *et al.*, 2004).

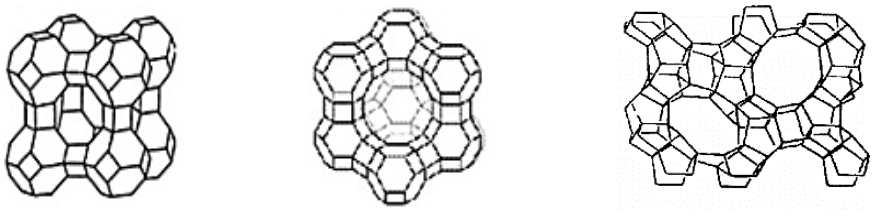

Figure 2.6. Varity of zeolite frameworks: (a) type A zeolite, (b) type X zeolite and (c) ZSM-5 type zeolite (Yang, 1986).

13X zeolite has been selected to be adsorbent model for preparing adsorbent hollow fibres. It is a molecular sieve zeolite with composition (1 Na_2O: 1 Al_2O_3: 2.8±0.2 SiO_2: xH_2O). This sodium form of zeolite adsorbs very small pores with less than 0.75 nm.

13X zeolite has high alumina content and a negative charge framework structure which contains channels and cavities taken by ions and water molecules. These active sites can enhance the reversible dehydration process and ion exchange. The main channels of 13X zeolite have a nearly spherical shape and are 13 Å in diameter. The thermal stability of 13X zeolite is 800°C with Si-to-Al ratio of 2.2 (İnel *et al.*, 2002) (Inel et al., 2002). Figure 2.7 shows the framework of 13X zeolite which consists of porous cages that are connected with pore window openings surrounded by 24 atoms (12 oxygen atoms). 13X zeolite has been used for VOCs recovery. In 2004, Díaz et al. reported that 13X zeolite has a higher adsorption capacity compared to 5A zeolite due to their pore size (Díaz *et al.*, 2004). Adsorbed n-butane can diffuse unrestricted throughout 13X zeolite as its pores are larger than the kinetic dimensions of n-butane. A potential disadvantage of zeolites as adsorbent in gas separation applications is their comparative affinity for water. For this reason, high Si/Al ratio zeolites were used in this research (Hisiv 1000 and Hisiv 3000).

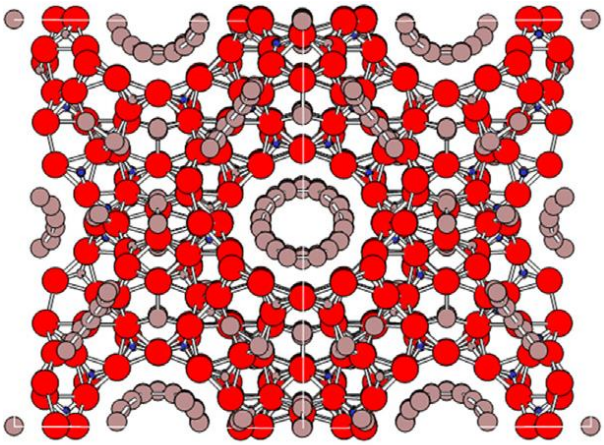

Figure 2.7. structure of 13X zeolite; -Si, -Al, -Na (Akhtar *et al.*, 2014)

In order to raise the Si/Al ratio, it is possible to substitute aluminium with silicon. This can be changed the type of zeolite from hydrophilic to hydrophobic and affects its properties. HiSiv 1000 and HiSiv 3000 high silica zeolites are a general term for adsorbent rich in the silica component with Si/Al ratio of 10 or higher. They are used in this work as moisture resistance high silica adsorbents. These high silica adsorbents are likely to be used as a functional material and have features such as hydrophobicity and excellent heat resistance.

HiSiv 3000 has a pore structure for adsorbing molecules with diameters up to 0.6 nm. The thermal stability of this high silica zeolite is 800°C with Si/Al ration of >1000 (UOP, 2006). However, HiSiv 1000 has pore size of 0.8 nm with Si/Al ratio of >20. The cation form of both adsorbents is Na^+. They have high capacity for organics at low feed concentrations. This characteristic permits easy removal of VOC from air to less than one ppm. They show classic zeolite isotherms, high capacity in the presence of water and stable mass transfer fronts. They are non-combustible and non-reactive with most compounds.

2.5 Structured adsorbents

The adsorbent as a powder is not suitable for direct use in industrial processes because of particle lifting at the packed bed and the high pressure drop. In an attempt to develop and improve the adsorption process and reduce costs, significant attention has been focused on the design of structured adsorbents in separation applications. Studies have found that the different structures of structured adsorbents have different benefits and drawbacks. The parameters which identify the quality of a structured adsorbent are low pressure drop, high adsorbent loading per unit volume, large surface area per unit volume, high pore volume, good mechanical strength properties and high mass transfer resistance (Rezaei and Webley, 2010). There are different types of structured adsorbents such as monoliths, foams, laminate adsorbents and hollow fibres. These structures will be reviewed in Sections 2.5.1-2.5.5.

At their most basic level, different forms of commercial adsorbents can be used in packed beds with particle sizes ranging from 50 μm to 1.2 cm, including pure powder adsorbents, beads, granules and spheres or pellets (Seader and Henley, 2011). Most of these forms can be chemically impregnated before being used in industrial processes.

2.5.1 Bead and granular adsorbents

In air separation processes, adsorbent packed beds filled with the particles mentioned above are used to recover polluted materials from gas steam. The structure, geometry and size of adsorbent particles are important parameters which can affect adsorption performance. The compromise between these parameters is difficult; for example, the very small size of an adsorbent can increase the pressure drop which leads to the lifting

of some particles off the bed, poor mass transfer and high energy cost. However, for the purposes of this study an adsorbent structure with low pressure drop and high adsorption performance will be used for cost-effectiveness (Akhtar *et al.*, 2014).

2.5.2 Monoliths

Recently, monoliths have been a focus of interest for research due to their low pressure structure, safer operations, large surface area and good mass transfer performance when compared to packed beds of pellets or beads (Williams, 2001). Monoliths are structures made up of parallel channels with different cross sections. They are made from different types of materials such as ceramics, metals and plastic depending on the type of processes they will be used for (Williams, 2001; Rezaei and Webley, 2010). In 2005, Crittenden and colleagues made monoliths out of activated carbon to use in gas separation (Crittenden *et al.*, 2005). Figure 2.8 shows a particular type of monolith.

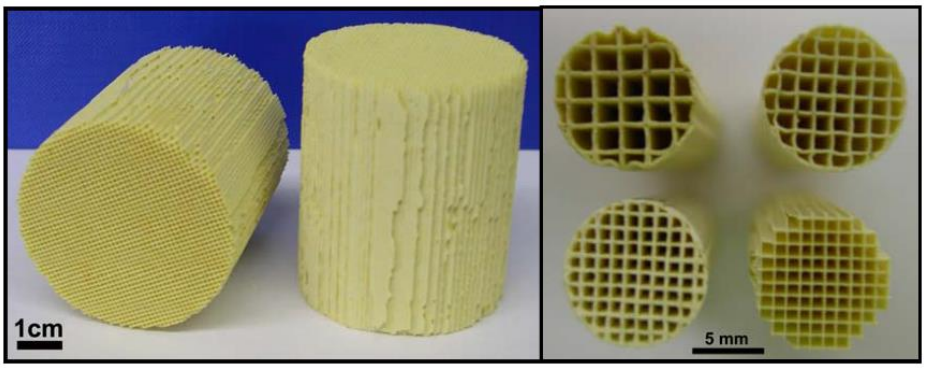

Figure 2.8. Ceramic monoliths with different cell density (Moreno-Castilla and Pérez-Cadenas, 2010).

As mentioned above, a monolith is a low pressure structure with providing high contact efficiencies between gas flow streams and monolith. Reduction in the monolith walls can optimise the adsorption kinetics which leads to a reduction in the adsorbent loading per unit volume. However, the monolith structure has a number of disadvantages. The preparation of monoliths with a high cell density and thin walls is expensive and difficult (Li *et al.*, 2009; Rezaei and Webley, 2010). Another disadvantage of monolith structures is the lack of control in larger-scale processes (Nijhuis *et al.*, 2001).

In general, monoliths have a good adsorption performance with many advantages which makes them a good choice for gas separation processes. However, the aim of this research is to develop multi-channel adsorbent hollow fibres for gas separation

with a flexible structure (can fit into any module), highly loaded with adsorbent and highly porosity and the monolith structure, being very rigid with low mechanical properties, is not the ideal structure to use.

2.5.3 Foams

Figure 2.9 shows an example of adsorbent foam. In comparison with a packed bed, the foam structure offers a higher pressure drop, better heat transfer, a lower mass transfer rate and a higher surface area. The higher voidage in the foams makes them a favourite for use in operations at high velocity where the pressure drop becomes of vital importance. Some studies classify foams as a type of monolith structure. High bed porosity is an advantage of the foam structure over the monolith structure. However, the very large porosity per unit volume can reduce the adsorption performance of foams (Rezaei and Webley, 2010). This type of adsorbent structure is not seen as appropriate for use in gas separation because of the issue of lower adsorption loading per unit volume and a higher pressure drop when compared to the monolith structure (Patcas et al., 2007).

Figure 2.9. 13X zeolite foam for gas separation fabricated at University of Bath.

2.5.4 Adsorbent fabric

An adsorbent fabric can be used for the air separation process. The natural fibre is composed of adsorbents (e.g. activated carbon) to provide very rapid mass transfer. In industrial processes, there are two types of structures of adsorbent fabric (spiral-wound and parallel sheets) prepared by coating adsorbents in fibre without any spacers or support. The potential advantages of using adsorbent fabric are a lower pressure drop,

lower attrition, good mechanical strength and high mass transfer when compared with granular or beads adsorbents (Rezaei and Webley, 2010). However, some research has been carried out on adsorbent loading considerations and it was found that there is poor adsorbent loading on fabrics when compared to the loading on granular or beads adsorbent (Golden *et al.*, 2005). Therefore, this structure is not a suitable choice for use in VOC separation, where high adsorbent loading for a range of gases is required.

2.5.5 Hollow fibres

Hollow fibre is a low pressure drop structure which offers a high surface area per unit volume. The first use of hollow fibres was as membranes during the 1960s (Pan and McMinis, 1992). In 1961, Loeb and Sourirajan discovered a dry-wet phase inversion technique which could be used to prepare hollow fibres. Several studies have subsequently used this method to produce hollow fibre membranes. The hollow fibres preparation technique is quite complicated as it uses inner and external fluid concurrently during the spinning process (Kneifel and Peinemann, 1992; Tan et al., 2001; Wang et al., 1999). The porous structure and cylindrical shape of hollow fibres lead to negligible transport resistance and a high resistance to transmembrane pressure (Peng, 2009). Initially, hollow fibres membranes were used in several commercial applications for long such as in the medical field (haemodialysis), for gas separation and for water purification. Polymeric hollow fibre membranes are potentially the superior choice for gas separation given their cost effectiveness, ease of operation, production of very little harmful waste and high permeability (Du *et al.*, 2012). Moreover, the use of these hollow fibres can save energy when compared with distillation operations which usually require a high amount of energy. Energy saving is currently one of the most active areas in terms of the development of environmental regulation. In contrast, the limitations associated with the use of polymeric membranes have mainly been the low mass transfer of some hydrocarbons over gas steam or water. Recently, the addition of different types of adsorbents has become increasingly significant for gas separation in order to improve the adsorption performance (Lasseuguette *et al.*, 2013; Dai *et al.*, 2012; Hasbullah *et al.*, 2011; Mao *et al.*, 2011).

In recent years, there have been an increasing number of studies on the applications of zeolite composite membranes for several types of gas separation processes (Shirzadeh-Gharacheh and Rahbari-Sisakht, 2016; Li *et al.*, 2013; Zhao *et al.*, 2016). However, it

is important to mention that this study focuses on the application of adsorbent hollow fibre for gas separation as storage unit with impermeable outer skin compared to hollow fibre membranes. Numerous studies have attempted to explain the effect of the addition of zeolites on the adsorption performance. In 2007, organic–inorganic hybrid (mixed matrix) asymmetric hollow fibre membranes were successfully used for gas separation by Hussain and Koros (Husain and Koros, 2007). It was found that Ultem 1000 polymer incorporated with small pore size zeolite produced a significant result with 17% for CO_2/CH_4 pure gases. Zulhairun et al. (2014) used polysulfone (PSF)-Cloisite®15A (C15A) to spin hollow fibre membranes. In this study, take-up speed, air gap height, force convection rate and polymer/adsorbent mixture extrusion rate were studied in order to optimise the fabrication conditions. The optimised hollow fibres showed over 46% selectivity improvement when compared to pristine PSF hollow fibres. It was conclusively shown that these composite membranes, containing zeolite-fillers, have higher adsorption capacity, and transfer resistance to gas streams and hydrophobicity (Zulhairun *et al.*, 2014).

Until now, most large-scale adsorption and catalytic applications usually used zeolites. The incorporation of zeolites in hollow fibre membranes offers an area-to-volume ratio of 30–250 m^2/m^3. However, it can yield ratios of almost more than 3000 m^2/m^3 with adsorbent hollow fibres (Tai and Wang, 2013). In 2007, the group at Bath developed adsorbent hollow fibres for gas separation containing porous materials merged with polymer and a low pressure drop (Perera and Tai, 2009). Adsorbent hollow fibres were produced by Tai using the dry-wet phase inversion. The method of immersion precipitation adsorbent hollow fibres can be explained as follows: a mixture consisting of a polymer, an adsorbent and solvent is immersed in two water baths. The water diffuses into the cast film while the solvent diffuses into the water baths. During this process, solvent is passed through the inner bore. Thus, a solid polymeric is obtained in the outer layer and a porous structure is obtained in the inner layer (Perera and Tai, 2009). The study is unique because porous hollow fibres provide light weight low pressure drop strutures and high mass transfer by reducing the mass transfer resistance due to the micro or macro size of adsorbent particles encapsulated within the structure. Therefore, adsorbent hollow fibres act as a gas storage because, unlike hollow fibre membranes, they have porous materials and an impermeable outer skin. Additionally,

adsorbent hollow fibres have a higher ability to recover. The bundle of adsorbent hollow fibre is shown in Figure 2.10.

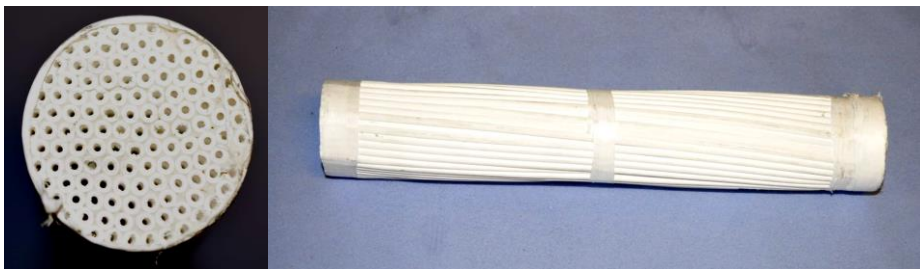

Figure 2.10. Adsorbent hollow fibre module fabricated from 13X zeolite and PESF at University of Bath.

In comparison to granular or bead beds, hollow fibres also have higher voidage and thinner walls which lead to a reduction in diffusion and improved mass transfer. Also, several adsorbents can be used to fabricate an adsorbent hollow fibre with the high chance to recover a wide range of toxic gases. Since adsorbent hollow fibre structures are similar to the structure of monoliths, they have almost similar advantages, such as organised parallel channels, improved mass transfer properties and a low pressure drop. However, hollow fibres are flexible which can enable the module to bundle into more specific shapes. Therefore, this research focuses on the development of multi-channel adsorbent hollow fibre with flexible structure, high adsorbent loading and highly porosity.

2.6 Formation of adsorbent hollow fibre

The formation of hollow fibres can be described by the Ternary Phase Diagram shown in Figure 2.11. It has three main regions which are single phase(I), meta-phase (II) and two phase region (III). The Ternary Phase Diagram represent three components. A point inside the triangle represents a mixture of these three components (polymer, non-solvent and solvent) whereas a point placed on one of the sides of the triangle represents a mixture containing of the two corner components such as solvent and polymer only. A bimodal and a spinodal curves can be detected. The path of the outer skin layer formation is illustrated by a spinodal line whereas the binodal line illustrates the formation of the substructure (porous structure). The meta-phase composition is indicated by the region between spinodal and binodal lines with separation of phase. In this case, the nucleation and growth of the skin layer occurs. Point C is very

important to clarify which type of process is taking place. In particular, the phase separation occurs when the precipitation line comes across the binodal line below point C; while the nucleation of the polymer lean phase could take place when the precipitation line comes across the binodal line above point C.

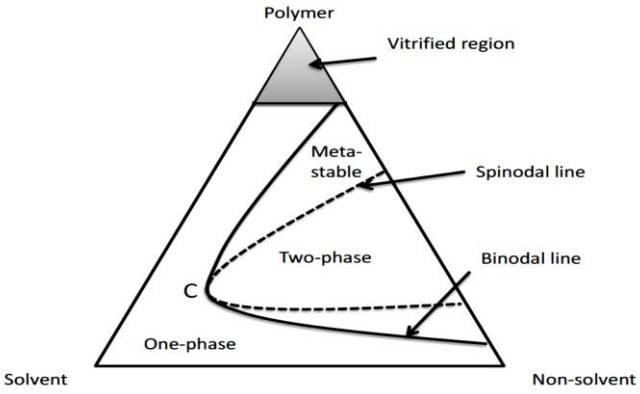

Figure 2.11. Ternary Phase Diagram Showing Phase Regions, Boundary Lines and the Formation of Skins.

Firstly, for adsorbent hollow fibre formation from ternary phase system, a homogenous polymer/adsorbent/solvent mixture is prepared. This will correlate to a point on the polymer/solvent axis. A non-solvent (water bath) can be added to this mixture. Then, phase inversion will occur at the point where the addition of the non-solvent (water) leads to the mixture becoming thermodynamically unstable. There are two different types of phase inversion processes which are delayed and instantaneous. Instantaneous phase inversion means that the hollow fibre is formed directly after immersion in the water bath (non-solvent) resulting in the formation of a hollow fibre with lower porosity. While in the case of delayed phase inversion, it takes more time before the hollow fibre is shaped and this leads to the formation of hollow fibre with higher porosity.

2.7 Effect of parameters on the adsorption performance through hollow fibres

There are several parameters that control the properties of the hollow fibres produced including the extrusion rate through the spinneret, the air gap length, the composition of the bore fluid, the dimensions of the spinneret, the composition of the coagulant bath and the ratio of solvent to adsorbent in the polymer mixture. Most of these studies

have been applied on the hollow fibre membranes. In this research, we are trying to adapt these studies on the adsorbent hollow fibres for VOC removal.

Studies on the influence of the polymer concentration in the polymer mixture show that high polymer concentrations decrease the flux and porosity in hollow fibre membranes, whereas low polymer concentrations result in weaker hollow fibres (Baker, 2012). For the purposes of this study, in order to obtain a highly porous structure in the adsorbent hollow fibre to provide easy access to the adsorbent, a low polymer concentration is desired without affecting the mechanical properties of the hollow fibre.

The effect of external and bore fluid concentrations has also been studied. A great difference between external bath and bore fluid concentrations was found to create finger-like macrovoids in the structure of the hollow fibre membranes due to instantaneous phase inversion process. However, a porous sponge-like structure is created when the difference between them is relative and there is a delay in the phase inversion process (Xu and Qusay, 2004). The effect of concentration of bore fluid is discussed in detail in Chapter 4.

When the longer air gap in the hollow fibre spinning process is adjusted, the pore size in the outer skin is increased, with the result that the phase inversion process is slowed down (Liu *et al.*, 2003). However, Kapantaidakis and Koops (2002) showed that a substantial air gap length let down the performance of the separation process because of the hollow fibre membranes losing a substructure of the porous layer (Kapantaidakis and Koops, 2002). Peng and Chung (2008) considered the effect of the dimensions of the spinneret and air gap distance on the performance of hollow fibre membranes. They suggested that a certain air gap distance and thicker spinneret annulus gaps can give rise to small, elliptical, teardrop shaped inward-pointed macrovoids. This type of macrovoid can help increase the performance of hollow fibres in gas separation processes (Peng and Chung, 2008). The effect of air gap on the adsorbent hollow fibres will be discussed in Chapter 5.

A suitable pre-treatment temperature in PESF/HiSiv 3000 hollow fibre was found to increase the porosity in the hollow fibre structure due to expose of adoption sites from polymer (Tai and Wang, 2013). With low pre-treatment temperature, the adsorption

sites of fibre are likely to cover by polymer. Also, a decrease in adsorption performance was seen above 250 ℃. This confirms that as the temperature exceeded the transition glass temperature of PESF (220℃), the PESF causes the adsorption sites of HiSiv 3000 to be blocked. The influence of pre-treatment temperature will also be discussed in Chapter 4.

Therefore, the quality of adsorbent hollow fibres can be controlled by changing the spinning conditions, the geometry of the fibres and the recipe of adsorbent/polymer mixtures. Most of these parameters have been tested for the purposes of this study which seeks to develop multi-channel adsorbent hollow fibres which would yield a high adsorption performance and have high mechanical stability and a low pressure drop for use in VOC removal.

2.8 High temperature polymers for structured adsorbents

Polymers are used in different chemical applications such as separation membranes. Polymers are a series of monomers linked into macromolecules. For the purposes of this study, which is concerned with the development of adsorbent hollow fibres for the removal of VOCs, the right choice of polymer is vital. Typically, polymers have different physical and chemical properties depending on the length of the chains and constituent monomers. The melting point, glass transition temperatures (T_g) and elasticity and tensile strength of polymers are also important properties by which to identify appropriate polymers for industrial applications. The molecular weight of polymers depends on the length of the chains and can affect the thermal stability. Polymers with higher molecular weight have a higher melting temperature.

In this research, a polymer was required that was stable to ~ 200 °C, soluble in NMP with glass transition temperature above this, to enable regeneration and drying. Furthermore, a good chemical resistance, high Young's modulus of at least 2 GPa and cost no higher than 11 €/kg in cost were needed. In general, the polymers with high enough temperature resistance such as polyimide, polyetherimide polysulfone and polyethersulfone used in membranes. However, polyetherimides and Polyimide are expensive, making these two less desirable than polysulfone and polyethersulfone (Jeffs, 2015). A range of polymers commonly used for VOC removal include polysulfone (PSU), polyetherimides (PEI) and polyethersulfone (PESF) (Kim *et al.*,

2002). PSU and PESF are comparable in terms of mechanical stability and price but polyethersulfone has a higher glass transition temperature than polysulfone due to a higher molecular weight. The thermogravimetric (TGA) analyses of polyethersulfone and polysulfone have also been carried out (Altinkok *et al.*, 2011; Forati *et al.*, 2014). It was found that the 5% weight loss of pure polysulfone, was observed at 356°C. However, the 5% weight loss of pure polyethersulfone, was observed at approximately 522°C. Therefore, polyethersulfone is thermally high stable than polysulfone.

The structure of PESF is shown in Figure 2.12. It is a thermoplastic which has good mechanical properties, temperature resistance and chemical resistance (Barth *et al.*, 2000). The glass transition temperature of PESF is 220°C. Also, it has high hydrolytic stability against steam, hot water and some chemical materials such as acids and bases. Additionally, this polymer is flexible which enables hollow fibre modules to be formed to fit the existing space. However, one potential drawback of this polymer composite is that access to the adsorption sites can be blocked by the polymer during the regeneration process. To avoid polymer shrinkage, the heating setting below the transition temperature should be applied.

Therefore, for the purposes of this study, PESF was selected for the preparation of the adsorbent hollow fibres to enhance their mechanical and thermal properties.

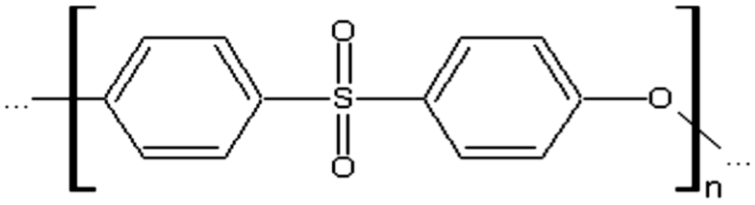

Figure 2.12. Polyethersulfone structure (Guan *et al.*, 2005).

2.9 Pore former

The addition of pore former in the adsorbent/polymer mixtures for hollow fibre fabrication was found to enhance the interconnectivity of pores and improve pore formation. The pore former can be achieved by mixing the pore formers with adsorbent/polymer mixtures and then eliminating them after the hollow fibres have been produced. The formation of pores can help enhance the adsorption performance due to increased porosity and provision of easier access to adsorption sites. Few studies

have been carried out on adsorbent hollow fibres; therefore, this literature review will give an overview of the studies carried out on the influence of pore former on the adsorption performance of hollow fibre membrane in liquid and gas separation.

Loh and Wang (2012) examined the effect of pore former on fabrication of hollow fibre membranes where Pluronic F127 was used as an additive. This study showed that pore former can modify the performance of hollow fibres and cut off the formation of macrovoids due to improved porosity (Loh and Wang, 2012). In 2012, Ismail et al. revealed that high concentration of pore former (glycerol) in the polymer mixture of hollow fibre membranes led to a high overall surface porosity with high adsorption performance (Rahbari-Sisakht *et al.*, 2012).

Previous study demonstrates a strong and consistent association between Licowax C micro powder PM and adsorption performance of adsorbent hollow fibres (Jeffs, 2015). It is an amide wax called N, N'-Bisstearoylethylenediamine with a melting point of 144°C. It offers anti blocking features to all polymers. Therefore, for the purposes of this study, Licowax C micro powder PM was used as an additive material to optimise the structure of adsorbent hollow fibres and the adsorption performance for VOC removal.

2.10 Mass transfer and transport resistance

Mass transfer is the movement of molecules from a higher concentration area (polluted gas) to a lower concentration area (adsorbent) in the adsorption processes. At equilibrium, no mass transfer occurs. The presence of large mass transfer resistance can affect the full use of the adsorbent module because of slow access to adsorption sites.

There are three types of mass transfer resistance: resistance to film transport, resistance to diffusion through the macropores of the adsorbent and resistance to diffusion on the surface of pores. The combination of all three types of resistance yields the overall mass transfer coefficient k. Hence, mass transfer resistance can be defined as 1/k. The types of adsorbent and adsorbate and conditions of process can control the steps mentioned above (Seader and Henley, 2011).

In chemical applications, adsorbents must be suspended in a binder such as ceramic and polymeric with the purpose of reducing the attrition related with very small particle size and withstanding pressure drop. In general, adsorbents are bound with for example ceramic to create a pellet having micro and macropores. These adsorbent pellets have complex structure where the molecules of adsorbate diffuse after passing the boundary layer. The framework structure of zeolite may contain uniform channels and windows, through which molecules of adsorbate can reach larger macro or mesopores. The binder such as clay also has micropores. This results can lead to a molecular sieving effect and in further resistance of zeolite intercrystalline diffusion (Ruthven, 2000).

In this study, polymers are used as a binder in adsorbent hollow fibres. When the access to adsorption sites is blocked, the mass transfer resistance is increased. This means that the diffusion of inlet gas will be through the polymer matrix. In comparison with adsorbent pellets, adsorbent hollow fibres have a lower mass transfer resistance because of their thin walls. The decrease in the size of pellets will lead to an increase in pressure drop. Therefore, hollow fibre modules have lower resistance, faster mass transfer and a lower pressure drop than granular bed modules.

2.11 Pressure drop

The development of new adsorption structures plays an important role in saving energy, which is a main environmental and economic concern in today's world. Adsorbents structured with a low pressure drop, a high surface area and low mass transfer resistance requires less operating costs than other comparable techniques (Brunazzi *et al.*, 1996). A low pressure drop for gas flow through an adsorber such as a hollow fibre is crucial for efficient fast-cycles within the process.

For the purposes of this research, adsorbent hollow fibres with minimal mass transfer resistance and low pressure drop were fabricated. The maintained contact between the gas stream and the adsorbent particles in hollow fibre structures is good. In experimental studies, the effect of the pressure drop on adsorbent hollow fibres with different structures was studied by changing the feed flow rate of the gas stream. All the flows used in this study are laminar flows. To identify the type of flow in hollow fibres the Reynolds number must be calculated as described in Equation 2.15.

$$Re = \frac{\rho u d}{\mu} \qquad (2-15)$$

where,

Re = Reynolds number

u = superficial velocity (m/s)

ρ = gas density (kg/m^3)

d = particle diameter (m)

μ = gas viscosity (Pa·s)

When the Re<2300 the flow is laminar, when the 6000>Re>2300 the flow is transitional and Re>6000 the flow is turbulent.

In modelling studies, three commonly used equations can be applied to model pressure drop depending on the types of flow and the adsorbent structure. The first equation is the Carman-Kozeny equation which applies to the laminar flow of a fluid in a packed bed of adsorbents (McCabe *et al.*, 1993).

$$\Delta P = L \frac{180\, u\, \mu\, (1-\varepsilon)^2}{\varphi_p^2\, d_p^2\, \varepsilon^3} \qquad (2-16)$$

where

ΔP = pressure drop (Pa)

L = bed length (m)

μ = fluid viscosity (Pa·s)

ε = Porosity

u = superficial velocity (m/s)

d_p = particle diameter (m)

φ_p = sphericity of the particles

The second equation is the Hagen-Poiseuille equation (Equation 2.17) which applies to the laminar flow of a fluid through a circular channel (Feng *et al.*, 1998).

$$\frac{\Delta P}{L} = \frac{8Q\mu}{\pi {r_i}^4} \qquad (2-17)$$

where,

ΔP = the pressure drop (Pa)

L =is the bed length (m)

Q= is the volumetric flow rate (m^3/s)

r_i = inner radius in the pipe (m)

μ= fluid viscosity (Pa.s)

The third equation is the Ergun equation (Equation 2.18) which applies to the turbulent flow of a fluid in a packed bed of adsorbents (Ergun, 1952).

$$\Delta P = L\left(\frac{150\ u\ \mu\ (1-\varepsilon)^2}{\varepsilon^3 d_p^2} + \frac{1.75(1-\varepsilon)\rho\ u^2}{\varepsilon\ d_p}\right) \qquad (2-18)$$

where

ΔP = pressure drop (Pa)

L = bed length (m)

μ = fluid viscosity (Pa·s)

ε = void space

u = superficial velocity (m/s)

d_p = particle diameter (m)

ρ = fluid density (kg/m^3)

For the purposes of this research the Hagen-Poiseuille equation was used to calculate the pressure drop through the model of adsorbent hollow fibres as it was deemed to be the most appropriate because the flow resembles laminar pipe flow.

2.12 Mechanical properties

Mechanical behaviour involves surface deformation of materials under the effect of applied forces. In membrane processes, mechanical properties are not important as most membranes are held by supporting materials. However, the mechanical properties are very important in the case of hollow fibres because they are self-supporting. In hollow fibre structures, the choice of a suitable type of material, the fibre diameter and the wall thickness is key to the structures' mechanical behaviour. The optimisation of these parameters can improve the mechanical properties of the structure and enable it to withstand high pressure (Mulder, 1996). The tensile modules (Young's modules)

can be obtained by plotting stress against strain at a constant rate, as shown in Figure 2.13.

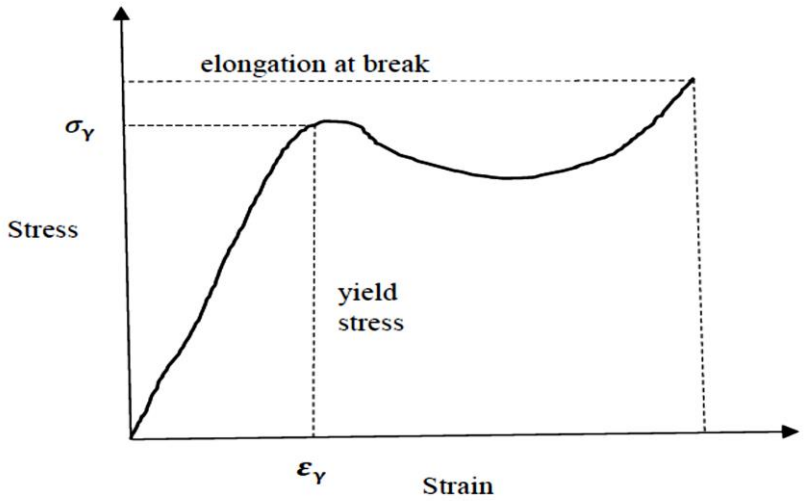

Figure 2.13 typical stress-strain curve adapted from (Mulder, 1996).

The initial slopes of the stress-strain diagram give the tensile modules.

$$E = \frac{d\sigma}{d\boldsymbol{\varepsilon}} \; at \;\; \boldsymbol{\varepsilon} = 0 \qquad (2-19)$$

where

E =tensile module

σ=stress which is force per cross-sectional area

$\boldsymbol{\varepsilon}$=strain which is (L-L_0)/L_0

The maximum point in the stress-strain curve can define the elongation at $\boldsymbol{\varepsilon}_Y$ yield stress and the stress at yield, $\boldsymbol{\sigma_Y}$**.** At the yield stress point, the materials have lost their mechanical properties. Single adsorbent hollow fibres have been used in previous studies for gas separation with some limitations in terms of their mechanical properties (Tai, 2007). In this research, single and multi-channel adsorbent hollow fibres were respectively optimised and developed to overcome the limitations of their mechanical properties. It was found that multi-channel adsorbent hollow fibres prepared using the new tri-bores spinneret have better mechanical properties when compared to single adsorbent hollow fibres obtained using a single spinneret.

2.13 Computational fluid dynamic modelling

Computational fluid dynamics (CFD) is the employment of applied physics, computational software and mathematics to visualise how a fluid flow. CFD is based on solving a set partial differential equations (PDEs) which describe the conservation of momentum, species transport and energy. These equations also describe the interaction between the gas or liquid and the surfaces and how the temperature, pressure, density and velocity of a moving gas or liquid are related. The definition of the boundary conditions of the system is important to obtain accurate solutions.

CFD has been attracting considerable interest since the early 20th Century and researchers are familiar with it as a useful tool for analysing fluid flow around aircraft and cars (Hess and Smith, 1962). Rapid development in computer technology, leading to increased computing power and memory capacity, has led to major improvement in CFD software which can now be used to obtain very accurate numerical solutions. CFD has replaced analytical PDE with its approximating analytical solutions when it comes to solving complex engineering issues (Wendt and Anderson, 2009).

A number of discretisation methods are used for discretised numerical approximations to the PDEs used in CFD modelling, such as, the Finite Difference Method (FDM), the Finite Element Method (FEM) and the Finite Volume Method (FVM). FEM is the most commonly used out of the other methods because it is simpler to use. The FEM and FVM are more complex, but are also more accurate and flexible methods to use to approximate the analytical solution of PDES. In general, quadrilateral or triangular elements which allow meshes will more accurately represent complex geometries (Wendt and Anderson, 2009). On the other hand, FDM is usually used in simple geometries whereby the partial derivatives given in PDEs of dynamic of flow are swapped with algebraic difference quotients (Dick, 2009).

In this research, the CFD commercial package that was employed to simulate the transport mechanism in adsorbent hollow fibres was COMSOL Multiphysics 5.2. This package is a finite element analysis, simulation software and solver for several engineering and physics applications. It is an easy-to-use, seamless interface between mass transfer and other fields of physics. Moreover, it provides the ability to modify governing equations and has superior mesh flexibility. The chemical reaction module

in COMSOL Multiphysics 5.2 contains the tool to simulate fluid (gases or liquid) transport through gases, porous media, within solid phases, liquids and on surfaces.

Hollow fibre-based separation processes have recently received increased attention in chemical applications. The application of mathematical models in chemical processes has many of significant advantages, such as flexibility and safety, cost effectiveness, the understanding of the influence of several process parameters and the possibility of analysing the fluid flow on hollow fibres for fluid separations. The hollow fibre module, which comprises a large number of hollow fibres packed in a module, has a wide range of applications. Mathematical modelling of hollow fibre applications has been carried out to model hollow fibre membranes for gas and liquid separation processes, but there has been no mathematical modelling of adsorbent hollow fibre carried out to date. Therefore, this section focuses on previous studies which carried out mathematical modelling and numerical simulation of gas transport through hollow fibre membranes.

The first simulation for membrane gas separation was developed by Weller and Steiner (1950) using a non-porous membrane. This mathematical model dealt with binary component gas mixtures (Weller and Steiner, 1950). The modelling of asymmetric hollow fibre membranes for high flux gas separation was reported by Pan (1986). The experimental results verified the modelling results and validated the technical feasibility of using the asymmetric hollow fibre for gas separation (Pan, 1986). In 1992, Kovvali and colleagues presented a comparison between flat sheet and tubular membrane modules for gas separation. They showed that a constant permeate pressure is reasonable for both modules but with small permeability, whereas a significant pressure drop was found when employing hollow fibre modules (Kovvali et al., 1992).

A novel approach was taken by Thundyil and Koros (1997) to solve and analyse the mass transfer issue through hollow fibre membrane posed by permeation processes (Thundyil and Koros, 1997). Moreover, Sohrabi et al. (2011) displayed a 2D model for the practical illustration of CO_2 separation using hollow fibre membranes and applying the finite element method for numerical solution of governing equations (Sohrabi et al., 2011). Khalilpour et al. (2013) put forward a general finite difference method combined with the Gauss-Seidel algorithm and analysed hollow fibre membrane separation to solve partial non-linear differential equations (Khalilpour *et al.*, 2013).

The modelling of hollow fibre membranes for VOC removal from wastewater using CFD has also been reported. In this system, VOC and air were simulated as stripping gas. The concentration changes and pressure drops were thus studied (Barati *et al.*, 2014).

This research deals with the development of adsorbent hollow fibres for VOC separation. While somewhat idealised, the understanding of mass transfer through fibres is important as a beginning for realistic modelling of this important separation. The permeation of gas is not considered in this research, unlike in other studies. Instead, the adsorbent hollow fibre was designed to allow no access through the wall of hollow fibres during the operation. Experimentally-validated adsorbent hollow fibre models were implemented in COMSOL Multiphysics 5.2 as a user defined unit operation using the finite element method. To design an adsorbent hollow fibre, the governing equations, which describe the relationships of the fluid properties, operation parameters and hollow fibre properties to the adsorption performance, were used. This work reports the results of a case study of VOC removal from steam gas using an adsorbent hollow fibre to assess the performance of a gas separation application. The adsorbent hollow fibre module characteristics, such as the diameter of the fibre, its geometries, bore shapes and porosity, were employed to yield different hollow fibre performance data. The details of the CFD model set-up will be included in Chapter 6.

2.14 Summary

The idea behind the use of hollow fibre for gas separation is convenient, and much has changed over time. Current studies should focus on improving the separation performance with low operation cost and minimal waste. In the following chapters, adsorbent hollow fibres are shown as being able to overcome a number of the problems which arise when using other structured adsorbents in gas separation processes for several reasons, given below:

1. Low mass transfer resistance results in very small adsorbent particles (between 1 and 2 mm).

2. Low pressure drop in fibres results in an open passageway for the fluid flow.

3. Light weight results in high porosity, so hollow fibre has a greater volume/length when compared to granules.

4. The uniform distribution of adsorbent particles along the hollow fibres structure minimise adsorbent dead spacing.

5. To actively pack granules, a special packing equipment is required while no special equipment is required to fill a cartridge with hollow fibres.

6. The presence of strong polymers in adsorbent hollow fibres can enhance the mechanical properties of fibres.

Therefore, in order to optimise and develop adsorbent hollow fibres:

1. Single adsorbent hollow fibres made up of a mixture of 13X zeolite and polyethersulfone (PESF) were optimised to achieve high adsorption performance with good mechanical properties.

2. Methods to improve the adsorption of n-butane as a VOC model gas were investigated, such as by changing the concentration of polymer/adsorbent/solvent mixtures, adding pore former and exposing the breakthrough curves of hollow fibres to a range of flow rates.

3. A multi-channel adsorbent hollow fibre was fabricated as a novel geometry of adsorbent hollow fibres. This fibre offers an improvement in adsorbent loading, mechanical properties and surface area when compared to a single hollow fibre at the same weight of bundles.

4. Adsorption using adsorbent hollow fibres were modelled using CFD, COMSOL 5.2. These models were used to understand the mechanism of fluid flow through the hollow fibres and predict the results.

Chapter 3: Development and Characterisation of Adsorbent Hollow Fibre

This study is based on a series of experimental procedures to produce single and multi-channel adsorbent hollow fibres. The materials used in this study are described in Section 3.1. The preparation of single and multi-channel adsorbent hollow fibres is described in Section 3.2. The viscosity of the polymer/solvent/adsorbent mixture was measured using a Bohlin CS 50 Rheometer before the spinning process of adsorbent hollow fibres. The procedure of the measurement of viscosity is described in Section 3.2.2. The spinning process of adsorbent hollow fibres used several types of spinneret is described in Section 3.2.3. The physical properties of 13X zeolite powder and adsorbent hollow fibres were explored using the nitrogen adsorption-desorption isotherm to determine their pore size distribution and surface porosity are given in Section 3.3.1. The Scanning Electron Microscope (SEM) was used to describe the morphology surface of adsorbent hollow fibres is describes in Section 3.3.2. The mechanical properties of the hollow fibres were obtained using an INSTRON 3369 fitted with a load cell. The details of the method used to determine the mechanical properties and pressure drop are given in Sections 3.3.3 and 3.3.4 respectively. The adsorption capacities of the produced adsorbent hollow fibres were tested using adsorption breakthrough experiments. In this experiment, n-butane was used as a VOC model gas. The procedures and apparatus used in the adsorption breakthrough experiment are described in Section 3.4.

3.1 Materials

The adsorbents used in this study were 13X zeolite (hydrophilic), HiSiv 1000 zeolite powder and HiSiv 3000 zeolite powder (hydrophobic). Both moisture resistance high silica hydrophobic adsorbents were purchased from Honeywell UOP, US. However, the 13X zeolite was purchased from Zeochem, Switzerland which has an average pore diameter of approximately 0.9 nm. The plyethersulfone (PESF) supplied by Solvay Performance, Brussels, were used as the polymers. 1-methyl-2-pyrrolidone (NMP) 99+%, Spectrophotometric Grade, supplied by Sigma-Aldrich, was used to dissolve the polymer. The pore former Licowax C micro powder PM was used in this work.

This is an amide wax called N, N'-Bisstearoylethylenediamine with a melting point of 144°C. It offers anti blocking features to all polymers. A summary of all the materials used in this research is given in Table 3.1.

Table 3.1: A list of the materials used in this work and the suppliers

Materials	**Purpose**	**Company, Country**
13X zeolite	adsorbent	Zeochem, Switzerland
HiSiv 1000 zeolite powder	adsorbent	Honeywell UOP, US
HiSiv 3000 zeolite powder	adsorbent	Honeywell UOP, US
NMP (1-methyl-2-pyrrolidone)	solvent	Sigma-Aldrich, UK
Polyethersulfone (PESF)	polymer	Solvay, Brussels
1000ppm n-Butane/Nitrogen 200bar	adsorbate	BOC Gases, UK
Nitrogen gas	carrier, system purge and regeneration	BOC Gases, UK
Hydrogen gas	FID fuel	BOC Gases, UK
Zero grade air	carrier	BOC Gases, UK
Silicone sealant	adhesive	Bostik, UK
Licowax C micro powder PM	pore former	Clariant, Switzerland

3.2 Types of spinneret

In this research, three different spinnerets were used to obtain different geometries of adsorbent hollow fibres, as shown in Figure 3.1. The spinnerets each comprised a different number of hollow tubes and a peristaltic pump was used to provide a different flow rate of internal coagulant (mixture of water and NMP) into these tubes. They were used to form bores and produce the different shape of adsorbent hollow fibres.

(a) Circular double orifice spinneret | (b) Tri-lobe with three tube spinneret | (c) Hexagonal with seven tube spinneret

Figure 3.1. The three types of spinneret used in this research to fabricate several geometries of adsorbent hollow fibres

3.2.1 Circular double orifice single bore spinneret

The first spinneret, shown in Figure 3.1 (a) and Figure 3.2, is a circular double orifice spinneret with one internal tube. This type of spinneret has been used previously to form double layer single channel adsorbent hollow fibres for several applications. It consists of an inner tube in the centre of an orifice. The tube has a diameter of 0.6 mm. With the presence of separator, the polymer/adsorbent/solvent mixture can be extruded through both layers to fabricate a double layer hollow fibre. The separator diameter of

the spinneret was 2 mm while the outer diameter was 3 mm. In this study, single hollow fibre has been spun to optimise the recipe of polymer/adsorbent/solvent mixture. The pressure used to transfer the optimum hollow fibre mixture (83 wt%: 17 wt% PESF) was 2 barg. The flow rate of bore fluid was 3 ml/min. In order to compare the adsorption capacity, mechanical properties and adsorbent loading of hollow fibres, the optimum recipe was used to fabricate multi-channel adsorbent hollow fibres using the tri-lobe three tube spinneret.

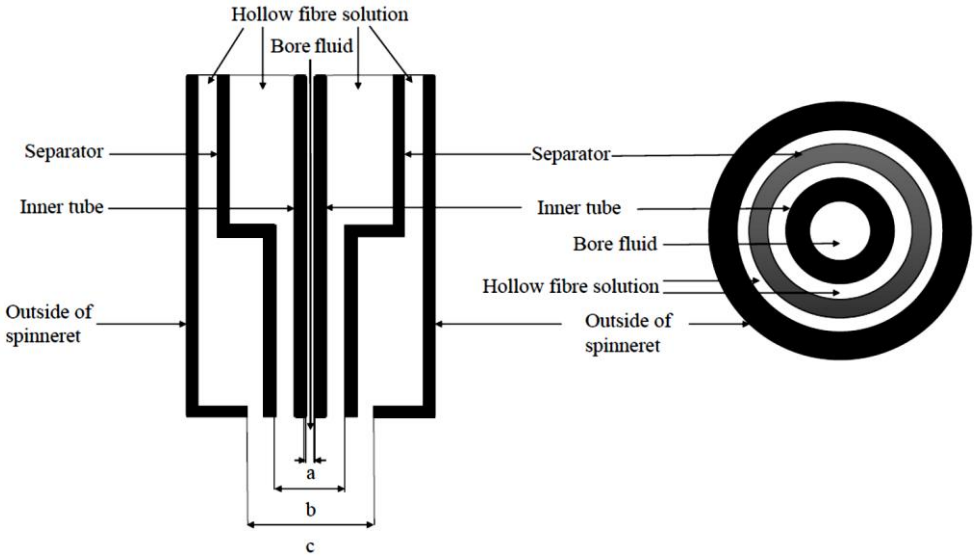

Figure 3.2. Diagram of the circular double orifice spinneret viewed from the side and above with the structure in place; where a). the tube diameter (0.6 mm); b). the diameter of the separator (2 mm), c). the outer diameter (3 mm) of the spinneret

The 13X zeolites and PESF were used to prepare three lengths (12, 17 and 22 cm) of single adsorbent hollow fibre. These were tested with 1 L/min 1000 ppm n-butane in a double layer configuration. The test results were used to study trends in the adsorption performance of the fibre module as length was increased. In addition, the effect of changing the gas flow rate on the dynamic adsorption challenge was tested. Three different gas flow rates were tested for adsorbent hollow fibres with the same compositions (83 wt% 13X and 17 wt% PESF) and module length (22 cm). Gas flow rates of 1, 2 and 3 L/min were examined and compared, to identify the optimum gas flow rate.

13X hollow fibres were prepared by extruding 13X/PESF mixture through a spinneret as mentioned in Section 3.3. With the purpose of maximising the adsorption

performance, mechanical properties and porous structure, adsorbent hollow fibres can be fabricated with different structures by changing the composition of adsorbent/PESF/solvent mixtures, bore fluid compositions and pre-treatment temperature. Therefore, the following procedure have been considered.

First, the adsorption capacity of 13X/polymer composite hollow fibres (83 wt% 13X and 17 wt% PESF) prepared using five different compositions of bore mixture (30 wt%, 40 wt%, 50 wt%, 60 wt% and 70 wt% NMP to water) were compared by studying the breakthrough curves of n-butane at a feed flow rate of 1.0 L/min, and with a feed concentration of 1000 ppm. The hollow fibre bundles were bundled into approximately 22cm lengths. These fibres were heat-treated for 24 hours at 200°C for exposing the adsorption sites.

Second, in order to study the influence of 13X zeolite concentration, three 13X/PESF mixtures were prepared with different 13X concentrations (83 wt%, 84 wt% and 85 wt%) to create adsorbent hollow fibres. The experiments were performed at feed flow rates of 1 L/min. In each adsorption experiment, the n-butane feed concentration was kept constant at 1000 ppm. Moreover, the influence of the morphology of all hollow fibres was studied.

Third, Licowax C micro powder PM (melting point at 144°C) will be incorporated into the 13X/PESF hollow fibre by adding this pore former to the 13X/PESF/NMP mixture. It can be removed from the hollow fibre by placing it in an oven at 200°C. The addition of pore former could help to enhance the adsorption kinetics of hollow fibres. To investigate the effect of adding the pore former, 1g of Licowax C micro powder PM was added to 13X/PESF mixtures (83 wt% 13X: 17 wt% PESF). All breakthrough experiments were carried out under the same adsorption conditions (1000 ppm of n-butane with a feed flow rate of 1.0 L/min). The length of the hollow fibre modules was kept at 22cm. The effect of adding pore former on the pore structure of hollow fibres was also investigated.

Finally, the influence of pre-treatment temperature on manufactured 13X/PESF adsorbent hollow fibre (83 wt% 13X and 17 wt% PESF) was investigated. A range of heat treatments (150°C, 180°C, 200°C and 250°C) for adsorbent hollow fibres were tested. This factor affects the adsorption performance of adsorbent hollow fibres and

was tested with 1 L/min 1000 ppm n-butane. The morphology of these fibres was also studied; Table 3.2 shows all single adsorbent hollow fibres compositions and parameters used in each experiment. It also shows the mixture compositions, spinning parameters and adsorption performance testing parameters of all single adsorbent hollow fibres manufactured in this research using the circular double orifice spinneret.

Table 3.2: Composition of the Polymer/Adsorbent/Solvent Mixture and Spinning Parameters to Fabricate Double Layer Single Adsorbent hollow fibres

Hollow fibre	Polymer/Adsorbent/Solvent Mixture Compositions				Spinning Parameters						Adsorption Performance Testing Parameters		
	PESF/NMP (wt%)	13X/PESF (wt%)	Licowax PM (g)	Viscosity (Pa.s)	Coagulation Bath Temperature (°C)	Bore Fluid Compositions NMP/Water (wt%)	Injection Rate of Bore Fluid (ml/min)	Nitrogen Pressure (bar)	Air Gap (cm)	Linear Extrusion Speed (rpm)	Volumetric Flow Rate of 1000 ppm n-butane (L/min)	Length of Fibre (cm)	Pre-treatment Temperature (°C)
SAHF 1	18/82	83/17	0	11.4	20	50/50	3	2	0	26	1	12	200
SAHF 2	18/82	83/17	0	11.4	20	50/50	3	2	0	26	1	17	200
SAHF 3	18/82	83/17	0	11.4	20	50/50	3	2	0	26	1	22	200
SAHF 4	18/82	83/17	0	11.4	20	50/50	3	2	0	26	2	22	200
SAHF 5	18/82	83/17	0	11.4	20	50/50	3	2	0	26	3	22	200
SAHF 6	18/82	83/17	0	11.4	20	30/70	3	2	0	26	1	22	200
SAHF 7	18/82	83/17	0	11.4	20	40/60	3	2	0	26	1	22	200
SAHF 8	18/82	83/17	0	11.4	20	60/40	3	2	0	26	1	22	200
SAHF 9	18/82	83/17	0	11.4	20	70/30	3	2	0	26	1	22	200
SAHF 10	18/82	84/16	0	12.7	20	50/50	3	2.25	0	26	1	22	200
SAHF 11	18/82	85/15	0	13.8	20	50/50	3	2.5	0	26	1	22	200
SAHF 12	18/82	83/17	1	11.4	20	50/50	3	2	0	26	1	22	200
SAHF 13	18/82	83/17	1	11.4	20	50/50	3	2	0	26	1	22	150
SAHF 14	18/82	83/17	1	11.4	20	50/50	3	2	0	26	1	22	180
SAHF 15	18/82	83/17	1	11.4	20	50/50	3	2	0	26	1	22	250

3.2.2 Tri-lobe three bore spinneret

The second spinneret was used to develop and fabricate a novel tri-lobe adsorbent hollow fibre with multi-channel (three bores) as shown in Figure 3.1 (b) and Figure 3.3. The spinneret has been done and manufactured in the University of Bath. This tri-lobe hollow fibres are novel and it has been reported for the first time. Tri-lobe spinneret consists of three hollow tubes in the centre, in this case, a reasonable mixture of NMP and water, injected through these tubes to form three bores and obtain the tri-lobe shape of the adsorbent hollow fibre. Each hollow tube diameter of the spinneret was 1 mm. The pressure used to transfer the optimum hollow fibre mixture (83 wt%: 17 wt% PESF) was 3 barg because of making the same average velocity. The flow rate of bore fluid was 3 ml/min. Tri-lobe multi-channel adsorbent hollow fibre structures have not yet been published and done the experiments for the first time.

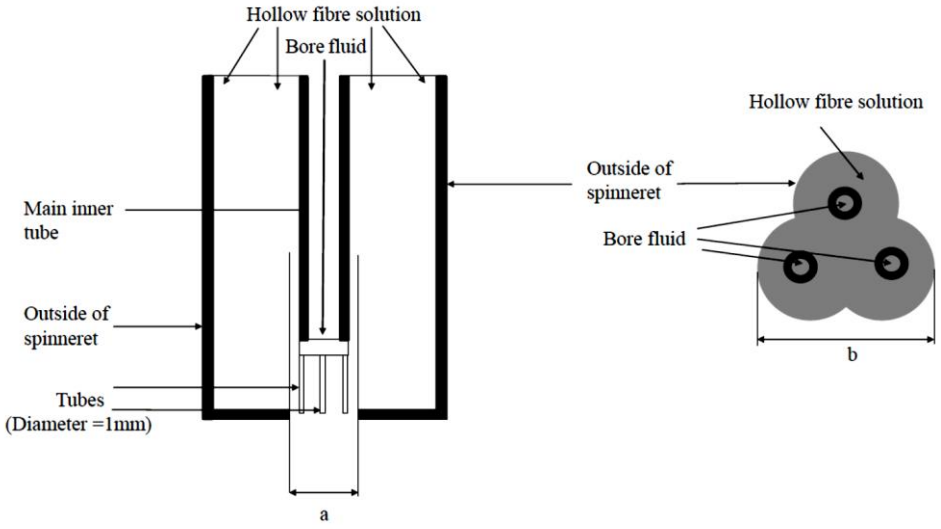

Figure 3.3. Diagram of the tri-lobe three bore spinneret viewed from the side and above with the structure in place; where a). the tube diameter (1 mm); b). the length of two lobe (11 mm), of the spinneret

3.2.3 Hexagonal seven bore spinneret

The work carried out using hexagonal seven bore spinneret to develop and produce hexagonal seven bore adsorbent hollow fibres. The third spinneret is shown in Figure 3.1 (c) and Figure 3.4. Hexagonal fibres are also novel and I have reported the work for the first time. Hexagonal spinneret has also been manufactured in the University of Bath. It consists of seven hollow tubes in the centre of orifice, in this case a

reasonable mixture of NMP and water, injected through these tubes to form seven bores and fabricate the hexagonal shape of the adsorbent hollow fibre. With the presence of hexagonal separator, the polymer/adsorbent/solvent mixture can be extruded through both layers to fabricate a double-layer hexagonal hollow fibre. The outer tube length of the spinneret was 7 mm. The hexagonal separator (outer tube) has a side length of 7 mm. Each hollow tube has a diameter of 1 mm. The pressure used to transfer the optimum hollow fibre mixture (83 wt%: 17 wt% PESF) was 5 barg because of making the same average velocity. The flow rate of bore fluid was 6 ml/min. Hexagonal multi-channel adsorbent hollow fibre structures have not also been published. The polymer/adsorbent/NMP mixture compositions, spinning parameters and adsorption performance testing of tri-lobe and hexagonal multi-channel adsorbent hollow fibres produced in this research are shown in Table 3.3.

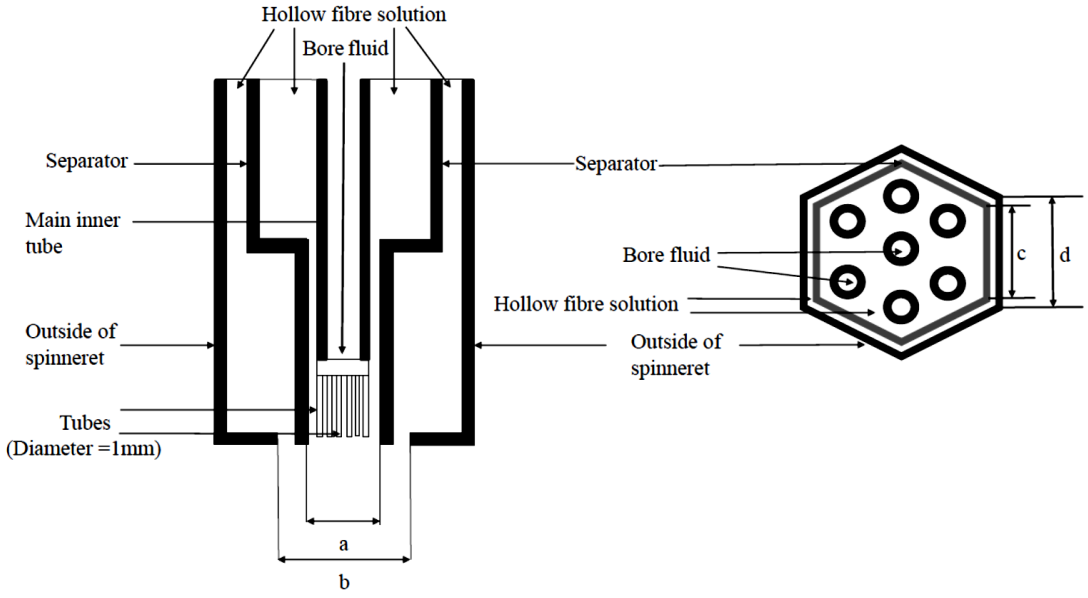

Figure 3.4. Diagram of the Hexagonal double orifice spinneret viewed from the side and above with the structure in place; where a). the outer tube length (7 mm); b). the length of the separator (9 mm), c). the inner hexagon side length (4 mm), d). the outer hexagon side length (5 mm) of the spinneret

Table 3.3: Composition of the Polymer/Adsorbent/Solvent Mixture and Spinning Parameters to fabricate tri-lobe and hexagonal Multi-channel Adsorbent hollow fibres

Hollow fibre	Polymer/Adsorbent/Solvent Mixture Compositions				Spinning Parameters						Adsorption Performance Testing Parameters		
	PESF/NMP (wt%)	Adsorbent/ PESF (wt%)	Licowax PM (g)	Viscosity (Pa.s)	Coagulation Bath Temperature (°C)	Bore Fluid Compositions NMP/Water (wt%)	Injection Rate of Bore Fluid (ml/min)	Nitrogen Pressure (bar)	Air Gap (cm)	Linear Extrusion Speed (rpm)	Volumetric Flow Rate of 1000 ppm n-butane (L/min)	Length of Fibre (cm)	Pre-treatment Temperature (°C)
TAHF 1	18/82	13X/PESF 83/17	1	11.4	20	50/50	3	3	0	24	1	22	200
TAHF 2	18/82	13X/PESF 83/17	0	11.4	20	50/50	3	3	0	24	1	22	200
TAHF 3	18/82	13X/PESF 84/16	0	12.7	20	50/50	3	3.25	0	22	1	22	200
TAHF 4	18/82	13X/PESF 85/15	0	13.8	20	50/50	3	3.5	0	20	1	22	200
TAHF 5	18/82	13X/PESF 83/17	0	11.4	20	50/50	6	3	0	24	1	22	200
TAHF 6	18/82	13X/PESF 83/17	0	11.4	20	50/50	3	3	0.5	24	1	22	200
TAHF 7	13/87	HiSiv 3000/ PESF 83/17	0	9.1	20	50/50	3	3	0	24	1	22	200
TAHF 8	12/88	HiSiv 1000/ PESF 83/17	0	9.5	20	50/50	3	3	0	24	1	22	200
HAHF 1	18/82	13X/PESF 83/17	0	11.4	20	50/50	6	4.5	0	18	1	22	200
HAHF 2	18/82	13X/PESF 83/17	0	11.4	20	50/50	6	4.5	0.1	18	1	22	200
HAHF 3	18/82	13X/PESF 83/17	0	11.4	20	50/50	6	4.5	0.5	18	1	22	200

3.3 Preparation of single and multi-channel adsorbent hollow fibres

The steps involved in preparing adsorbent hollow fibres are described below in chronological order.

3.3.1 Preparation of the polymer/solvent/adsorbent mixture

Polymer/solvent/adsorbent mixture were prepared to fabricate adsorbent hollow fibres. Firstly, a polymer mixture was prepared by dissolving polyethersulfone (PESF) in an NMP solvent. This mixture was prepared in different ratios, one of which was, for example, 180 g of NMP to 40g of PESF. These compositions were stirred on the laboratory roller mixer series SRT6D (manufactured by Stuart Equipmentat) at 18 rpm for 24 to 48 hours until the PESF was completely dissolved in each. Secondly, the polymer mixtures were stirred using an electric stirrer and the adsorbent powder was slowly added in small amounts over 2 days to ensure thorough mixing. When a hydrophobic adsorbent such as HiSiv 1000 was used, an additional amount of solvent was added to ensure that a homogenous mixture with a suitable viscosity was obtained. Thirdly, to optimise the adsorption performance of the adsorbent hollow fibres, additives were added to some of the mixtures. Finally, the polymer/solvent/adsorbent mixtures were vacuumed for 25 minutes with the aim of removing any bubbles. These bubbles could cause the hollow fibre to break during the spinning process.

3.3.2 Viscosity of mixtures

The viscosity of all polymer/solvent/adsorbent mixtures was measured. In order to spin adsorbent hollow fibres the viscosity of the adsorbent/polymer mixture must be high (between 7 and 15 Pa.s). Over viscosity or under viscosity values can cause a failure of spinning. The critical concentration of polymer is described in Appendix III. The viscosity values were obtained using a Bohlin CS 50 Rheometer. All samples were placed on the sample placement as per operating instructions. It is important when applying an adsorbent/polymer/solvent mixture that a suitable amount is used to provide an accurate value. Under filling or over filling can introduce errors in the values measured. The temperature was then set at 20°C and the shear stress software was selected and measured. The apparatus was then set to complete the test automatically.

3.3.3 Spinning process of adsorbent hollow fibres

The prepared solvent/polymer/adsorbent mixtures were transferred to a vessel which was extruded with compressed nitrogen. The pressure ranged from 0.5 to 5 barg depending on the prepared adsorbent/polymer/solvent mixture viscosity and type of spinneret used, as mentioned in Section 3.2. Figure 3.5 shows how the adsorbent hollow fibre mixture was extruded through one of the spinnerets used in this research and passed in a bath filled with water. It was important to adjust the air gap length between the water bath and the spinneret to achieve the required air gap. It is indicated that the greater weight of adsorbent into polymer/solvent mixture used to fabricate adsorbent hollow fibre can enhance the gravitational effect with large air gap. Therefore, in this research, zero air gap was selected as favourite air gap length to enhance the adsorbent hollow fibre porosity and keep the fibre strong. It was also important to adjust desired bore fluid flowrate depending on the type of spinneret. A peristaltic pump provided a constant flow of bore fluid into the bore of hollow fibre.

The extruded adsorbent fibre mixture began the phase inversion process at contact with the water bath. During phase inversion, the solvent in the polymer/adsorbent mixture exited into the bath water. Then, the formed adsorbent hollow fibre was passed through the first water bath to a second for further phase inversion before collecting in the third water container. A Parvalux motor with a Mitsubishi S500 controller provided a constant removal rate of adsorbent hollow fibre from the coagulation baths. Also, it is important to set the controller to allow the hollow fibre as long as possible in the water baths but avoid mechanical damage to the hollow fibres. The macrovoids were formed as the adsorbent hollow fibres coagulated; the bore surface is highly porous due to the use of a mixture of NMP/water in the bore fluid, whereas the poorly porous outer skin is as a result of spinning into a water bath with no solvent. The use of several compositions of NMP/water leads to delay or instantaneous coagulation process in the bore of hollow fibre. This will be discussed in details in Chapter 4.

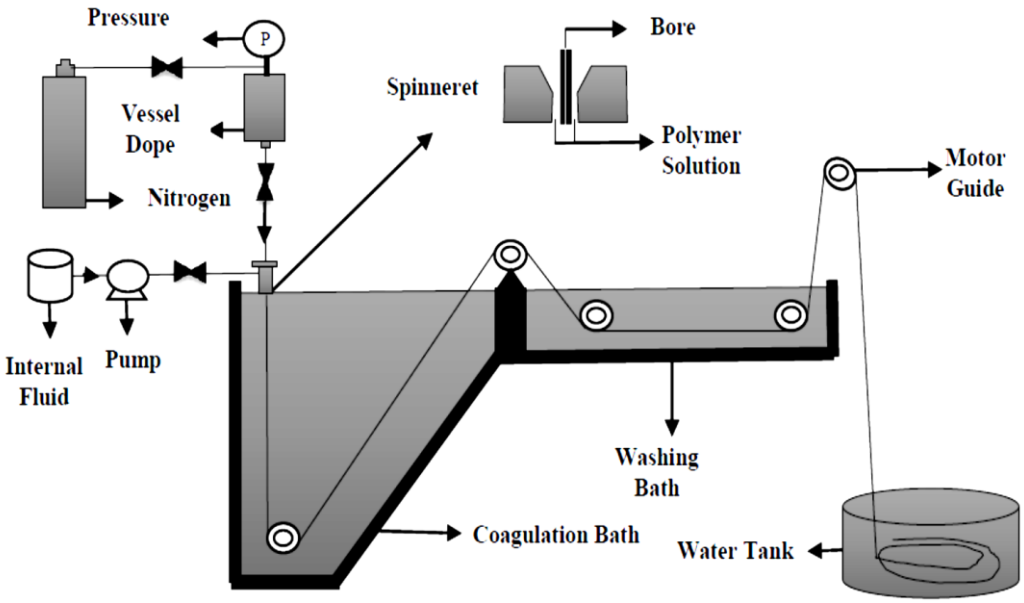

Figure 3.5. Diagram of the adsorbent hollow fibre spinning process.

3.3.4 Delayed phase inversion

At the end of the spinning process, the adsorbent hollow fibres were left in a water container to soak between three and four days. This soaking step allowed the residual solvent to be removed from the fibres and completed the phase inversion process. During this step, the water was changed daily. After washing, the adsorbent hollow fibre was straightened and cut into about 26 cm length and then dried at ambient conditions for two days before preparing of adsorbent hollow fibre modules, pre-treatment and characterisation.

3.3.5 Preparation of adsorbent hollow fibre column for dynamic adsorption testing and pressure drop challenge

In order to be used in gas separation applications, a specific number of fibres should be bound into a module. Adsorbent hollow fibres were formed into cartridges for dynamic adsorption testing and the pressure drop challenge. In this work, the module used was a stainless-steel cylinder with a 2 cm diameter and a length of 25 cm. The fibres were straightened, cut to a length which was 26 cm longer than the required length (which is 22 cm) and bundled together into a cylindrical shape to pack the stainless-steel module. Then, both ends of the cartridge were sealed with a suitable amount of silicone and wrapped in PTFE gas tape to make sure that the gas would only

pass through the lumen of the adsorbent hollow fibres. After nearly 24 hours, in order to expose the bores of hollow fibres and obtain the desired length, nearly 2 cm was cut from every sealed end.

3.3.6 Pre-treatment of adsorbent hollow fibre modules

The adsorbent hollow fibre module was pre-treated by heating to 200°C for 24 hours under vacuum. It was important to keep the pre-treatment temperature below the glass transition temperature (T_g) of the polymer. The polymer used in this research was polyethersulfone (PESF) which has a T_g of 220°C. The aim of this stage was to remove any residual solvent and water from the fibres and improve access to the adsorption sites. The effect of heat treatment on the adsorption performance and morphology of adsorbent hollow fibre will be discussed in Chapter 4.

3.4 Characterisation of adsorbent hollow fibres

The single and multi-channel adsorbent hollow fibres were investigated by using a number of characterisation techniques described in Sections 3.4.1-3.4.4.

3.4.1 Nitrogen adsorption-desorption isotherm

The nitrogen adsorption-desorption isotherm analyses of the adsorbent hollow fibres and adsorbent powders were performed at 77 K on a Micromeritics 3Flex Surface Area and Pore Analyser (ASAP), as shown in Figure 3.6. They were used to measure the pore size distribution, the surface area and pore volume of adsorbent hollow fibres and 13X zeolite powder. This apparatus is provided with software packages for calculating the data from the measured nitrogen adsorption different models, such as the BET (Brunauer, Emmett and Teller), Langmuir and the Horvath-Kawazoe.

This analysis method is to measure the quantity of gas adsorbed onto a porous material at various equilibrium vapour pressures by the constant volumetric method. As adsorption occurs, the pressure in the sample changes until equilibrium is reached. The volume of gas adsorbed is the difference between the amount of gas admitted and the amount of gas filling the sample cell space around the adsorbent. The volume-pressure data is transformed into BET surface area, adsorption/desorption isotherms, micropore analysis and pore size distribution based on the selected models.

The 13X zeolite powder and adsorbent hollow fibre samples analyses were carried out using a sample of approximately 0.15 g. All samples are contained inside the sample analysis port, as shown in Figure 3.6. Prior to the adsorption measurements, they were degassed at 473 K for 24 hours in a vacuum to determine the dry weight, followed by the nitrogen isotherm under increasing pressure (range of 0.001 to 780 mmHg). The pure nitrogen charges to the system were determined using the pressure transducer and dosing volume, and the system operates automatically. Nitrogen adsorption isotherms were measured at the Chemical Engineering and Chemistry Departments (University of Bath).

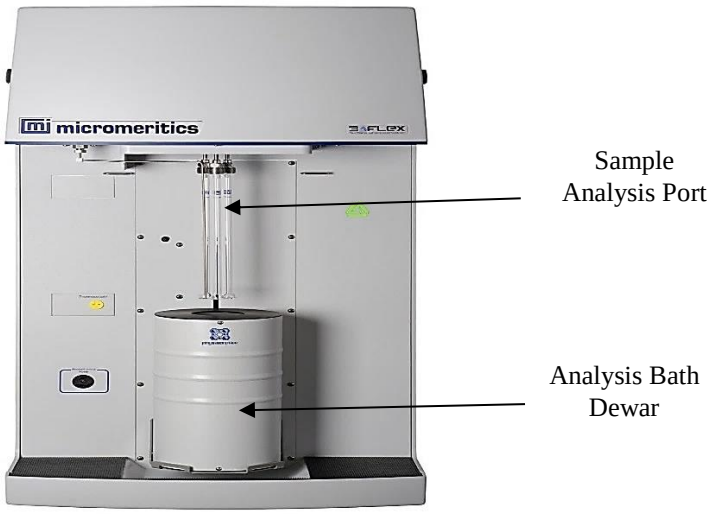

Figure 3.6. Micromeritics 3Flex Surface Area and Pore Analyser (Micromeritics.com, 2016)

3.4.2 Scanning electron microscope (SEM)

Adsorbent hollow fibres were characterised using a scanning electron microscope (SEM). This technique is useful for producing images of surface structure, distribution in the matrixes and particle size. Firstly, all samples were frozen for 30 seconds using liquid nitrogen and then sectioned using a sharp blade. Secondly, a number of the small sample was placed on a specimen stub with a double sided carbon adhesive. Then, a specimen was coated with gold for 3-5 minutes using the Edwards Sputter Coater to create a conductive layer on the sample for reducing thermal damage and improving the secondary electron signal. Finally, SEM micrographs were taken using a JEOL JSM63 10 model with a voltage of 10 kV at different magnifications.

3.4.3 Mechanical properties

The mechanical properties of the adsorbent hollow fibres were estimated using the INSTRON 3369 fitted with a load cell for 1 KN. It has upper and lower crosshead: the lower one is fixed and the other is used to apply tension. The specimen grips use to hold the specimen during the tensile test. The hollow fibres were placed in the specimen grips with 9 cm gauge length in between. The upper crosshead speed was adjusted to 0.2 mm/min. The gauge length of the specimen has a cross-sectional area that the load will be applied across, generating a stress. The calculations and plotting of the extension, breaking load and strain of hollow fibres were performed automatically. Figure 3.7 shows a schematic of a standard tensile specimen.

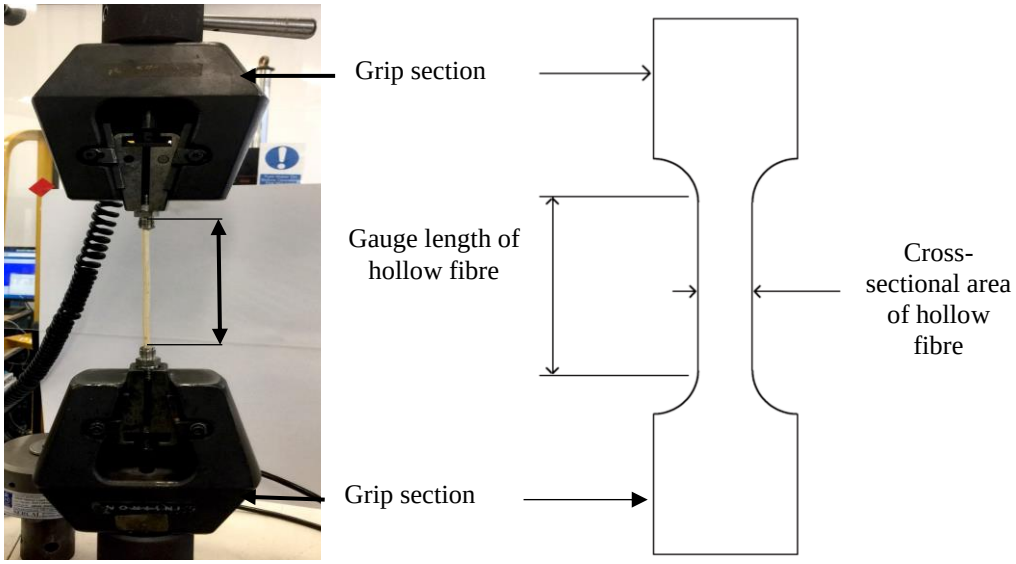

Figure 3.7. Photo and schematic of a tensile specimen

The following are equations used to calculate the strength of adsorbent hollow fibres:

$$Stress\ (Mpa)\ = \frac{Load\ (N)}{Cross-sectional\ area\ (cm^2)}$$

Where, stress describes the ratio of applied load to the cross-sectional area of fibre in tension or the maximum load a fibre can stand before it breaks.

$$Strain = \frac{Extention\ (cm)}{Gauge\ length\ of\ fibre\ (cm)}$$

Where, strain is a measure of the deformation of the fibre.

$$Young`s\ modulus\ of\ elasticity\ (Gpa) = \frac{Stress\ (Mpa)}{Strain}$$

Where, Young`s modulus of elasticity is a measure of the stiffness of a hollow fibre.

3.4.4 Pressure drop testing of adsorbent hollow fibres

The pressure drop in an adsorbent hollow fibre is very important to consider as a high pressure drop leads to a low adsorption performance. The pressure will vary for different hollow fibre modules depending on the bore diameter and the geometry of the adsorbent hollow fibres. This means that adsorbent hollow fibres with larger bore diameters will have a lower pressure drop than ones with a smaller bore diameter as a result of the lower superficial velocity through larger bores and smaller friction against the inner wall of the bore. Figure 3.8 shows a u-tube manometer used to determine the pressure drop in different structure of adsorbent hollow fibre modules with the same weight and composition over a range of flow rates.

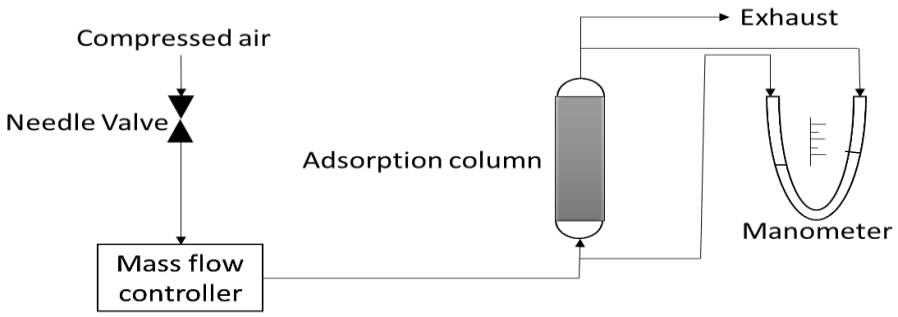

Figure 3.8. A diagram of the U-tube manometer attached with adsorbent hollow fibre bed in order to determine the pressure drop.

The equation below can be used to calculate the pressure drop.

$$\Delta P = h_m \rho_m g$$

where

ΔP = pressure drop (N/m^2)

h_m= height difference between liquid levels on manometer (m)

ρ_m= density of water (kg/m^3)

g = acceleration due to gravity (9.81 m/s^2)

The module was connected to the manometer. An air cylinder provided the test gas through the valve. The flow rates were set by a mass flow rate controller from 0.5 to 5 L/min. When the pressure drop reached equilibrium state, the difference in liquid level h_m was measured at several flow rates. Test air gas was passed to exhaust. The adsorbent hollow fibre module lengths tested were 22 cm long.

3.5 Adsorption performance testing

Adsorbent hollow fibres are used to remove toxic gases from gas steam under dynamic conditions. In this research, dynamic adsorption tests were performed, in which the adsorbent hollow fibre modules were challenged with a flow of 1000 ppm n-butane, which was used as a VOC model gas, in order to obtain the value of adsorption capacity that the adsorbent hollow fibres could provide. A flame ionising detector (FID) was used to measure the VOC concentration leaving the outlet of an adsorption module over time. This gas detector can be used to calculate the breakthrough time and loading by plotting a breakthrough curve.

The FID is designed to monitor hydrocarbon compounds with a low boiling point (< 200°C) such as toluene and n-butane. This detector works during the combustion of the hydrocarbon samples in an ionisation hydrogen flame. This burning process produces a number of positive carbon ions and an electrode above the flame collects these ions. The concentration of the hydrocarbon compounds in the stream can then be measured from the current generated. Generally, the FID can be used to monitor a number of low boiling point VOCs.

To prepare the dynamic gas breakthrough system, the zero grade air cylinder was opened (V1) and set to 2 bar pressure. The instrument was turned on for approximately 2 hours to warm up. Figure 3.9 provides a diagram of the dynamic adsorption test apparatus. The temperature during the experiment was graded between 20°C and 25°C. The nitrogen generator was opened (V2) to remove contaminated materials in the tubes. After 2 hours, the nitrogen and hydrogen (V3 and V4) were opened and set to 3.5 bar and 2 bar respectively. The adsorbent hollow fibre column was placed in the system. To begin the dynamic gas breakthrough studies, the n-butane cylinder was opened (V5) and set to 1.25 bar pressure. N-butane flow rate set at 1 L/min. The concentration of gas at the outlet was measured by a gas detector and recorded using

particular software. The waste gas was removed by the ventilation system. This experiment was tested under 1 bar of pressure. It was completed to reach equilibrium concentration (1000 ppm). Then, both valves (V6 and V7) were opened and started running. During the reading, V8 and V9 were closed. In this experiment, the concentration of test gas was recorded in ppm every 2 minutes. To obtain the breakthrough curve, the outlet concentration was divided by the initial concentration over time and plotted, to obtain the breakthrough curve. When the experiment reached equilibrium, the n-butane flow was stopped and the rig was purged with nitrogen to remove any remaining toxic gas. It is important to weight the adsorbent hollow fibre column before and after the dynamic adsorption experiment and compare the result with the result from the breakthrough curve calculations to ensure consistent results.

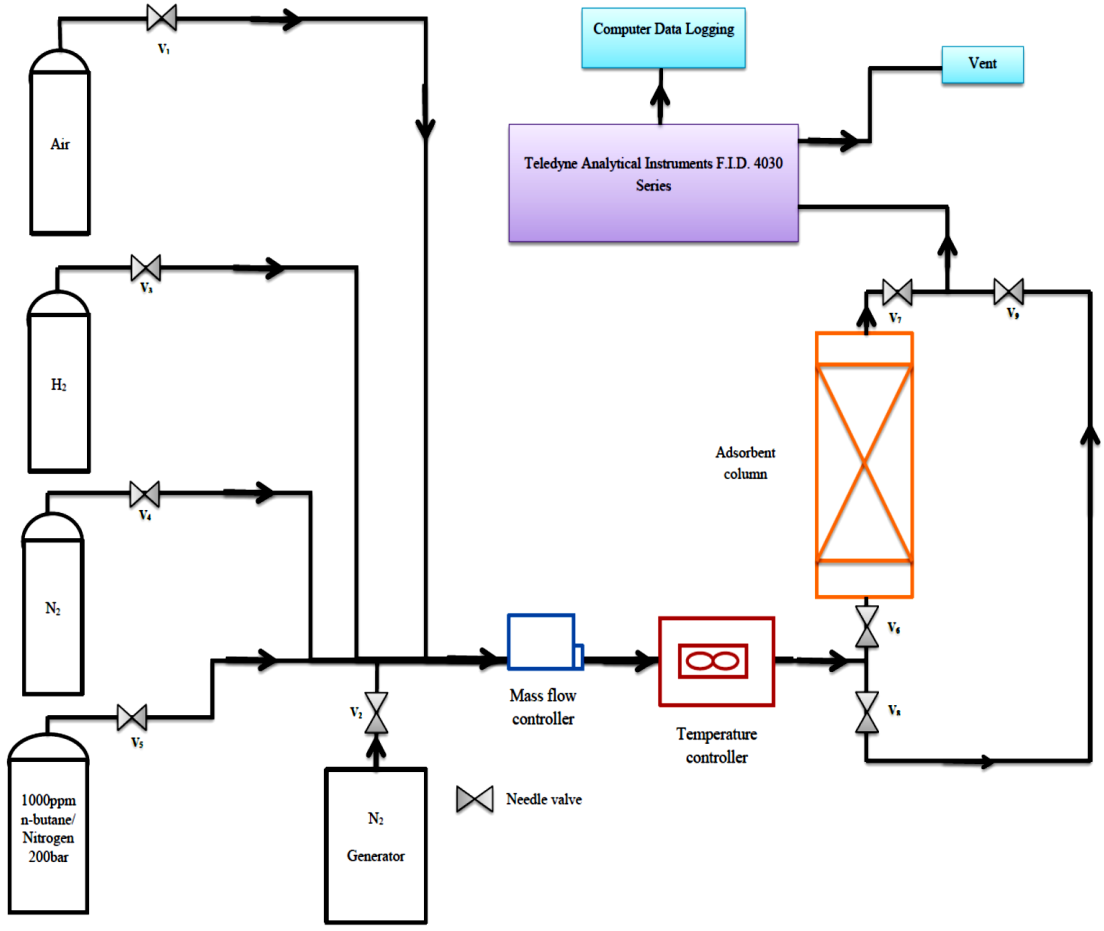

Figure 3.9. Schematic diagram of the dynamic adsorption apparatus.

Chapter 4: Optimisation of Single Adsorbent Hollow Fibre

To maximise the adsorption capacity, surface area, mechanical properties of single channel adsorbent hollow fibres for VOC removal, several methods to produce single bore adsorbent hollow fibre (SAHF) were conducted. This technique utilises wet/wet spinning followed by a phase inversion process. First, a range of pre-treatment temperatures, hollow fibre lengths and flow rates of bore fluid will be investigated, in order to identify the optimum bed length, pre-treatment temperature and flow rate for further study. Second, to improve the porous structure, mechanical properties and adsorption capacity, the effect of primary factors, such as composition of solvent and bore fluid, will be examined. Chapter 3 described the methodology and experimental preparation phases, spinning and testing. In addition, the characterisation methods for adsorbent hollow fibres were also explained in detail in Chapter 3.

4.1 Results and discussion

4.1.1 Effect of hollow fibre length

Double layer 83% 13X fibres were dynamically challenged with 1000 ppm n-butane at 1 L/min; the results are presented in Figure 4.1. Figure 4.1 shows that an increase in breakthrough time as length increased was clearly observed for all adsorbent hollow fibres with the same compositions and experimental conditions. As is apparent from Table 4.1, 12cm and 17cm adsorbent hollow fibres have very similar breakthrough loading, and the 22cm long fibres have higher breakthrough loading (3.1%). The hollow fibre length caused a linear increase in the breakthrough and equilibrium loading as it increased. This increased breakthrough time was even more noticeable taking the weight of hollow fibres into consideration. It was not surprising to have this trend. Unfortunately, as shown in Table 4.1, in all cases, it was difficult to determine the MTZ length which are most likely anomalous results due to the small size of hollow fibres.

Therefore, according to combine resistance to the applied pressure and acceptable pressure drops inside the adsorbent hollow fibre, optimum outer and inner hollow fibre diameters were identified for acceptable module length. Ideally, the longest hollow fibre should be used, providing lowest pressure drop (Schweitzer, 1988). Moreover, in

line with the study of Ren et al., (2005), it is accepted that when aspect ratio L/D (length to diameter) for a granular bed exceeds 30-40, entrance or wall effects might be neglected (Ren *et al.*, 2005). In this study, the aspect ratios of 12, 17, and 22 cm long adsorbent hollow fibre modules with 0.5 cm diameter respectively are 24, 34, and 44. However, this study was for granular bed, it is unreliable how this would apply to adsorbent hollow fibre and may be an interesting topic for further investigation. Therefore, the 22cm hollow fibre was selected as the optimum module length depending on the study of Schweitzer (1988).

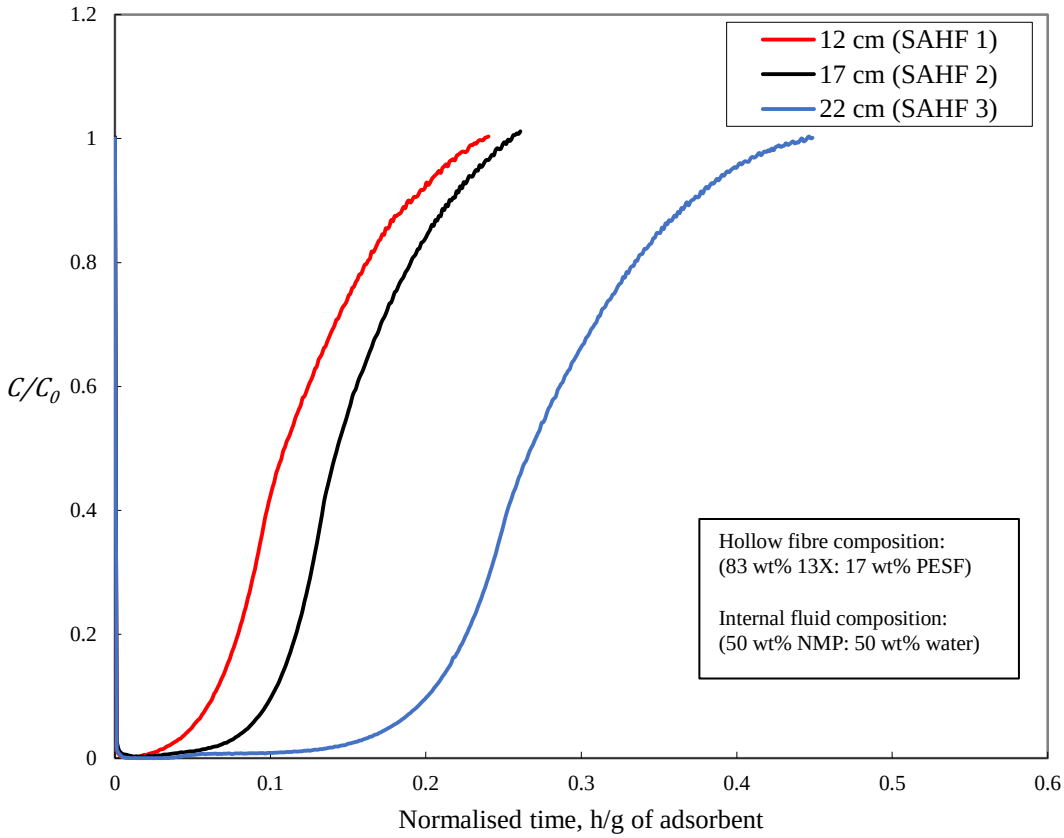

Figure 4.1. Breakthrough curves for 1000 ppm 1 L/min n-butane challenge on double layer 13X/PESF hollow fibres with different module lengths

Table 4.1: Dynamic breakthrough data for double 13X/PESF hollow fibres (83 wt% NMP: 17 wt% PESF) with different module lengths

Hollow fibre	Length (cm)	Weight (g)	t_b (h/g)	Breakthrough loading (%)	t_{eq} (h/g)	Equilibrium loading (%)	MTZ length (cm)
SAHF 1	12	15.7	0.05	2.4	0.24	3.8	24.3
SAHF 2	17	22.7	0.09	2.4	0.26	3.2	9.5
SAHF 3	22	29.8	0.17	3.1	0.45	5.1	21.3

The adsorption breakthrough experimental conditions were with n-butane at a feed flow rate of 1.0 L/ min and a concentration of 1000 ppmv.

4.1.2 Effect of gas flow rate

Three gas flow rates, 1, 2 and 3 L/min, were tested for the same composition (83 wt% 13X: 17 wt% PESF), length (22cm) of 13X/PESF hollow fibres with 1000 ppm n-butane. Figure 4.2 shows the breakthrough curves as n-butane flow rate was increased for the adsorbent hollow fibres, while Table 4.2 shows the values associated with these breakthrough curves.

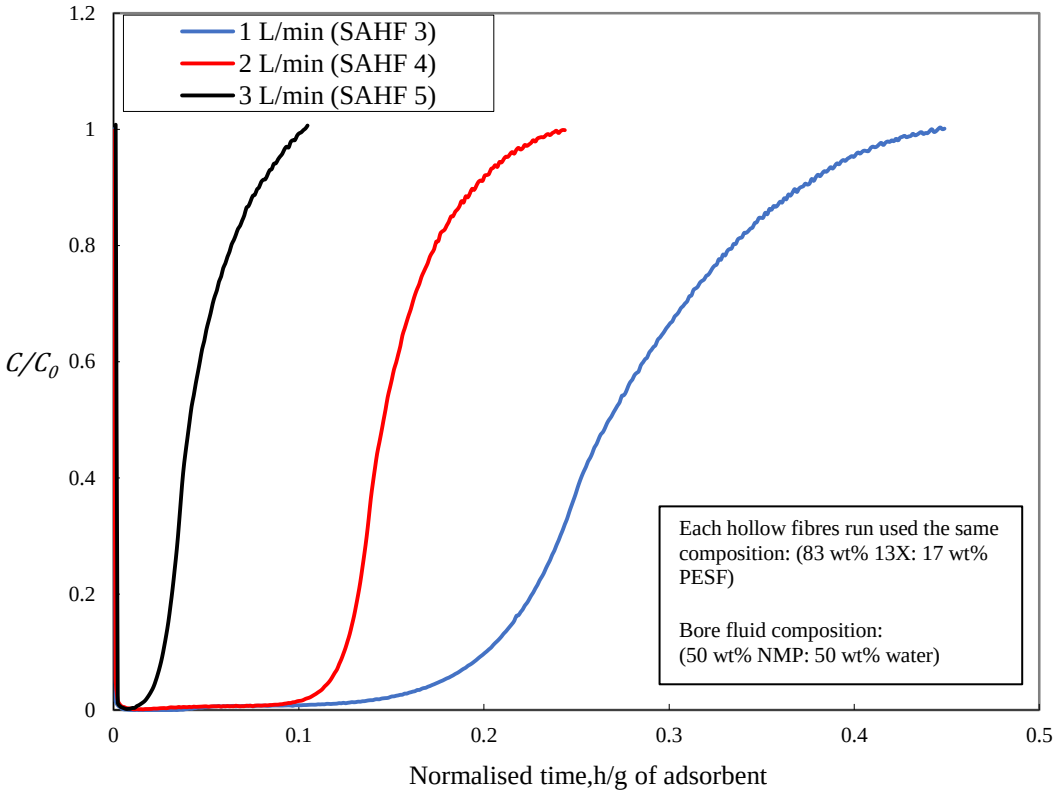

Figure 4.2. Breakthrough curves for 1000 ppm n-butane on 13X/PESF hollow fibre as flow rate was increased

Table 4.2: Dynamic breakthrough data for double 13X/PESF hollow fibres (83 wt% NMP: 17 wt% PESF) tested with different flow rates for 1000 ppm n-butane

Hollow fibre	Flow rate (L/min)	t_b (h/g)	Breakthrough loading (%)	t_{eq} (h/g)	Equilibrium loading (%)
SAHF 3	1	0.17	3.1	0.45	5.1
SAHF 4	2	0.11	1.9	0.24	2.6
SAHF 5	3	0.02	0.4	0.1	0.8

The adsorption breakthrough experimental conditions were with n-butane at a concentration of 1000 ppmv.

Figure 4.2 shows low breakthrough time and equilibrium loading for n-butane adsorption on adsorbent hollow fibre at 3 L/min compared to hollow fibres at 2 and 1 L/min. For 13X/PESF hollow fibres, at 2 and 3 L/min the hollow fibres have a sharper breakthrough curve. However, at 1 L/min the hollow fibres have higher breakthrough time than the hollow fibres at a flow rate of 3 and 2 L/min. As can be seen in Table 4.2, the difference in breakthrough loading becomes greater as gas flow rate increases, meaning a more noticeable drop in equilibrium loading and breakthrough loading was observed as gas flow rate increased for hollow fibres at 1 L/min than hollow fibres at 2 and 3 L/min. The increase in breakthrough loading as flow rate decreased was most likely due to entrance effects, as the modules tested were only 22cm in length. Gas flow rates of 3 and 2 L/min will pass through these hollow fibres quickly, and almost certainly without the chance for flow to fully develop. Therefore, the 1 L/min flow rate was selected as the optimum flow rate for all other experiments.

4.1.3 Effect of bore fluid composition

In this part of the experiment, several bore mixture compositions (NMP: Water) were selected for testing; 22cm 13X/PESF hollow fibres (83 wt% 13X: 17 wt% PESF) were tested with 1 L/min 1000 ppm n-butane. The results are shown in Figure 4.3 and Table 4.3.

4.1.3.1 Adsorption performance testing

As can be seen in Figure 4.3, the hollow fibre with (50 wt% NMP: 50 wt% Water) bore fluid has the highest breakthrough time, at 0.18 hours/g of adsorbent, followed by the hollow fibre with (60 wt% NMP: 40 wt% Water) bore mixture, at 0.12 hours/g of adsorbent. The other hollow fibres with (70, 30 and 40 wt% NMP) bore mixtures have lower breakthrough times. The hollow fibre with 50 wt% NMP: 50 wt% Water bore fluid composition (SAHF 3) also demonstrated greater equilibrium loading than other fibres, as shown in Table 4.3. Results of adsorption performance testing indicated that low or high concentration of NMP in the bore fluid decreased the n-butane adsorption of the adsorbent hollow fibre. Also, Figure 4.3 shows that the SAHF 3 gave significantly sharper breakthrough curves. This result can be explained by their lower diffusion resistance and higher effective surface area from the bore surface to the outer wall of hollow fibre. This allows n-butane molecules easily reaching more adsorption

sites of hollow fibre. One possible reason for this is that these differences in adsorption capacity could be related to the rate of hollow fibre phase inversion process occurred in the bore surface which can decrease the porosity in bore surface, creating limited access to adsorption sites. By repeating the same experiments, the same trend can be observed for the n-butane dynamic challenge, as shown in Figure 4.3. More details will be described and confirmed by scanning electron microscopy in the next section.

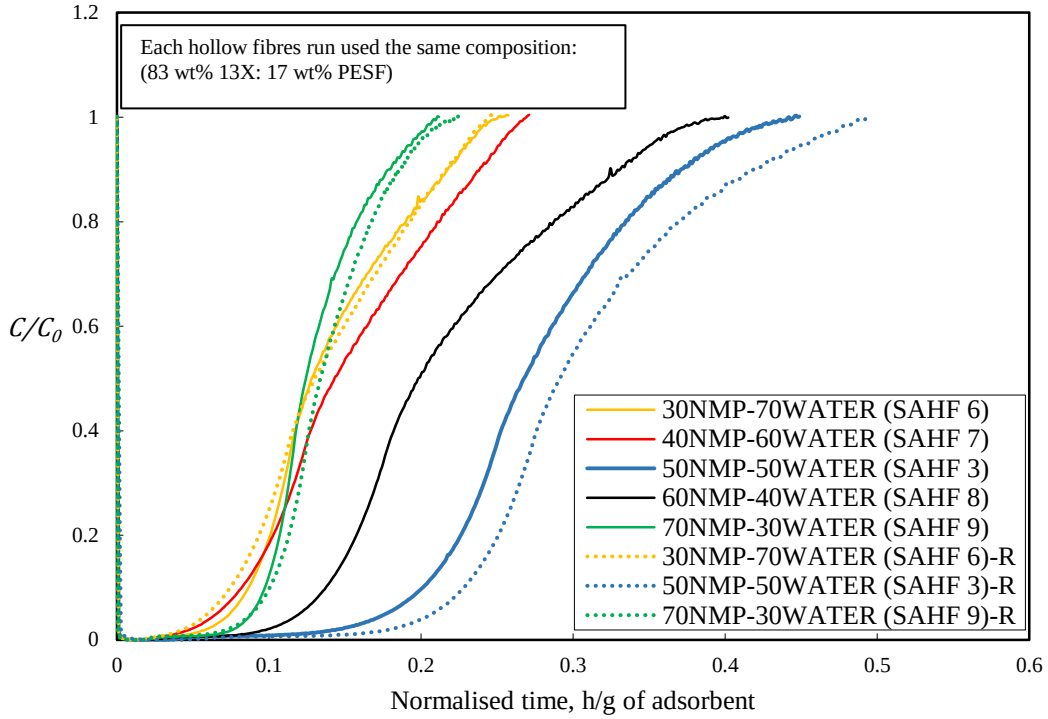

Figure 4.3. Comparing the breakthrough curves of n-butane with 1 L/min flow rate and 1000 ppm concentration for the adsorbent hollow fibres (17% PESF: 83% 13X) prepared from five different bore mixtures (30, 40, 50, 60 and 70% NMP), showing repeated breakthrough curves with dotted lines

Table 4.3: Summary of the adsorption performance of the 13X/polymer hollow fibres (83 wt% 13X: 17 wt% PESF) with different compositions of bore fluid

Hollow fibre	Bore fluid composition	t_b (h/g)	Breakthrough loading (%)	t_{eq} (h/g)	Equilibrium loading (%)
SAHF 6	30 wt% NMP: 70 wt% Water	0.07	1.3	0.25	2.6
SAHF 7	40 wt% NMP: 60 wt% Water	0.06	1.2	0.27	2.7
SAHF 3	50 wt% NMP: 50 wt% Water	0.18	3.2	0.45	5.1
SAHF 8	60 wt% NMP: 40 wt% Water	0.12	2.1	0.4	3.9
SAHF 9	70 wt% NMP: 30 wt% Water	0.09	1.6	0.21	2.3

The adsorption breakthrough experimental conditions were with n-butane at a feed flow rate of 1.0 L/ min and a concentration of 1000 ppmv.

4.1.3.2 Scanning electron microscopy

When the external coagulant (water) is used for the spinning of the adsorbent hollow fibre, a smooth and dense structure with no pores in the outer surface is formed. Therefore, the outer surface of adsorbent hollow fibre is impermeable. However, the formation of a porous surface in the inner surface requires the mixing of water with an appropriate solvent. The effect of different bore fluid compositions on the surface morphology of the 13X/PESF hollow fibre is presented in Figure 4.4. This figure shows the SEM morphology of the hollow fibre with various bore fluid compositions (30, 50 and 70% NMP to water). Figure 4.4(a) shows a weaker bore fluid composition (30 wt% NMP), which can be employed to form the low porous inner surface of hollow fibre. In this case, the phase inversion of the bore skin of the adsorbent hollow fibre begins instantaneously after extrusions from spinneret. This instantaneous phase inversion process in the bore skin seems to allow very short time to provide porous inner skin, and therefore provides limited accessibility for adsorbate to reach the adsorption sites. When water and 50 wt% NMP was used as a bore fluid, the porosity of bore skin of hollow fibre increased, as can be seen in Figure 4.4(b). The results reveal that using the hollow fibre with 50% NMP bore mixture during the spinning process has a significant effect on the inner skin structure, the micro porosity of the adsorbent hollow fibre, and the mass transfer kinetic properties of the fibre. In this composition, a delayed phase inversion in the bore skin of hollow fibre seems to allow enough time to create a porous structure during diffusion processes, and hence provides better accessibility for n-butane molecules to reach the adsorption sites. Figure 4.4 (c) shows that the hollow fibre prepared from 70% NMP bore mixture showed a low breakthrough time, as no phase inversion process occurred during the spinning process, meaning the bore skin remained in the one phase region until it was placed in the water tank. The further addition of NMP delays the phase inversion process and a polymer leans can be covered the adsorption sites, as can be seen in Figure 4.4(c). This concentration of bore fluid reduces the diffusion of water into the inner surface of the adsorbent hollow fibre, and therefore decrease the porosity.

The 50% NMP bore mixture provides the best adsorption capacity, and creates high bore surface porosity compared to the other samples, ensuring that the cylindrical structure was maintained during the spinning process. It can thus be concluded that the

influence of a reasonable bore mixture composition ensures good adsorption performance and high inner surface porosity.

Melted polymer leans and low porosity

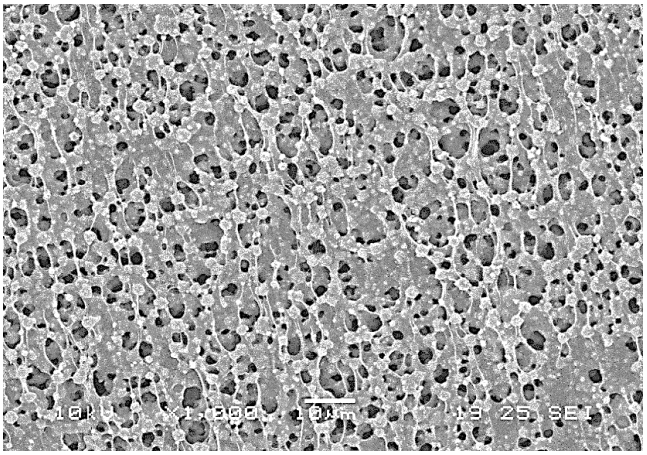

(a) Cross section of bore surface (SAHF 6), x1000

Better porous structure

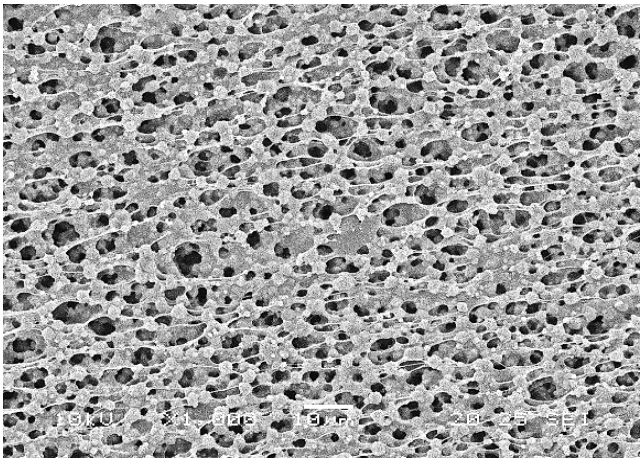

(b) Cross section of bore surface (SAHF 3), x1000

Melted polymer leans and low porosity

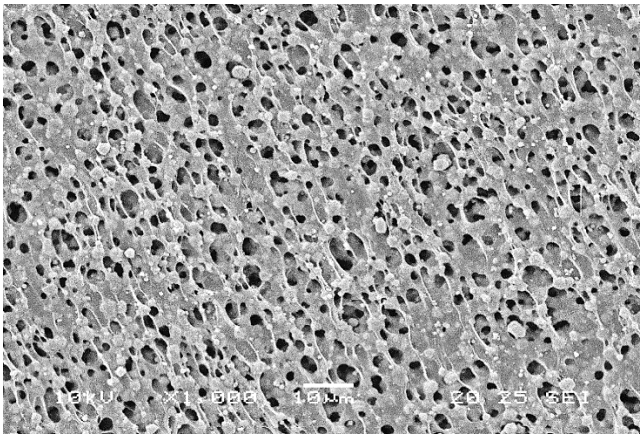

(c) Cross section of bore surface (SAHF 9), x1000

Figure 4.4. Scanning electron micrographs of 13X hollow fibres 17 wt% PESF: 83 wt% 13X with different bore mixture compositions in the range of bore mixtures (a) (30 wt% NMP: 70 wt% Water), (b) (50 wt% NMP: 50 wt% Water) and (c) (70 wt% NMP: 30 wt% Water)

4.1.4 Effect of 13X concentration

Dynamic adsorption experiments testing different 13X zeolite (83, 84 and 85 wt%) compositions of hollow fibre were performed at feed flow rates of 1.0 L/min of 1000 ppm n-butane.

4.1.4.1 Adsorption performance testing

Cartridges of 13X/PESF hollow fibres made with 83, 84 and 85 wt% 13X content was fitted to the experimental column. Figure 4.5 shows the changes in breakthrough curves when n-butane is passed through the different 13X hollow fibre cartridges. Table 4.4 presents the calculated values of all hollow fibres. The breakthrough times of the hollow fibres (83, 84 and 85 wt% 13X) were 0.18, 0.21 and 0.27 hours/g of adsorbent, respectively. These results show that the breakthrough times increased alongside the increase in 13X zeolite. Moreover, Table 4.7 also shows the BET surface area values for these samples. It was found that an increase in 13X loading led to an increase in the surface area of hollow fibres. The open structure of the high 13X composition hollow fibres appeared to provide greater accessibility for the n-butane to reach the 13X sites, thus enabling lower mass transfer resistance and better kinetic performance. The results clearly show that an increase in 13X zeolite has a significant effect on the porosity and adsorption capacity of the fibre. However, the increase in 13X zeolite concentration in hollow fibre could give lower mechanical strength. Also, Figure 4.5 shows that the SAHF 11 provides significantly broader breakthrough curves compared to SAHF 3 and SAHF 10. This result could be described by their lower effective surface and higher diffusion resistance. This prevents adsorbate molecules easily reaching the adsorption sites. By repeating the same experiments, the same trend can be detected for the n-butane dynamic challenge, as shown in Figure 4.5.

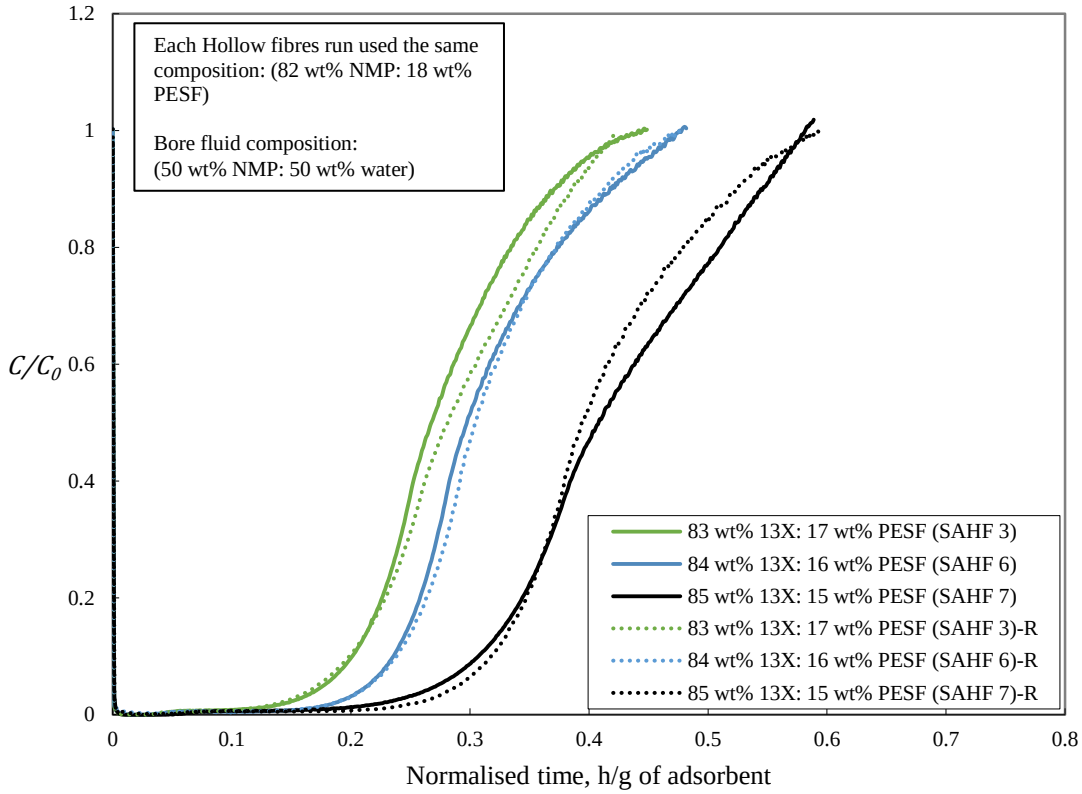

Figure 4.5. Comparison between the adsorption breakthrough curves of single adsorbent hollow fibres with 1 L/min flow rate 1000 ppm concentration of n-butane with different concentration of 13X zeolite in hollow fibre mixture, showing repeated breakthrough curves with dotted lines

Table 4.4: Summary of adsorption performance of the 13X/polymer hollow fibres with different composition of 13X

Sample	SAHF 3	SAHF 10	SAHF 11
13X/PESF/NMP mixture	82 wt% NMP: 18 wt% PESF 83 wt% 13X: 17 wt% PESF	82 wt% NMP: 18 wt% PESF 84 wt% 13X: 16 wt% PESF	82 wt% NMP: 18 wt% PESF 85 wt% 13X: 15 wt% PESF
Viscosity (Pa.s)	11.4	12.7	13.8
t_b (h/g)	0.18	0.21	0.27
Breakthrough loading (%)	3.2	3.6	4.5
t_{eq} (h/g)	0.45	0.5	0.6
Equilibrium loading (%)	5.1	5.3	6.9
BET surface area (m^2/g)	447.1	464.3	474.5

The adsorption breakthrough experimental conditions were with n-butane at a feed flow rate of 1.0 L/ min and a concentration of 1000 ppmv.

4.1.4.2 Scanning electron microscopy

Figures 4.6 shows the SEMs of cross sections of 13X/PESF hollow fibres prepared from 83 wt%, 84 wt% and 85 wt% 13X zeolite using the similar experimental conditions. From Figure 4.6(b), when the 13X zeolite loading is increased to 84 wt%, the cross-section morphology shows a denser distribution of 13X zeolite particles compared with Figure 4.6(a) (13X/PESF, 83/17 wt%). The cross-sectional structure of sample SAHF 10 seems to change from a long and sponge-like structure with voids like spheres (SAHF 3) to a short and denser finger-like structure. The 85 wt% 13X loading in the PESF/NMP mixture leads to more dense structure, as shown in Figure 4.6(c). By increasing the 13X zeolite content in the PESF/NMP mixture, the concentration of polymer decreases. Therefore, the mechanical strength of the adsorbent hollow fibre becomes weaker as the connection between the polymer chains is lost. The higher adsorbent loading results in a higher 13X zeolite packing and distribution, but this also reduces the mechanical strength of the fibres. This will be confirmed by mechanical properties testing in the next section.

Therefore, it is important to optimise that composition of PESF/13X mixture to have both good mechanical strength and good adsorbent loading.

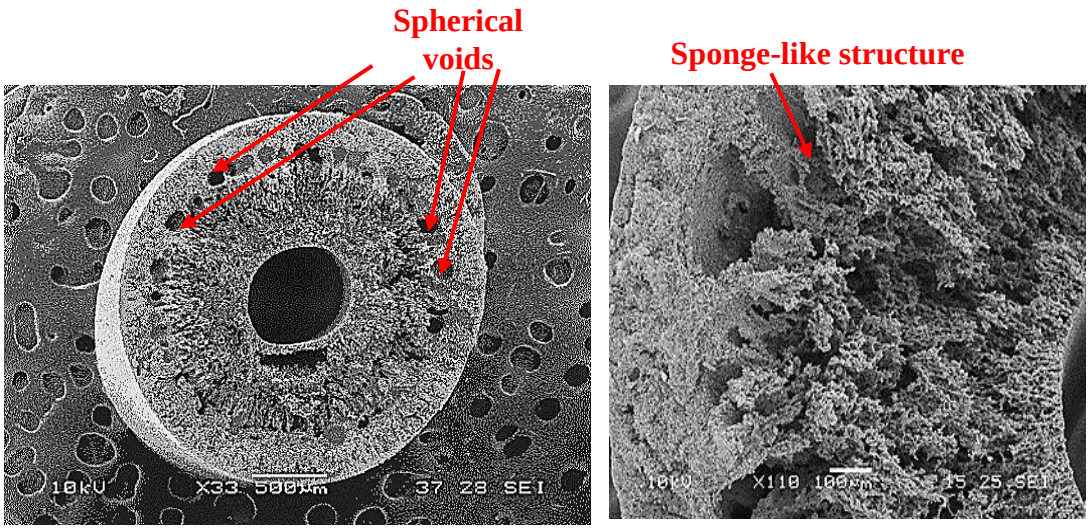

(a) SAHF 3 (83 wt% 13X: 17 wt% PESF), x33 and x110

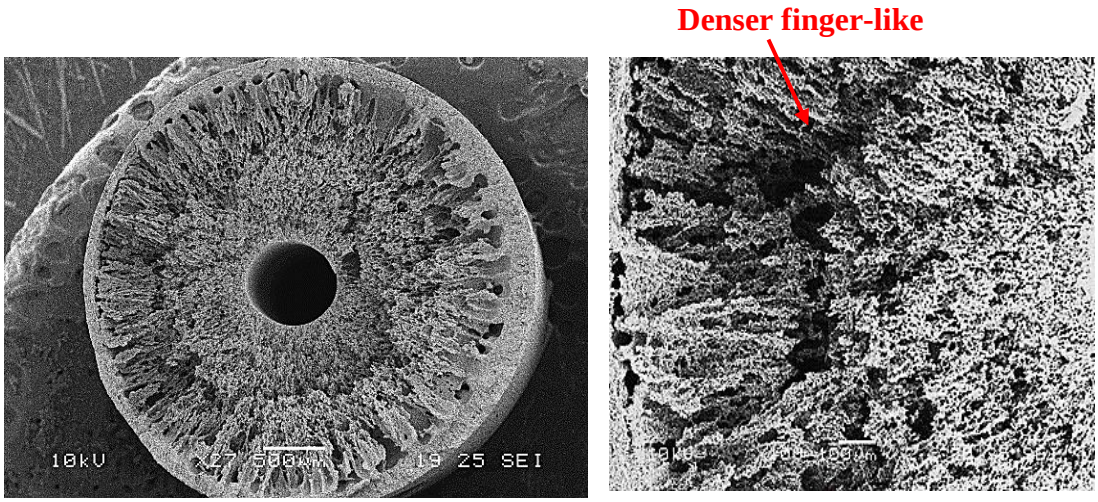

(b) SAHF 10 (84 wt% 13X: 16 wt% PESF), x27 and x100

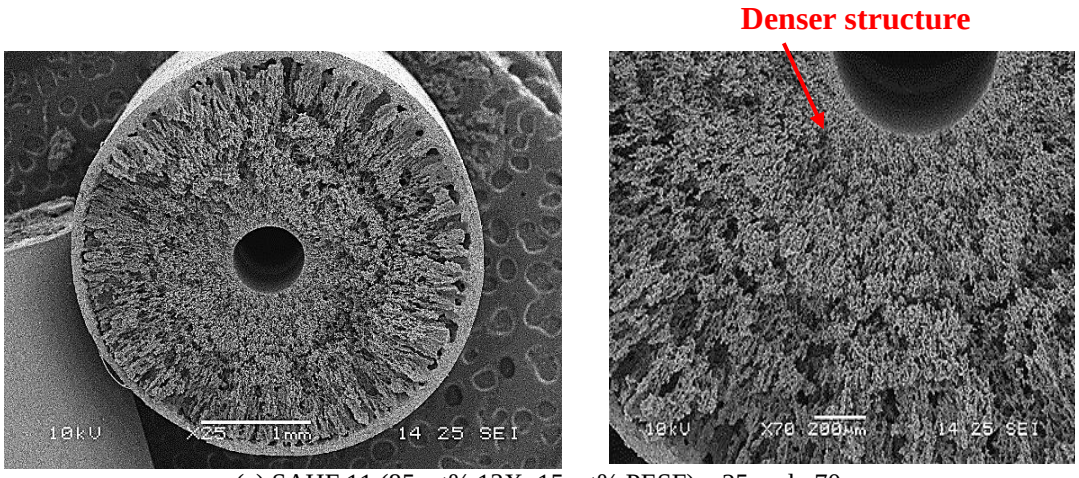

(c) SAHF 11 (85 wt% 13X: 15 wt% PESF), x25 and x70

Figure 4.6. Scanning electron micrographs of 13X hollow fibres (18 wt% PESF: 82 wt% NMP) at different 13X zeolite compositions.

4.1.4.3 Mechanical properties testing

To correlate the effects of 13X zeolite concentrations and the mechanical properties of adsorbent hollow fibres, Figure 4.7 and Table 4.5 show the data obtained from a tensile test on a specimen of gauge length 90 mm. It was found that the decrease of polymer loading with increase of 13X zeolite concentration leads to decrease in the ultimate tensile strength (stress). Moreover, there seems to be a direct relationship between the 13X concentration and the Young's modulus of the adsorbent hollow fibres. It was found that SAHF 3 has a lower Young`s modulus compared to SAHF 10 and SAHF 11. This means SAHF 3 with finger-like structure and lower 13X zeolite concentration is more flexible compared to other samples due to increase in the composition of polymer.

Therefore, in order to spin hollow fibres with high adsorption capacity and mechanical properties, the suitable amount of 13X should be detected without affecting the mechanical properties of hollow fibres.

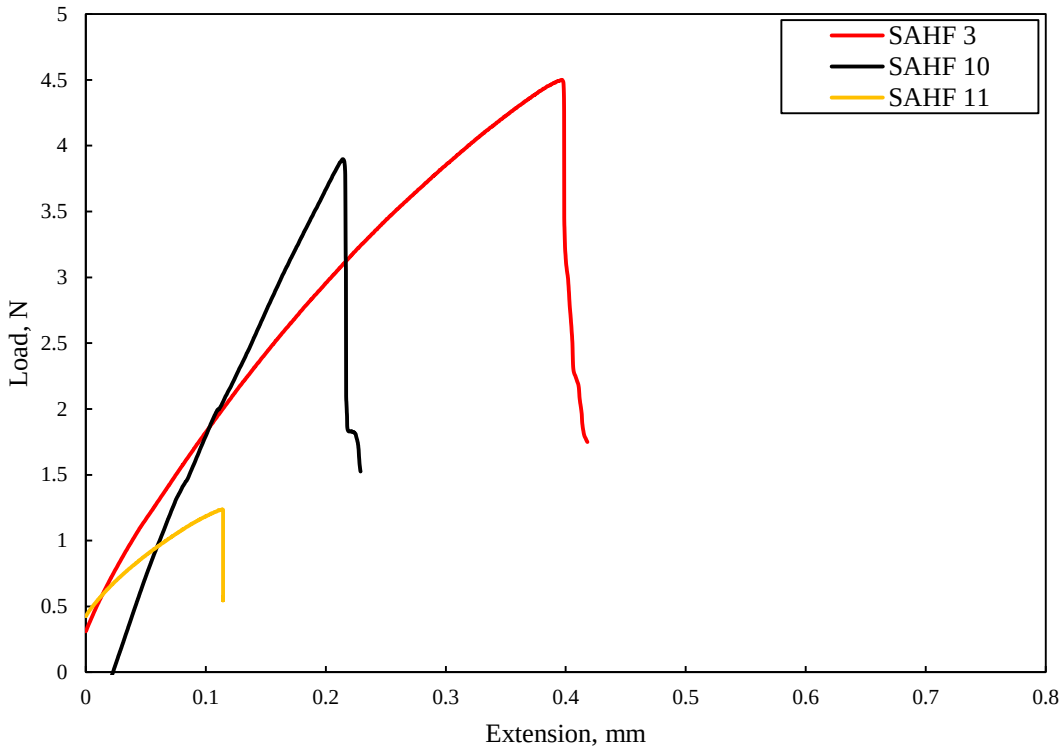

Figure 4.7. Tensile stress and elongation at the break of adsorbent hollow fibre with different 13X compositions.

Table 4.5: Stress, Strain and Young`s modulus of adsorbent hollow fibres with different concentration of 13X zeolite

Hollow fibre	Cross sectional area (cm^2)	Maximum load (N)	Stress (MPa)	Strain	Young`s modulus of elasticity (GPa)
83 wt% 13X: 17 wt% PESF (SAHF 3)	0.062	4.48	0.72	0.004	180
84 wt% 13X: 16 wt% PESF (SAHF 10)	0.063	3.85	0.61	0.002	305
85 wt% 13X: 18 wt% PESF (SAHF 11)	0.064	1.23	0.19	0.001	190

4.1.5 Effect of adding pore former

In this study, all experiments were run at a 1 L/min feed flow rate, with concentration of polymer and adsorbent in hollow fibre bundle (83 wt% 13X: 17 wt% PESF).

4.1.5.1 Adsorption performance testing

Pore former was spun into adsorbent hollow fibres, using a mixture mixture prepared by the method described in Section 3.3, with 1g weight pore former included in the (82 wt% NMP: 18 wt% PESF) and (83 wt% 13X: 17 wt% PESF) mixture. The pore former used was Licowax C micro powder PM. Following spinning, adsorbent hollow fibre with pore former (SAHF 12) was successfully spun. SAHF 12 was bundled into 22 cm test modules and heated to 200°C to remove the pore former from structure of hollow fibre.

Dynamic 1000 ppm n-butane tests were carried out, which were compared to a PESF/13X hollow fibre 83 wt% 13X: 17 wt% PESF without and with the pore former, as shown in Figure 4.8; the calculated results are given in Table 4.6. Figure 4.8 shows that the breakthrough curves of both samples are sharp. Also, it was found that 1g of Licowax C micro powder PM pore former (SAHF 12) fibre significantly improved breakthrough and equilibrium loading, as well as increasing breakthrough time from just over 20% for the 1g of pore former. SAHF 12 clearly have a higher adsorption performance than that of SAHF 3 fibre which provides a better adsorption curve. This was likely due to the increased porosity and surface area and improved adsorption kinetics. The nitrogen isotherm study shows that the BET surface area of SAHF 12 (with pore former) is greater than it in the SAHF 3 (without pore former). By repeating the same experiments, the same trend can be detected for the n-butane dynamic challenge, as shown in Figure 4.8.

Possible structural causes for the improvement in adsorption performance will be investigated by SEM in the next section.

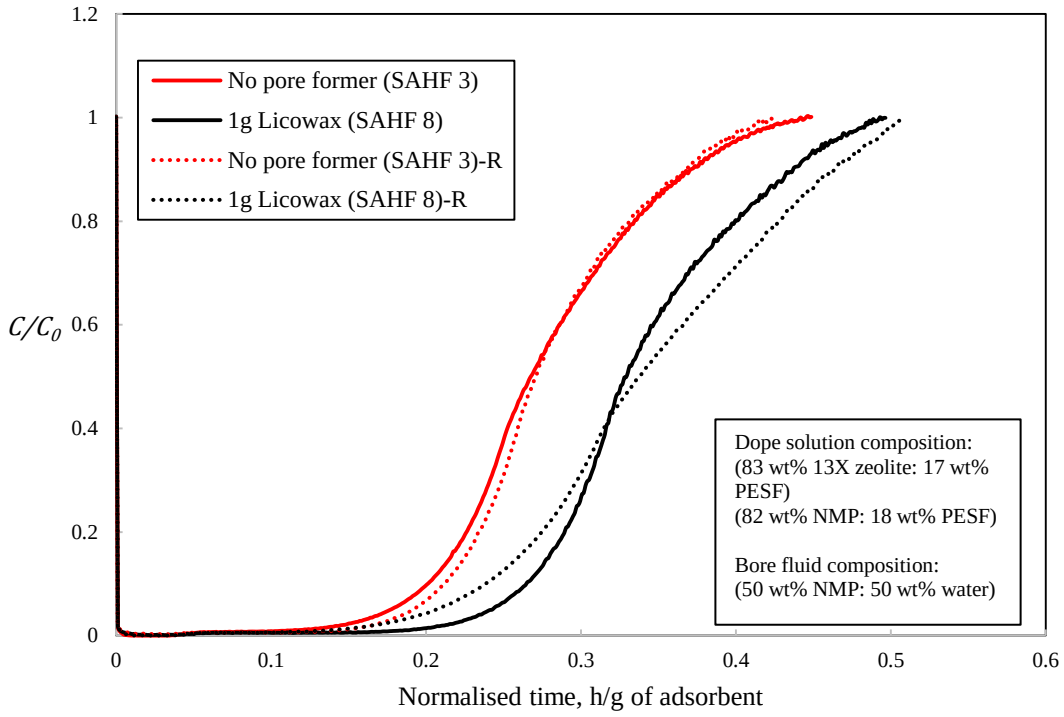

Figure 4.8. Comparison between the adsorption breakthrough curves of single adsorbent hollow fibres with 1 L/min flow rate 1000 ppm concentration of n-butane with 1g of Licowax C micro powder PM and without pore former, showing repeated breakthrough curves with dotted lines

Table 4.6: Summary of adsorption performance of the 13X/polymer hollow fibres with adding pore former

Sample	SAHF 3	SAHF 12
13X/PESF/NMP mixture composition	82 wt% NMP: 18 wt% PESF 83 wt% 13X: 17 wt% PESF	
Licowax C micro powder PM pore former (g)	0	1
t_b (h/g)	0.18	0.24
Breakthrough loading (%)	3.2	4.3
t_{eq} (h/g)	0.45	0.5
Equilibrium loading (%)	5.1	6.2
BET surface area (m^2/g)	447.1	476

The adsorption breakthrough experimental conditions were with n-butane at a feed flow rate of 1.0 L/ min and a concentration 1000 ppmv.

4.1.5.2 Scanning electron microscopy

Some possible structural reasons for the enhancement in adsorption capacity were explored using SEM. The results are shown in Figure 4.9. The 1g Licowax hollow

fibre (Figure 4.9(b)) appeared to have a more porous inner surface compared to the no Licowax C (Figure 4.9(a)) hollow fibre. It is possible that enhanced adsorption performance was observed with the 1g Licowax C due to the uniform distribution of the pore former around the inner bore enhancing the porosity of hollow fibre and providing better accessibility for the n-butane molecules to reach the adsorption sites and hence provide better adsorption and kinetic performance.

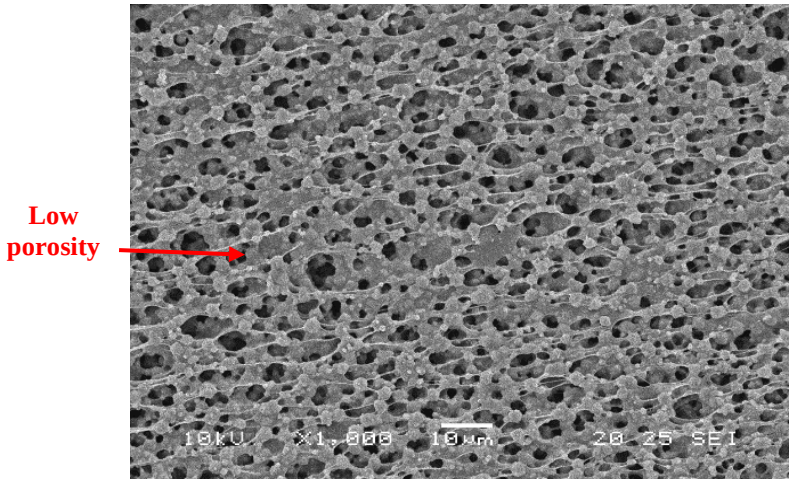

(a) Bore surface of hollow fibre with no pore former, 1000x

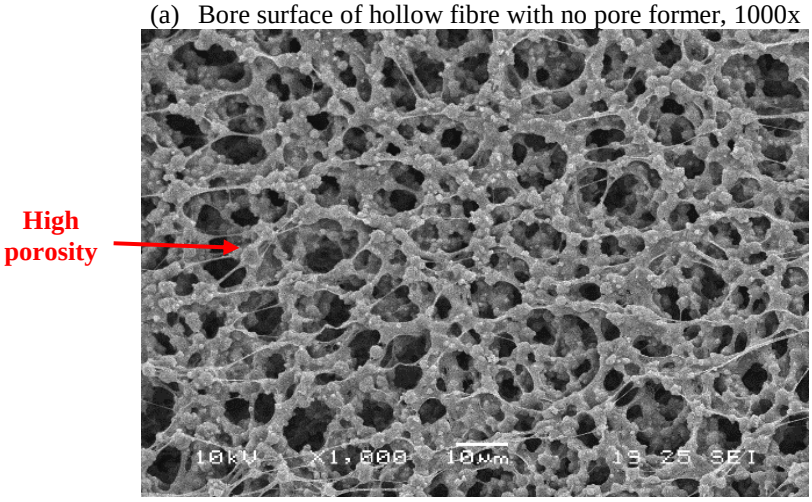

(b) Bore surface of hollow fibre with 1g pore former, 1000x

Figure 4.9. Scanning electron micrographs of 13X hollow fibres (18 wt% PESF: 82 wt% NMP) and (83 wt% 13X: 17 wt% PESF) at different pore former amounts in the range of (a) SAHF 3 (0g) and (b) SAHF 12 (1g Licowax)

4.1.5.3 Mechanical properties testing

The tensile properties of adsorbent hollow fibres with pore former is compared with those of hollow fibres without pore former in Figure 4.10 and Table 4.7. As can be seen the hollow fibres with pore former (SAHF 12) tend to have lower ultimate tensile strength (Stress) but higher Young`s modulus. The reason for the differences in stress

is the increased porosity in hollow fibre with pore former. Therefore, the decreased mechanical strength of the adsorbent hollow fibres is in line with the increase of porosity.

It was concluded that the addition of 1g of pore former led to increased adsorption performance with little effect on the mechanical strength of the adsorbent hollow fibre.

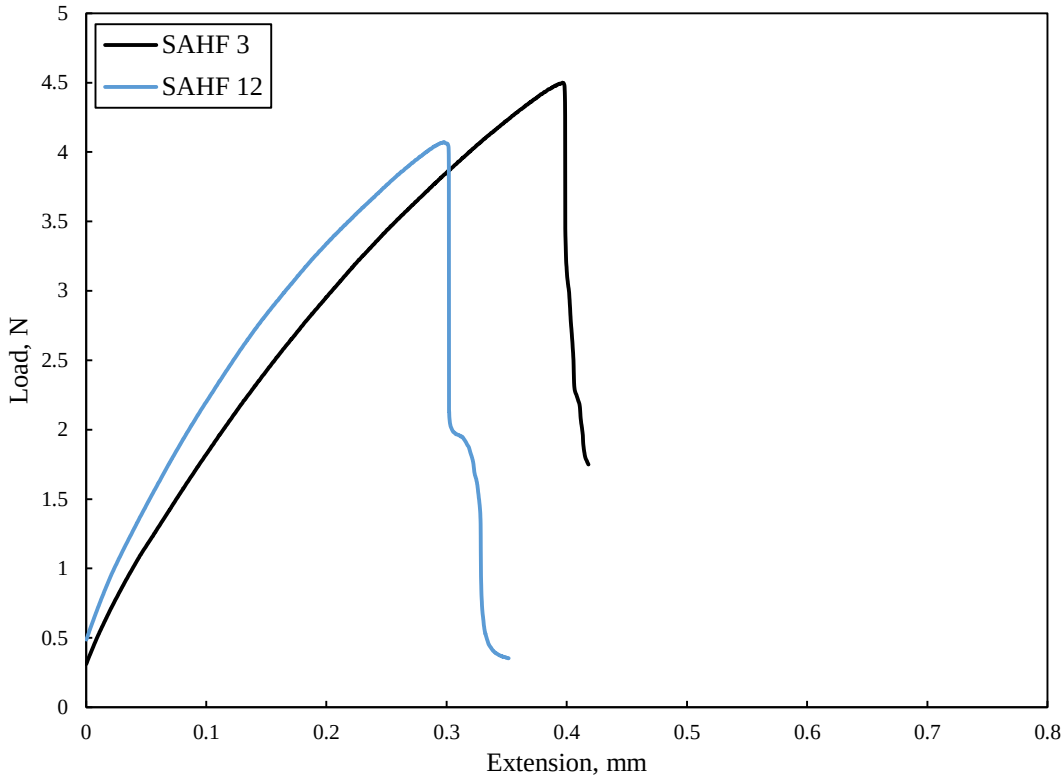

Figure 4.10. Tensile stress and elongation at the break of adsorbent hollow fibre with different pore former adding.

Table 4.7: Stress, Strain and Young`s modulus of adsorbent hollow fibres with 1g pore former and without pore former

Hollow fibre	Cross sectional area (cm^2)	Maximum load (N)	Stress (MPa)	Strain	Young`s modulus of elasticity (GPa)
SAHF 3	0.062	4.48	0.72	0.004	180
SAHF 12	0.061	4.1	0.67	0.003	223.3

4.1.6 Pre-Treatment temperature

To test the effect of pre-treatment of the 13X/PESF hollow fibres on adsorption performance, the hollow fibres were subjected to a range of pre-treatment conditions. Figure 4.11 presents the experimental breakthrough curves obtained using 13X/PESF hollow fibre (83 wt% 13X: 17 wt% PESF) after pre-treating at 150, 180, 200 and 250°C for 24 hours.

4.1.6.1 Adsorption performance testing

Figure 4.11 and Table 4.8 show the adsorption breakthrough curves of sample SAHF 13, SAHF 14, SAHF 12 and SAHF 15 prepared with four pre-treatment temperatures. The equilibrium loading for 150, 180, 200 and 250°C are approximately 3.1, 4.6, 6.2 and 3.1%, respectively. The breakthrough times of 13X/PESF hollow fibre treated at 150, 180, 200 and 250°C, were 0.08, 0.18, 0.24 and 0.08 hours/g of adsorbent, respectively. It is found that the breakthrough time and equilibrium loading increase with increasing pre-treatment temperatures, as the porosity of hollow fibre surfaces and adsorption sites of 13X zeolites are improved. Adsorbent hollow fibre with 200°C pre-treatment shows far sharpest breakthrough curves and longest times to breakthrough for n-butane which are indicative of a lowest resistance to adsorption. Also, Figure 4.11 shows that the breakthrough curve for hollow fibre with 180°C pre-treatment is broader than those for the 200°C pre-treatment hollow fibre. This fibre with 180°C pre-treatment have a poorer adsorption performance than that of fibre with 200°C pre-treatment which give a better adsorption curves. However, with 250°C heat treatment, a reduction in adsorption capacity was seen. This confirms that as the pre-treatment temperature exceeded the PESF T_g (220°C), the 13X zeolite adsorption sites were blocked and covered by the degrading PESF. This can be confirmed by scanning electron microscopy in the next section.

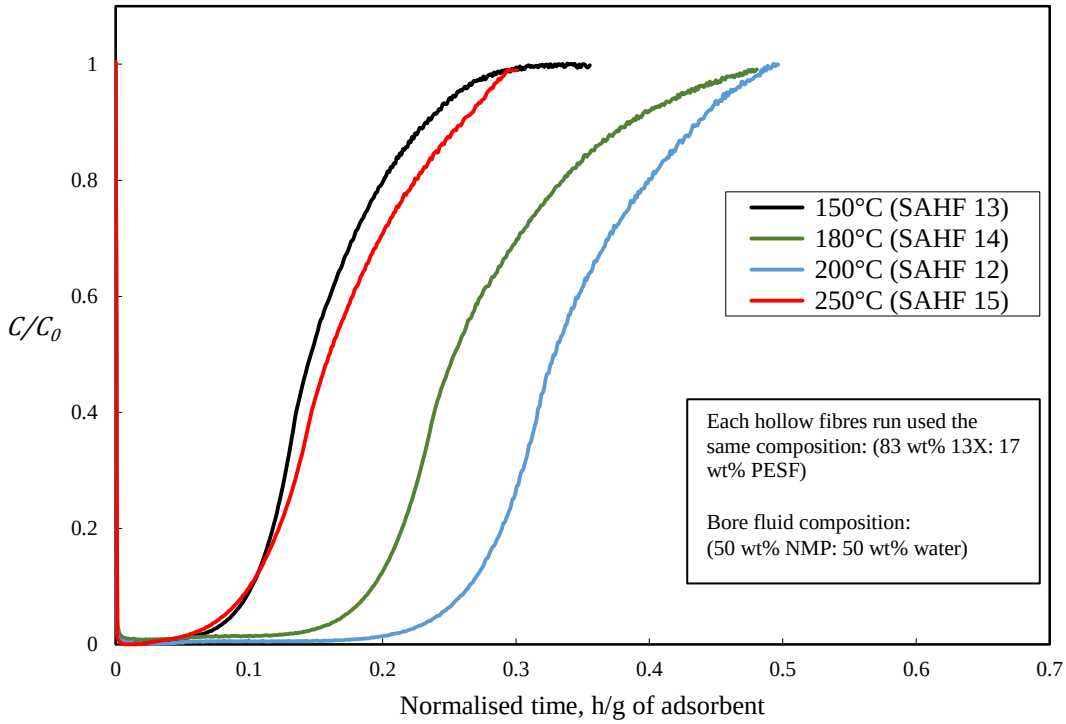

Figure 4.11. Breakthrough curves for 1000 ppm n-butane on 13X/PESF hollow fibre as pre-treatment temperature was changed.

Table 4.8: Dynamic breakthrough data for double 13X/PESF hollow fibres (83 wt% NMP: 17 wt% PESF) tested with different pre-treatment temperature.

Hollow fibre	Pre-treatment temperature (°C)	t_b (h/g)	Breakthrough loading (%)	t_{eq} (h/g)	Equilibrium loading (%)
SAHF 13	150	0.08	1.4	0.3	3.1
SAHF 14	180	0.18	2.8	0.5	4.6
SAHF 12	200	0.24	4.3	0.5	6.2
SAHF 15	250	0.08	1.4	0.3	3.1

The adsorption breakthrough experimental conditions were with n-butane at a feed flow rate of 1.0 L/ min and a concentration of 1000 ppmv

4.1.6.2 Scanning electron microscopy

The influence of pre-treatment temperature on 13X hollow fibre structure was also investigated using scanning electron microscopy (SEM). Figure 4.12 shows the SEM morphology of the hollow fibre bore surface at 150, 180, 200 and 250°C. The bore surface structure of hollow fibre at 150°C pre-treatment temperature has a continuous long polymer leans and bridges surrounding the 13X particles, as shown in Figure 4.12(a). The 13X zeolite particles seem to be covered by PESF. In Figure 4.12(b), the

SEM of bore surface of hollow fibre with 180°C pre-treatment temperature has high surface porosity and short polymer lean. Figure 4.12(c) with 200°C pre-treatment temperature shows that the PESF created nodular chains and has shrunk as result of higher surface porosity. Therefore, the PESF leans in the previous SEM micrographs become shorter and fewer by increasing the pre-treatment temperature. Also, it is found that the 13X zeolite particles are uniformly distributed and more uncovered on the surface of hollow fibre after pre-treatment at temperatures between 150 and 200°C. Nevertheless, In Figure 4.12(d), the bore surface of hollow fibre with 250°C pre-treatment shows that the PESF has covered the 13X zeolite particles and slightly degraded resulting in the pre-treatment temperature exceeded its Tg (220°C).

Therefore, the results of this study indicate that the combined effects of a suitable polymer and reasonable pre-treatment temperature can provide good adsorption capacity and create high surface porosity for 13X zeolite hollow fibres.

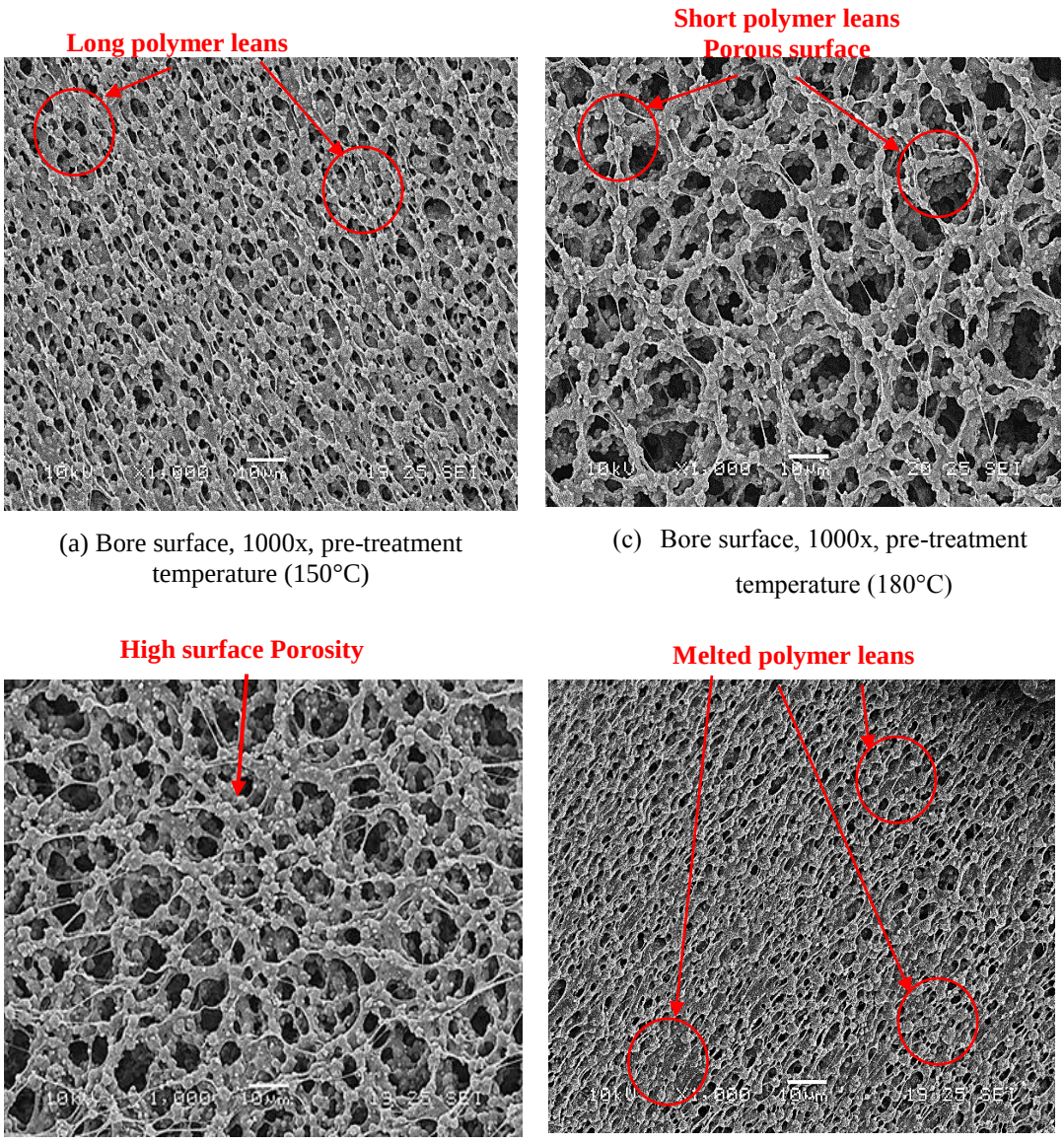

(a) Bore surface, 1000x, pre-treatment temperature (150°C)

(c) Bore surface, 1000x, pre-treatment temperature (180°C)

(c) Bore surface, 1000x, pre-treatment temperature (200°C)

(d) Bore surface, 1000x, pre-treatment temperature (250°C)

Figure 4.12. Scanning electron micrographs of the bore surface of 13X hollow fibres 17 wt% PESF: 83 wt% 13X at the range of pre-treatment temperatures.

4.2 Nitrogen isotherms of single adsorbent hollow fibres

To confirm the observations from the n-butane breakthrough challenge, nitrogen adsorption isotherms at 77 K were determined for different single adsorbent hollow fibres. Nitrogen uptake was compared on SAHF 3 (83 wt% 13X), SAHF 10 (84 wt% 13X), SAHF 11 (85 wt% 13X) and SAHF 12 (83 wt% 13X and 1g Licowax), all of which having been spun into a 50/50 water/NMP bore mixture. It can be seen in Figure 4.13 that there was a significant increase in uptake, from 10.7 w/w% on the SAHF 11 fibres to 14.9 w/w% on the SAHF 12. This increase in uptake was predictable, given

the great surface area of hollow fibre with 1g Licowax, meaning the binder could have contributed to adsorption and improved adsorption kinetics. In addition, the increase in 13X composition in hollow fibres leads to increase in nitrogen uptake. These results confirm the results of dynamic n-butane breakthrough challenge. Table 4.9 presents the results of BET surface area, Langmuir maximum adsorption capacity and pore size distribution for these adsorbent hollow fibres.

Therefore, it can be concluded that a single adsorbent hollow fibre (83 wt% 13X: 17 wt% PESF) with 1g pore former was successfully prepared with higher nitrogen uptake, higher equilibrium loading in n-butane breakthrough challenge, good mechanical properties and good BET surface area compared to the other single adsorbent hollow fibres.

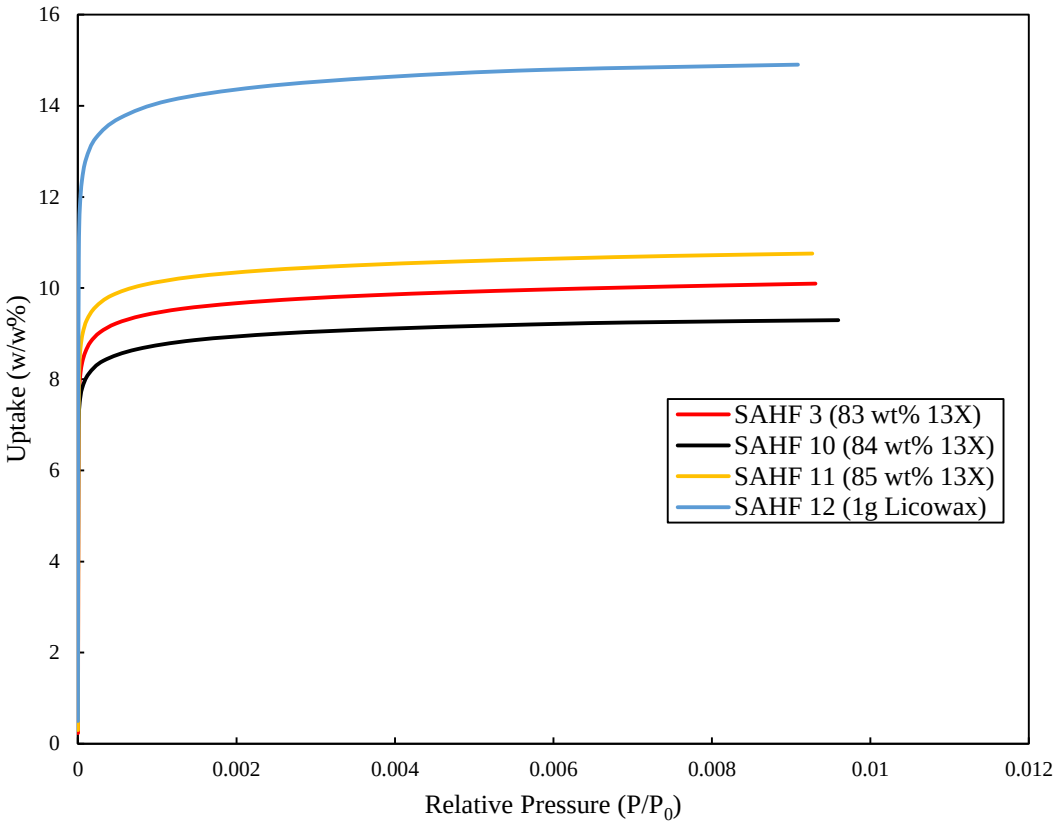

Figure 4.13. Nitrogen uptake on 83% 13X, 84% 13X, 85% 13X and 1g Licowax single adsorbent hollow fibres.

Table 4.9: The surface area and structural properties of several samples of single 13X/PESF hollow fibres from the N_2 adsorption isotherm

	SAHF 3	SAHF 10	SAHF 11	SAHF 12
BET surface area m^2/g	447.5	473.1	517.2	475.6
Langmuir surface area m^2/g	452.4	477.1	521.6	479.7
Total pore volume cm^3/g	0.16	0.17	0.18	0.17
Langmuir maximum adsorption capacity (cm^3/g)	104.6	110.2	120.5	110.2

4.3 Summary

In this study, single bore adsorbent hollow fibres were successfully prepared through wet/wet spinning a PESF mixture containing suspended 13X zeolite powders in a hollow fibre mixture. In this stage of the experiment, n-butane adsorption was tested with a range of 13X/PESF/NMP mixture compositions, bore fluid compositions, bundle lengths, flow rates and pre-treatment temperatures, to identify the optimum levels to use in the testing and preparation of single bore adsorbent hollow fibres and achieve the best adsorption performance. It was found that the parameters affecting the adsorbent hollow fibre structure are the ratio of the adsorbent to the polymer, the addition of pore former, and the pre-treatment temperature. However, it should be noted that the viscosity of adsorbent/polymer/NMP mixture must be between 9-14 Pa.s. The mixtures where the viscosity was higher or lower than this range were difficult to spin. This has been confirmed by Tai and appendix III.

The conclusions of this chapter will be summarised below:

The bundle length of the adsorbent hollow fibre and flow rate of n-butane during dynamic adsorption tests both affected the adsorption performance. The bundle length testing showed that the increased breakthrough time and equilibrium loading achieved with a 22cm bundle length was even more noticeable when considering the weight of hollow fibres. In line with the study of Schweitzer, (1988), it is accepted that the longer adsorbent hollow fibre has lower pressure drop. However, this study could be unreliable and may be an interesting topic for further investigation.

It was found that the 85 wt% 13X: 15 wt% PESF ratio of adsorbent hollow fibre has the highest breakthrough time and equilibrium loading. This was most likely due to the greater surface area and adsorbent loading, which attracts n-butane molecules to adsorption sites more effectively, as well as providing better kinetic performance. This result was confirmed by nitrogen isotherm in Section 4.4. However, one problem with a high ratio of 13X is that the rapid increase in the loading of zeolites leads to single hollow fibres with lower mechanical strength. Similar result was found by Tai (2009), who prepared a hollow fibre decrease in mechanical properties as adsorbent concentration was increased. This is in line with the study of Baker (2012), as low polymer concentration may provide weak hollow fibre due to high adsorbent concentration.

The bore wall and porosity of the adsorbent hollow fibres was also controlled by varying the bore fluid compositions. It was found that the hollow fibre prepared with 30 wt% NMP: 70 wt% water bore fluid demonstrated instantaneous phase inversion. This is because there was no time to create the porous structure, and the bore wall transferred to the two-phase region immediately after immersion. While a high ratio of NMP led to a low breakthrough time, due to no phase inversion process occurring during the spinning process and the bore wall remaining in the one phase region until it was placed in the water tank, in bore fluid with 50 wt% NMP, delayed phase inversion in the bore wall appeared to allow plenty time to create a porous structure during the diffusion process. These results were similar with results from a work by (Xu and Qusay, 2004), who found that by using bore fluid with 50 wt% solvent or close to this concentration it could create sponge-like structure due to delay in the phase inversion process.

This work assessed the use of pore formers to improve adsorption of n-butane on adsorbent hollow fibres. Licowax C has been used in previous work on adsorbent hollow fibre structures for Removal of toxic industrial chemicals (Jeffs, 2015). In this application, a several pore formers can be used due to their low melting temperatures. It was suitable because of formation of pores throughout the adsorbent hollow fibre structure. Licowax pore former was successfully added to the 13X/PESF/NMP mixture, which enhanced the overall loading of n-butane on adsorbent hollow fibres, due to increased porosity and surface area. This result was confirmed by nitrogen isotherm which enhance the speed of hollow fibre uptake in Section 4.4. However, the

use of pore former in the preparation of hollow fibre can slightly affect the mechanical strength, due to increased porosity. From these results, an appropriate heat treatment temperature can be identified for capturing n-butane from air.

The effect of pre-treatment temperature on adsorbent hollow fibres shows that suitable heat treatment can allow 13X particles to be released from the PESF structure, and enhance the accessibility of adsorbate molecules to adsorption sites. However, it is important to keep the regeneration temperature below the glass temperature (Tg) of PESF (220°C), to avoid polymer melting when the temperature reaches Tg. Moreover, the pre-treatment temperature can also affect the breakthrough time and equilibrium loading, which increase alongside temperature. Tai *et al.*, (2013), found similar results that 200°C pre-treatment temperature was improved adsorption performance of HiSiv 3000/PESF hollow fibre by increasing the porosity of hollow fibres.

It is possible to conclude that the combined effects of appropriate adsorbent/PESF/NMP mixture composition, reasonable heat treatment, and bore fluid composition can enable the preparation of adsorbent hollow fibres of superior quality. However, there are some limitations to this tubular structure of adsorbent hollow fibre. Module of SAHF 12 was chosen for further study since its good adsorption capacity, good mechanical strength is comparable with those of other single adsorbent hollow fibres. The problem with such fibres is that the improvement in adsorption capacity can cause a decrease in mechanical strength. Nonetheless, it is possible to further improve the efficiency of adsorption performance with good mechanical properties at low cost. In pursuit of this goal, the present study seeks to develop novel multi-channel adsorbent hollow fibres for pollution control applications, which will be described further in the next chapter.

Chapter 5: Development of Multi-channel Adsorbent Hollow Fibre

The previous chapter described how single adsorbent hollow fibres were optimised to have a good adsorption %wt loading for VOC removal. In general, these hollow fibres have reasonable breakthrough times due to their good surface area, but have poor mechanical properties. The highest uptake of n-butane, 6.2%wt equilibrium loading and 0.24 hours/g of asorbent' breakthrough time, were seen in single adsorbent hollow fibres impregnated with Licowax C micropowder PM. Modifications with the potential to improve the adsorption capability and mechanical properties of adsorbent hollow fibre were considered. Therefore, an optimised recipe of adsorbent/polymer/NMP mixture based on the work described in the previous chapter was used to develop multi-channel adsorbent hollow fibres to improve mechanical strength and to enhance the adsorbent weight in a given volume. As such, this chapter explores techniques for spinning adsorbent hollow fibres with multi-bores and different geometries using specially designed spinnerets at the University of Bath, as shown in Section 3.2.3. Its particular focus is on improving the efficiency of VOC adsorption and mechanical properties, as single hollow fibres were fragile and difficult to handle in industrial applications. This chapter also includes an investigation into the effect of multi-channel hollow fibres on pressure drop and adsorption performance compared to single hollow fibres with the equivalent weight of adsorbent. In addition, a hydrophobic adsorbent high silica zeolite, HiSiv 1000, was used as the model adsorbent to spin multi-channel fibres.

5.1 Multi-channel adsorbent hollow fibres

A multi-channel highly adsorbent loaded hollow fibre structure to achieve efficient VOC adsorption was developed and optimised. The creation of highly adsorbent loaded multi-channel fibres with an impermeable outer skin is novel and has not previously been achieved. The addition of pores and adsorbent loading into the hollow fibres was carried out using spinnerets with multiple inner tubes to produce hollow fibres with multi-bores. The methodology used in the preparation, testing and characterisations was explored in depth in Chapter 3.

This chapter describes several studies that tested multi-channel adsorbent hollow fibres for the recovery of VOC:

1. A comparison of new tri-lobe three bore adsorbent hollow fibres and a tubular single hollow fibre membrane for use in n-butane adsorption. In this study, both hollow fibres were prepared using the same composition of 13X/PESF/NMP mixture (optimised recipe from previous chapter); spinning experiment parameters excluded the type of spinneret. Their adsorption properties were tested using dynamic n-butane breakthrough studies. They were also characterised using scanning electron microscopy (SEM), mechanical study and the adsorption-desorption isotherm.

2. A study of the effect of solvent compositions, adsorbent compositions and air gap on the adsorption performance of tri-lobe three-bore adsorbent hollow fibres. SEM and the dynamic breakthrough challenge were also used to characterise all hollow fibres.
3. The use of moisture-resistant high silica zeolite HiSiv 1000 as model adsorbents to fabricate tri-lobe three-bore adsorbent hollow fibres. SEM and dynamic breakthrough studies were also used.
4. Fabrication of hexagonal seven bore adsorbent hollow fibres and an examination of the effect of air gap on shape and adsorption capacity. Dynamic breakthrough studies and SEM were used to investigate these hollow fibres.

5.2 Results and discussion

In this chapter, all adsorbent hollow fibres were characterised according to their adsorption performance, surface morphology, pore size distribution and mechanical strength. These techniques were described in Chapter 3.

5.2.1 Dynamic n-butane adsorption in single adsorbent hollow fibres and tri-lobe three-bore adsorbent hollow fibres

A 1000 ppm n-butane breakthrough test was carried out at 1 L/min on a 22cm module length of tubular single bore hollow fibres and tri-lobe three-bore fibres. This is shown in Figure 5.1. The optimisation of the PESF/13X/NMP composition used to fabricate both hollow fibres was described in the previous chapter. Table 5.1 shows the experimental details and results of both hollow fibre modules. As can be seen in Table 5.1, similar experimental parameters were used to spin and test both hollow fibres.

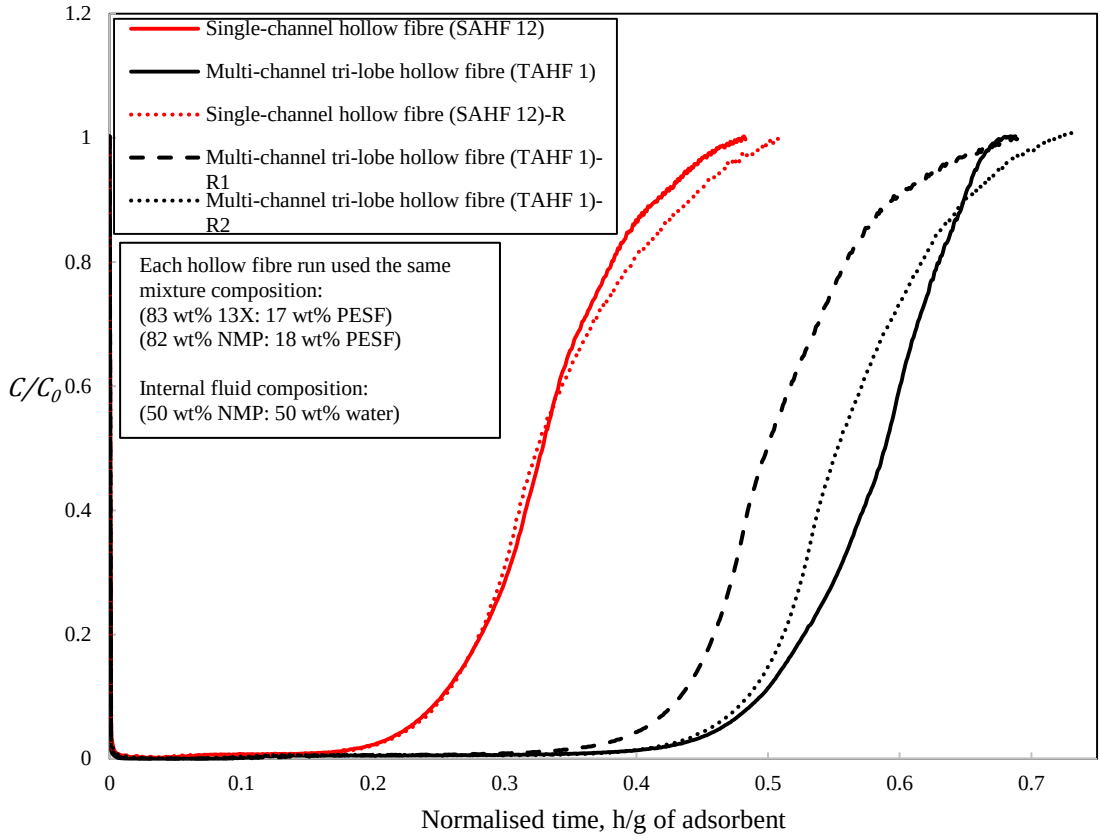

Figure 5.1. 1 L/min 1000 ppm n-butane dynamic challenge on tubular single bore and tri-lobe three bore hollow fibres, showing repeated breakthrough curves with dotted lines.

Table 5.1: Summary of the adsorption performance of the 13X/PESF single and three bore hollow fibres.

Sample	Single hollow fibres (SAHF 12)	Tri-lobe hollow fibres (TAHF 1)
13X/PESF/NMP mixture composition	82 wt% NMP: 18 wt% PESF 83 wt% 13X: 17 wt% PESF	
Bore fluid compositions	(50 wt% NMP: 50 wt% water)	
Bore fluid flow rate, ml/min	3	3
Licowax pore former (g)	1	1
Number of fibres	60	34
Number of bores	60	102
Regeneration Temperature,	200°C	200°C
t_b (h/g)	0.24	0.46
Breakthrough loading (%)	4.3	8.7
t_{eq} (h/g)	0.5	0.7
Equilibrium loading (%)	6.2	10.9

The adsorption breakthrough experimental conditions with n-butane at a feed flow rate of 1.0 L/ min and a concentration 1000 ppmv.

Despite the improved loading observed in n-butane in single-bore hollow fibres and full access to the adsorbent, as described in the previous chapter, greater adsorption capacity in the breakthrough study was noted in tri-lobe three-bore hollow fibres of

equivalent weight under adsorbent and experimental conditions. As shown in Figure 5.1 and Table 5.1, the breakthrough curve shifted from left to right and the breakthrough time for the hollow fibre modules increased from 0.24 to 0.46 hours/g of adsorbent as the hollow fibre geometry was changed from single-bore hollow fibres to tri-lobe three-bore hollow fibres, indicating the increase in adsorption performance because of the gain of 13X active sites. The adsorption capacities up to the point of equilibrium and the breakthrough of the tri-lobe hollow fibre module are calculated to be 10.9 and 8.7%, respectively. However, in single adsorbent hollow fibres, the adsorption capacities up to the point of equilibrium and breakthrough are calculated to be lower, at 6.2 and 4.3% respectively. By repeating the same experiments, the same trend can be detected for the n-butane dynamic challenge, as shown in Figure 5.1. This confirms that a tri-lobe three-bore adsorbent hollow fibre module provides improved adsorption performance.

5.2.2 Characterisation of single adsorbent hollow fibres and tri-lobe three bores adsorbent hollow fibres

5.2.2.1 Scanning electron microscopy

To investigate why the tri-lobe three-bore hollow fibres have greater adsorption capacity per weight for n-butane than the single hollow fibres, scanning electron micrographs were taken for both hollow fibres. It is apparent in Figure 5.2(c) and Figure 5.3(c) that the single and tri-lobe adsorbent hollow fibres are perfectly formed, with a bore diameter of 0.5 mm and 1 mm, respectively. The tri-lobe adsorbent hollow fibre has a very open macrostructure with high loaded zeolite crystals held within to provide easier access to the adsorption sites; this reduces voidage, which leads to improved adsorption capacity, as shown in Figure 5.3(d and e). In this hollow fibre, there are more macrovoids around bores compared to single hollow fibres. These macrovoids and bores are presented throughout the hollow fibre structure, as can be seen in Figure 5.3(f). However, Figure 5.2(a, b and d) shows that the open porous structure of single adsorbent hollow fibre appears to consist of fewer zeolite crystals, possibly giving rise to zeolites coated in PESF. It is important to ensure that the 13X particles are not covered by a PESF coating and that the adsorbate molecules can easily access the adsorption sites. Figure 5.2(f) also shows that the single hollow fibre has a sponge-like structure extending from the bores to the outer layer, while the tri-lobe hollow fibre has a long thin finger-like structure around the bores, and a sponge-like

structure in the outer layer with some large macrovoids, as shown in Figure 5.3(f). The combination of sponge-like and finger-like can enhance the mass transfer processes and provide easy gas channelling. Figure 5.2(e) shows that single hollow fibres have a denser structure in the outer wall, compared with tri-lobe hollow fibres, as shown in Figure 5.3(a).

It may be concluded that the increase in 13X zeolite loading and the formation of macrovoids in tri-lobe hollow fibre may be a result of the use of three inner tubes in the spinneret to pass a mixture of NMP/water during the spinning experiment. In contrast, the lower number of macrovoids obtained in the single hollow fibre and lower 13X loading are result of spinning hollow fibre using of a mixture of NMP/water in one inner tube, as shown in Figure 5.2(f and b). Therefore, in tri-lobe fibre the molecules of n-butane can easily diffuse to adsorption sites with minimal resistance compared with single hollow fibre.

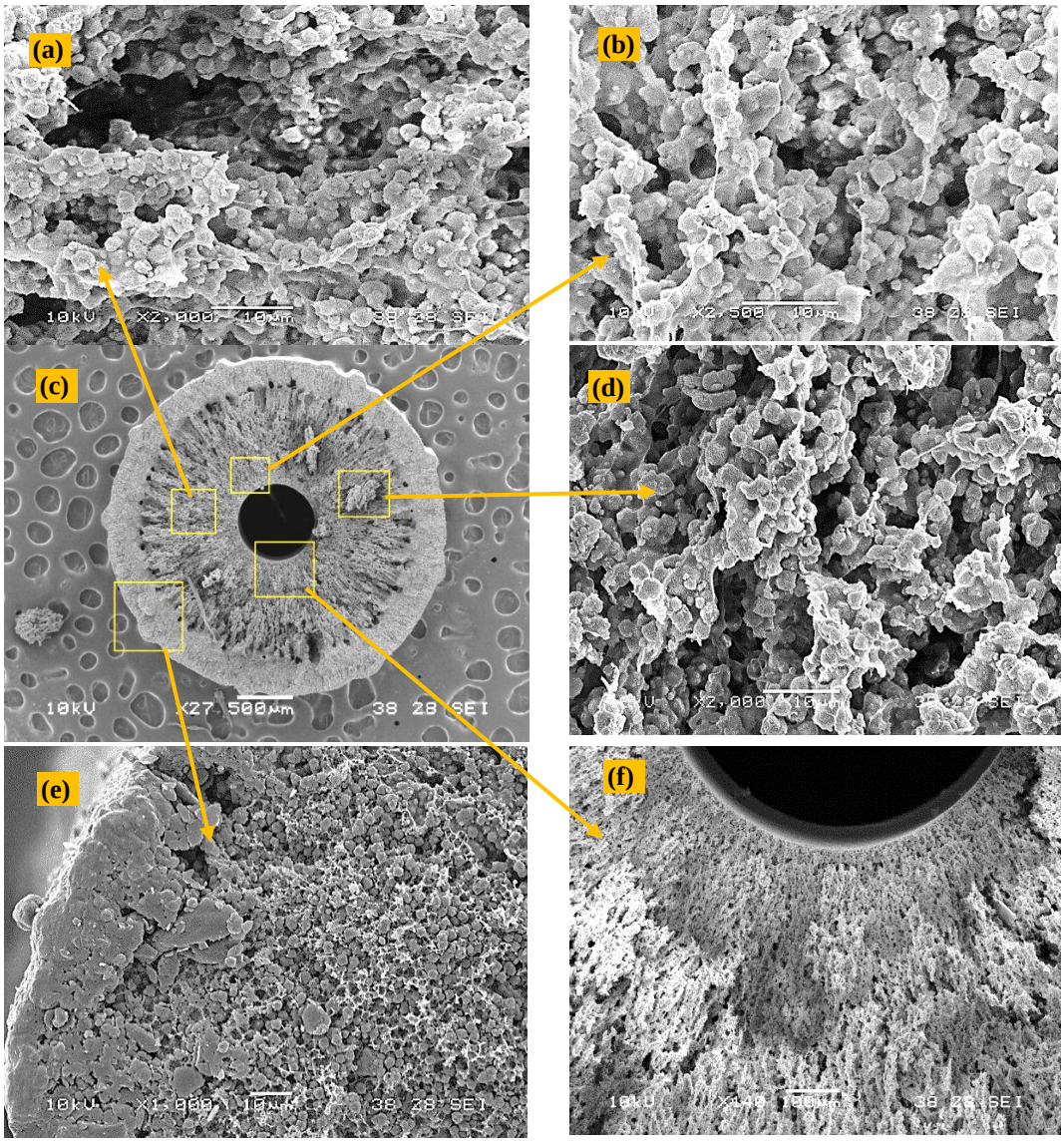

Figure 5.2. Single bore adsorbent hollow fibre (83 wt% 13X: 17 wt% PESF) cross-section a) x2000, b) x2500, c) x27, d) x2000, e) x1000, f) x140.

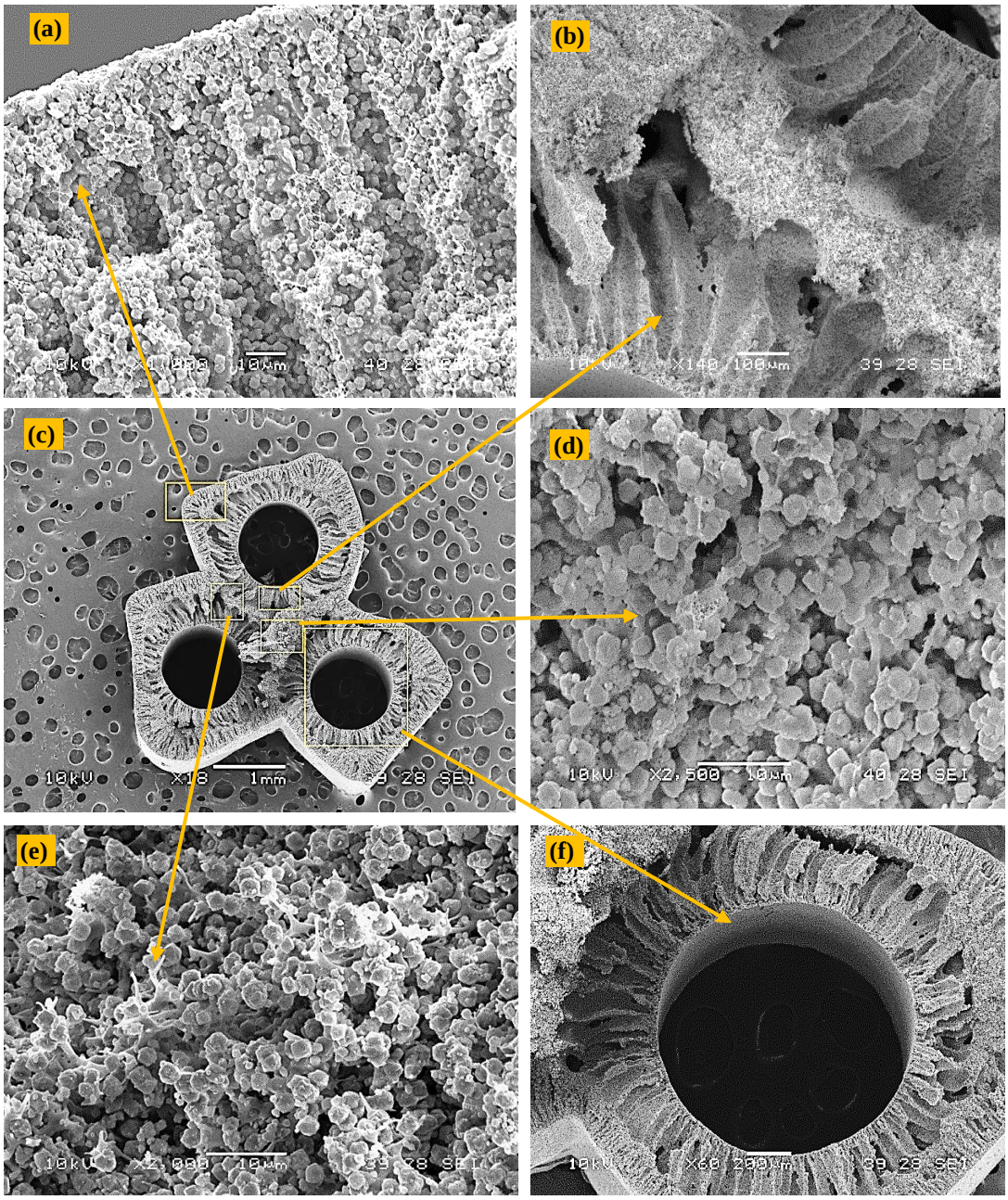

Figure 5.3. Tri-lobe three bore adsorbent hollow fibre (83 wt% 13X: 17 wt% PESF) cross-section a) x1000, b) x140, c) x18, d) x2500, e) x2000, f) x60.

5.2.2.2 Nitrogen adsorption isotherm

Nitrogen isotherms relating to 13X zeolite powder are shown in Figure 5.4, and are typical for a porous material. In Figure 5.4, it can be observed that the adsorption isotherm rises steeply in the low relative pressure range ($2.32x10^{-7}$-$5x10^{-4}$) with N_2 at 77K and reach plateau. It shows that the molecules of N_2 are adsorbed by microspores and that the 13X hollow fibre and 13X powder exhibit a narrow range of (P/P_0) due to a limited range in pore size. According to the IUPAC classification, these adsorption

isotherms of the samples are microporous (Type I). The Brunauer-Emmett-Teller (BET) and Langmuir methods were used to determine the specific surface area in the relative pressure (P/P_0) between 1e-4 and $5x10^{-4}$. 13X zeolite powder and tri-lobe 13X hollow fibre have high apparent BET surface areas of 586.7 m^2/g and 560.5 m^2/g respectively, as shown in Table 5.2. However, single 13X/PESF hollow fibre has a lower BET surface area of 475.6 m^2/g. Pore size distributions were evaluated according to the Horvath-Kawazoe method. The total pore volume of samples was calculated from the quantity adsorbed at 0.0286 relative pressure. It was found that the 13X zeolite powder and tri-lobe 13X/PESF hollow fibres have roughly the same values of pore volume, pore size distribution and maximum adsorption capacity. However, there are differences in these values in the case of single 13X/PESF hollow fibres. This shows that the polymer incorporated with 13X in single hollow fibre may influence the surface area, adsorption capacity and pore size distributions compared to tri-lobe hollow fibres. This was confirmed in the beginning of this section by scanning electron microscopy (SEM). Therefore, the values shown in Table 5.2 and Figure 5.4 confirm that the tri-lobe 13X hollow fibres have higher porosity than single hollow fibres, which can provide high adsorption performance for organic gases with low transport resistance.

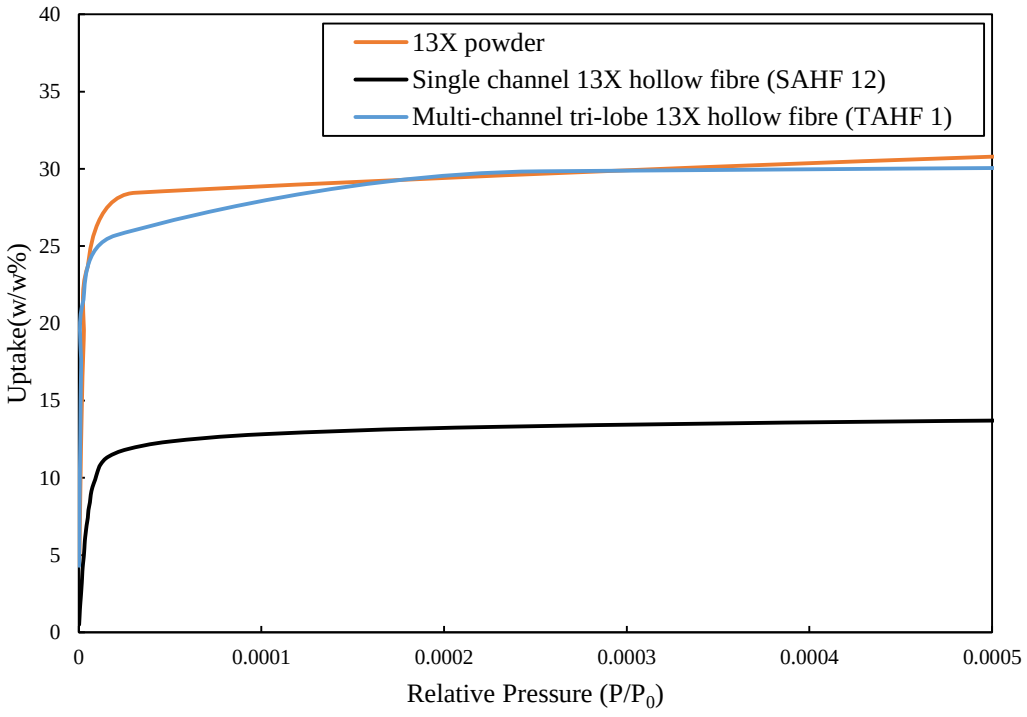

Figure 5.4. N_2 adsorption isotherms at 77K for 13X zeolite powder, single hollow fibre and tri-lobe three bore hollow fibre.

Table 5.2: The surface area and structural properties of 13X powder, single 13X/PESF hollow fibre and tri-lobe three bore 13X/PESF hollow fibre from the N_2 adsorption isotherm.

	13X powder	Single 13X/PESF hollow fibre	Tri-lobe 13X/PESF hollow fibre
BET surface area m^2/g	586.7	475.6	560.5
Langmuir surface area m^2/g	595.7	479.7	576.6
Total pore volume cm^3/g	0.27	0.17	0.25
Horvath-Kawazoe pore size distributions (nm)	0.56	0.66	0.55
Langmuir maximum adsorption capacity (cm^3/g)	136.8	110.2	132.4

5.2.2.3 Pressure drop in adsorbent hollow fibres

The adsorbent hollow fibres fabricated in this research have minimal resistance to n-butane flow, with pore openings in the microfiltration range. The 13X zeolite particles can be incorporated in the hollow fibre structure; the gas stream flowing through the bore of hollow fibre can maintain good contact with the adsorbent. The pressure drop measurements were carried out on the single and tri-lobe adsorbent hollow fibres (83 wt% 13X: 17 wt% PESF) using air as the gas module. The module's lengths tested was 22cm long. The gas flow rate was controlled by a mass flow controller (5850S, BROOKS Instrument, Holland). The hollow fibre outlet was open to the exhaust during the measurements. Figure 5.5 shows the experimental effects of the pressure drop in single and tri-lobe adsorbent hollow fibres as a result of feed flow changes. The results show that a lower pressure drop can be achieved using the tri-lobe hollow fibres compared to single hollow fibres, which have already been confirmed as having a higher adsorption performance.

The data for the single hollow fibre (diameter of bore = 0.5 mm; column length = 22 cm) and tri-lobe hollow fibre (diameter of bore = 1 mm; column length = 22 cm) were obtained from experimental data. For a given flow rate, the pressure drop is much lower in the tri-lobe hollow fibre than in a single hollow fibre of the same length. A benefit of the tri-lobe hollow fibre is that it allows higher flowrates to be used without considerably increasing the pressure drop.

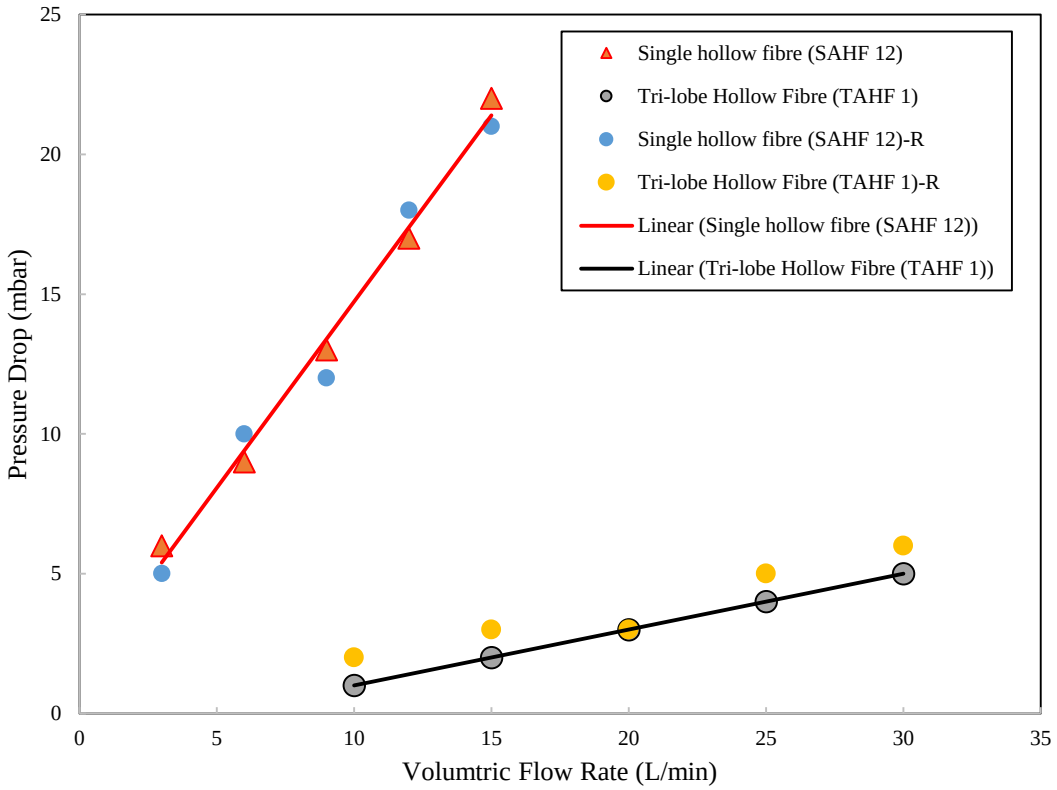

Figure 5.5. Comparison of experimental pressure drop in single hollow fibre unit with that in a tri-lobe hollow fibre.

5.2.2.4 Mechanical strength

To determine the best combination of adsorption capacity, pressure drop and mechanical strength, the tri-lobe hollow fibre and single hollow fibres were prepared using the same compositions of 13X/PESF/NMP mixture. Previous sections have confirmed that tri-lobe hollow fibres have a higher adsorption capacity and lower pressure drop compared to single hollow fibres. The mechanical properties of adsorbent hollow fibres are important parameters for their separation applications. In production of adsorbent hollow fibre, the cross-section structure of fibre could play an important challenging for achieving some better values of mechanical properties. In this study, the stress, strain and Young`s modulus of elasticity of single and tri-lobe adsorbent hollow fibres were investigated. Both single and tri-lobe hollow fibre contained 83 wt% 13X: 17 wt% PESF in the fibre structure. As shown in Figure 5.6, the tri-lobe hollow fibre can withstand a stress of 0.84 MPa, which is better than those of single adsorbent hollow fibre under the same experimental conditions. By repeating the same experiments, the same trend can be detected for the n-butane dynamic challenge, as shown in Figure 5.6.

The aim of this research is to develop multi-channel adsorbent hollow fibres for gas separation with a flexible structure (can fit into any module). Table 5.3 shows the Young`s modulus of elasticity values of both hollow fibres. The tri-lobe hollow fibre has lower Young`s modulus of elasticity than those of single hollow fibre. This means that tri-lobe hollow fibre is more flexible than single adsorbent hollow fibre.

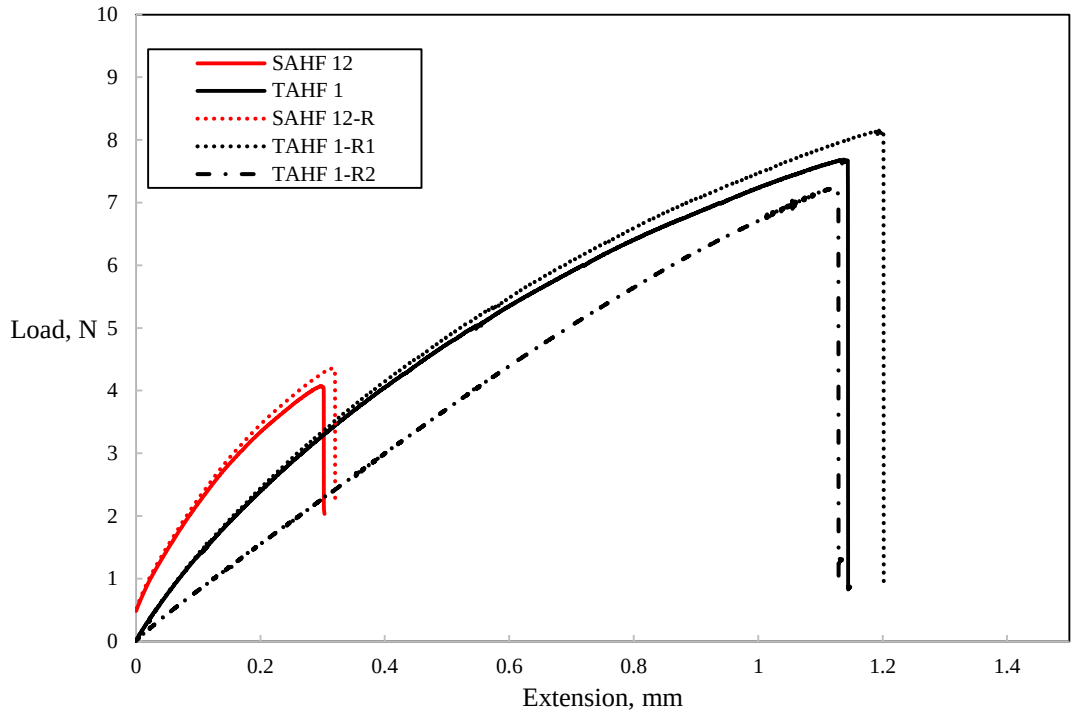

Figure 5.6. Tensile stress and elongation at the break of single and tri-lobe adsorbent hollow fibres, showing repeated measurement of mechanical properties with dotted lines.

Table 5.3: Stress, Strain and Young`s modulus of single and tri-lobe adsorbent hollow fibres

Sample	Cross sectional area (cm^2)	Maximum load (N)	Stress (MPa)	Strain	Young`s modulus of elasticity (GPa)
Single adsorbent hollow fibre (SAHF 12)	0.062	4.5	0.72	0.004	163.6
Tri-lobe adsorbent hollow fibre (TAHF 1)	0.092	7.7	0.84	0.013	64.2

5.2.3 Effect of adsorbent concentration on tri-lobe adsorbent hollow fibres performance

In previous sections, it was confirmed that the adsorption capacity, mechanical properties and pressure drop are much better in the tri-lobe adsorbent hollow fibres than in single hollow fibres. However, tri-lobe hollow fibres do not have a perfect shape. In this section, two main approaches were considered to optimise the adsorption capacity of VOC separation and the shape of fibres by changing the compositions of adsorbent/polymer/NMP mixtures and spinning conditions, such as air gap and flow

rate of bore fluid. To start the adsorbent/polymer/NMP mixture reformulation, the viscosity of the mixture must be between 9-14 Pa.s.

5.2.3.1 Adsorption performance testing

To investigate the effect of 13X zeolite concentration on adsorption performance and mechanical properties, tri-lobe hollow fibres were spun from 83 wt%, 84 wt% and 85 wt% 13X zeolite. Figure 5.7 shows a comparison of adsorption breakthrough curves. The breakthrough curve for the 85 wt% 13X zeolite tri-lobe hollow fibre module is much steeper than for the other tri-lobe hollow fibres. This shows that the tri-lobe hollow fibre module with higher 13X zeolite concentration has much better kinetic characteristics. As can be seen from Table 5.4, the equilibrium loading increased due to the increase of 13X zeolite in tri-lobe hollow fibres. The breakthrough times for sample 83 wt%, 84 wt% and 85 wt% 13X zeolite tri-lobe hollow fibres were 0.4, 0.46 and 0.55 hours/g of adsorbent, respectively. Hence, from these results it may be concluded that the adsorption capacity of the 85 wt% 13X tri-lobe hollow fibre is greater than that for the 83 wt% and 84 wt% 13X tri-lobe hollow fibres under identical feed conditions.

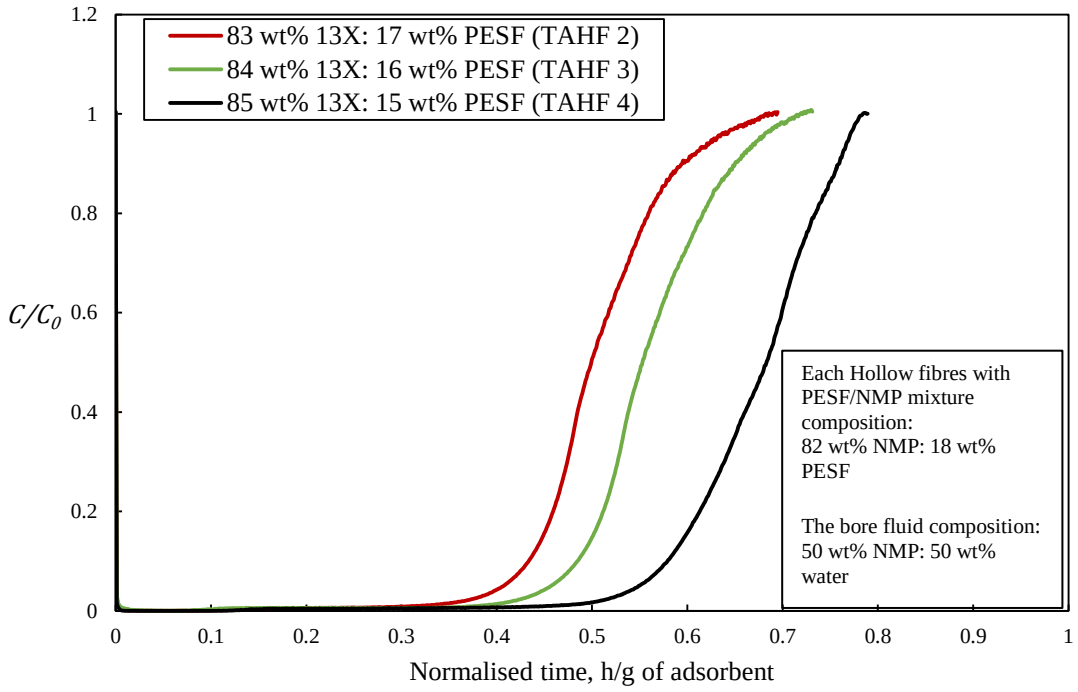

Figure 5.7. Comparison of the adsorption breakthrough curves of tri-lobe adsorbent hollow fibres with 1 l/min flow rate 1000 ppm concentration of n-butane with different amounts of 13X zeolite.

Table 5.4: Summary of adsorption performance of the tri-lobe 13X/PESF hollow fibres with different composition of 13X

Sample	TAHF 2	TAHF 3	TAHF 4
13X/PESF/NMP mixture composition	82 wt% NMP: 18 wt% PESF 83 wt% 13X: 17 wt% PESF	82 wt% NMP: 18 wt% PESF 84 wt% 13X: 16 wt% PESF	82 wt% NMP: 18 wt% PESF 85 wt% 13X: 15 wt% PESF
Viscosity (Pa.s)	11.4	12.7	13.8
t_b (h/g)	0.4	0.46	0.55
Breakthrough loading (%)	6.9	7.9	9.9
t_{eq} (h/g)	0.71	0.73	0.79
Equilibrium loading (%)	8.6	9.7	12.2

The adsorption breakthrough experimental conditions used n-butane at a feed flow rate of 1.0 L/ min and a concentration 1000 ppmv.

5.2.3.2 Scanning electron microscopy

The morphologies of 13X/PESF composite tri-lobe hollow fibres with different 13X compositions are shown in Figure 5.8. 83 wt% and 84 wt% 13X tri-lobe hollow fibre can allow 13X particles to be covered by the PESF structure, as shown in Figure 5.8(a and b).

The cross-section structure of tri-lobe hollow fibre with 85 wt% 13X zeolite has a higher loading of 13X particles and lower outer wall thickness compared to the samples of tri-lobe hollow fibres with 83 wt% and 84 wt% 13X zeolite. This pore system of the 85 wt% 13X tri-lobe hollow fibre is much more porous, and the finger-like structures allow the n-butane to obtain rapid access to the adsorption sites of the 13X particles. The superior structure of this hollow fibre in terms of capturing gas molecules could be attributed to the high effective surface area of the fibre structure and the diffusion rate. However, as noted in Chapter 4, the increase in 13X zeolite leads to a decrease in the mechanical properties of hollow fibres. Therefore, the tri-lobe hollow fibre with 85 wt% 13X was weaker and more difficult to form as a cartridge module for the dynamic breakthrough challenge. From this, it may be concluded that the increase in 13X zeolite composition with the lower polymer content enhanced adsorption capacity affects the mechanical properties of tri-lobe hollow fibres, thereby weakening the overall structure without improving the tri-lobe hollow fibre shape. Furthermore, the hollow fibres were more likely to crack with high loading

of 13X zeolite. It therefore follows that to produce tri-lobe hollow fibres with good mechanical properties and good flexibility, a higher 13X zeolite content in the structure should be avoided.

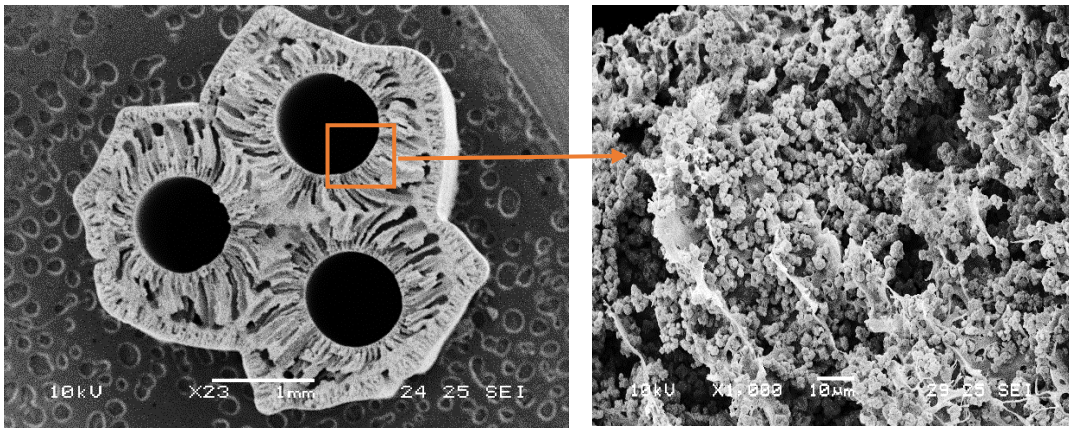

(a) Cross-section of 83 wt% 13X tri-lobe hollow fibre (TAHF 2), x23 and x1000

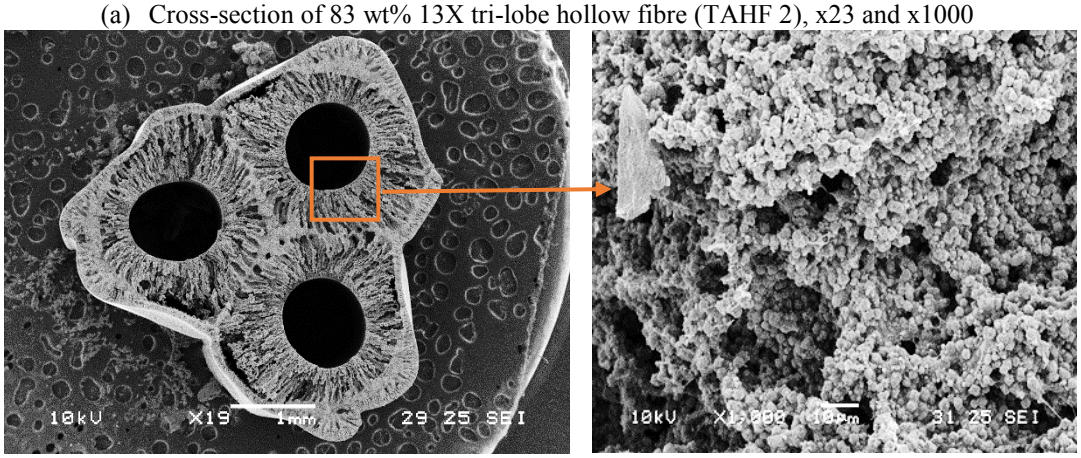

(b) Cross-section of 84 wt% 13X tri-lobe hollow fibre (TAHF 3), x19 and x1000

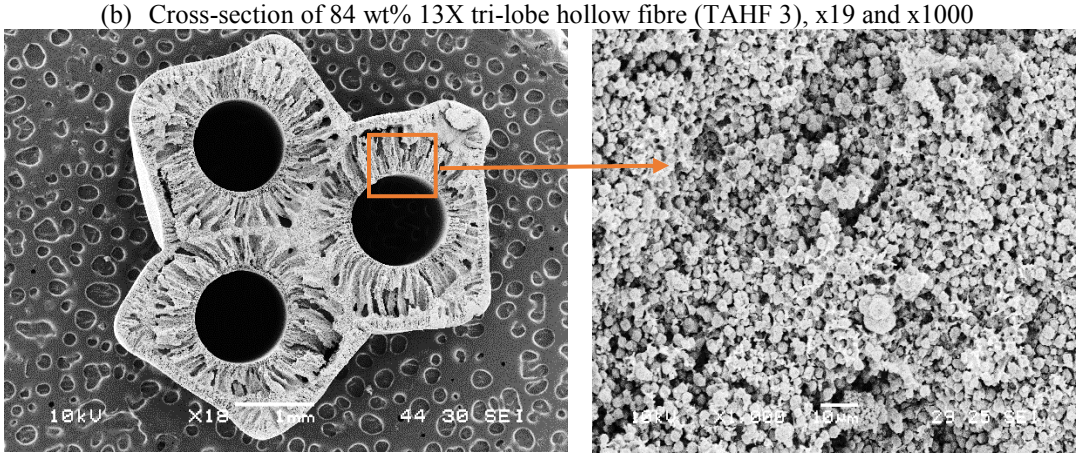

(c) Cross-section of 83 wt% 13X tri-lobe hollow fibre (TAHF 4), x18 and x1000

Figure 5.8. Scanning electron micrographs of tri-lobe hollow fibres (18 wt% PESF: 82 wt% NMP) at different 13X zeolite compositions in the range of (a) (83 wt% 13X: 17 wt% PESF), (b) (84 wt% 13X: 16 wt% PESF) and (c) (85 wt% 13X: 15 wt% PESF).

5.2.4 Effect of bore fluid flow rate

This section examined the effect of the flow rate of bore fluid on adsorption performance and the shape of tri-lobe hollow fibres.

5.2.4.1 Adsorption performance testing

Figure 5.9 shows the breakthrough curves of tri-lobe hollow fibres as a function of the flow rate of bore fluid during the spinning experiment. The breakthrough time decreased as the flow rate of bore fluid increased, in this case from 0.41 to 0.28 hours/g of adsorbent as the flow rate was increased from 3 to 6 ml/min under the same experimental conditions. Table 5.5 shows the equilibrium loading of the tri-lobe hollow fibre modules, which was calculated to be 8.6 and 5.7%, for the bore fluid flow rate of 3 and 6 ml/min, respectively. By repeating the same experiments, the same trend can be detected for the n-butane dynamic challenge, as shown in Figure 5.9.

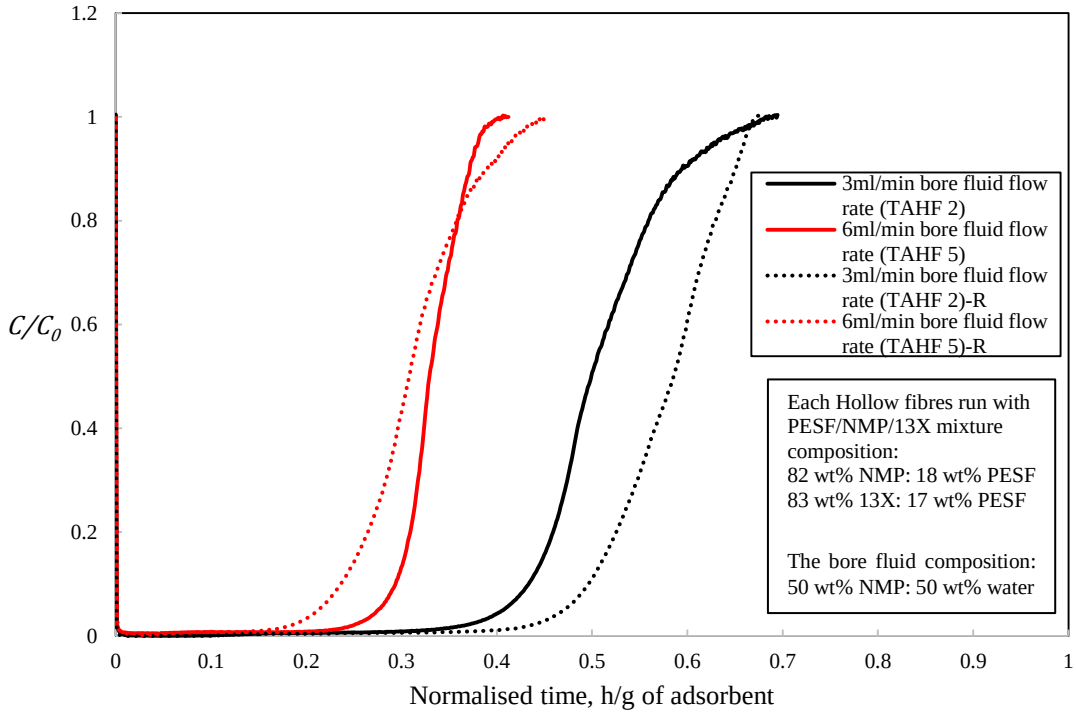

Figure 5.9. Comparison of the adsorption breakthrough curves of tri-lobe adsorbent hollow fibres with 1 l/min flow rate at 1000 ppm concentration of n-butane with a different flow rate of bore mixtures, showing repeated breakthrough curves with dotted lines

Table 5.5: Summary of the adsorption performance of the tri-lobe 13X/PESF hollow fibres with different flow rates of bore fluid

Sample	TAHF 2	TAHF 5
13X/PESF/NMP mixture composition	82 wt% NMP: 18 wt% PESF 83 wt% 13X: 17 wt% PESF	
Bore fluid compositions	(50 wt% NMP: 50 wt% water)	
Bore fluid flow rate, ml/min	3	6
Regeneration Temperature,	200°C	200°C
t_b (h/g)	0.41	0.28
Breakthrough loading (%)	6.9	4.7
t_{eq} (h/g)	0.71	0.41
Equilibrium loading (%)	8.6	5.7

The adsorption breakthrough experimental conditions with n-butane at a feed flow rate of 1.0 L/ min and a concentration 1000 ppmv.

5.2.4.2 Scanning electron microscopy

The SEM micrographs show that a reasonable bore fluid flow rate can allow 13X particles to be released from the PESF structure and to create better access to adsorption sites. As can be seen in Figure 5.10(b), the tri-lobe hollow fibre with a 6 ml/min flow rate of bore fluid has a slightly circular shape. This could be due to an increase in the inner diameter and a decrease in the wall thickness of the fibre. It is very important to keep the flow rate of bore fluid at a suitable value. This is because at 6 ml/min the bore fluid will pass rapidly through the bores without allowing sufficient time to create a sponge finger-like structure. However, the 3ml/min flow rate of bore fluid could provide sufficient time to enhance the process of coagulation, as shown in Figure 5.10(a).

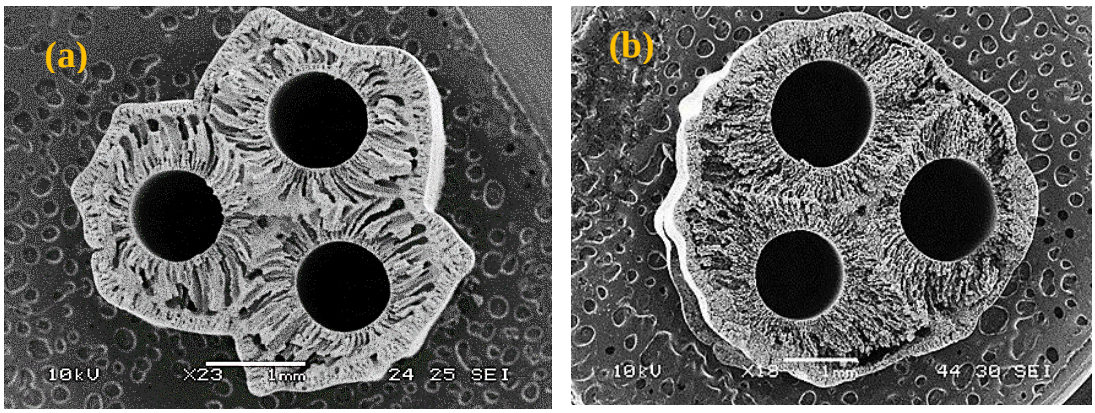

Figure 5.10. Scanning electron micrographs of tri-lobe hollow fibres (83 wt% 13X: 17 wt% PESF) at different bore fluid flow rates in the range of (a) 3 ml/min, x23 (b) 6 ml/min, x18.

5.2.5 Effect of air gap distance

The tri-lobe hollow fibre spinning conditions were tested by varying the air gap distance to improve the adsorption capacity and shape of fibres.

5.2.5.1 Adsorption performance testing

The effect of air gap on the n-butane adsorption of tri-lobe hollow fibre spun from 83 wt% 13X: 17 wt% PESF was examined. Figure 5.11 shows that an increase in air gap leads to a significant decrease in adsorption capacity. A reduction in the air gap distance to 0cm increased the time to breakthrough for tri-lobe hollow fibres from 0.08 to 0.41 hours/g of adsorbent. The equilibrium loading was calculated to be 8.6 %, as shown in Table 5.6. This may be a result of the elongation-induced polymer chain orientation and the different precipitation paths that occurred during wet/wet spinning and dry/wet spinning. By repeating the same experiments, the same trend can be detected for the n-butane dynamic challenge, as shown in Figure 5.11.

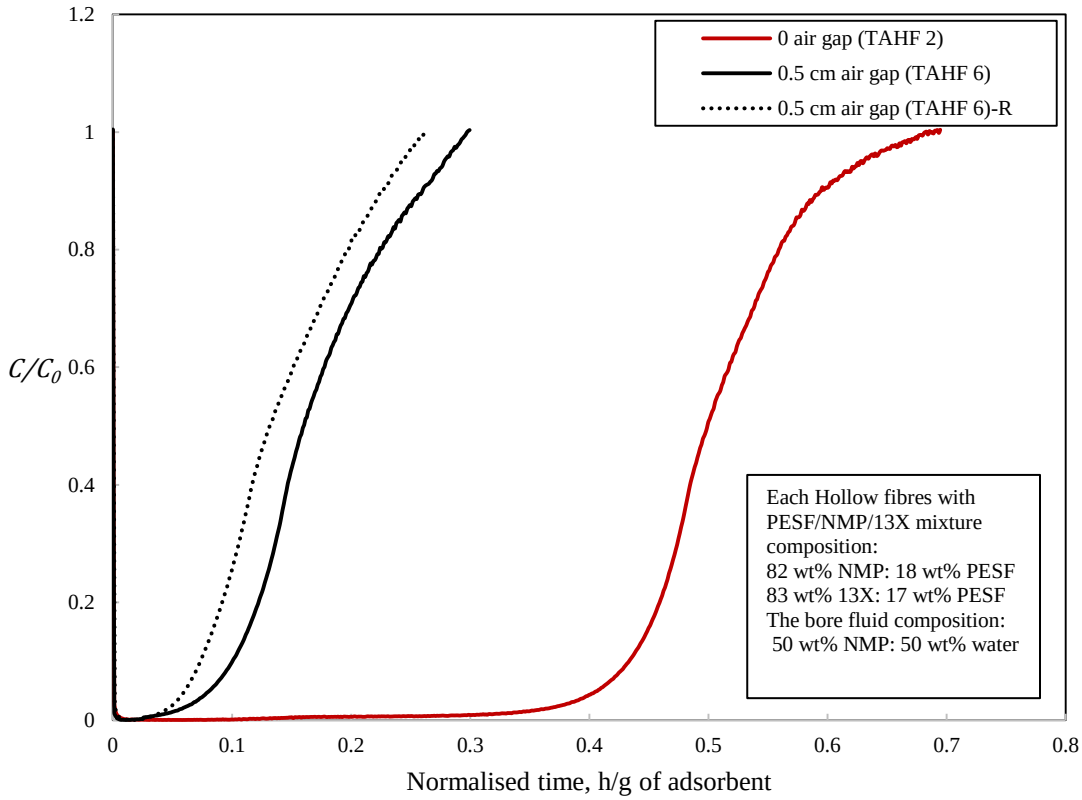

Figure 5.11. The effect of air gap length on the adsorption breakthrough curves of tri-lobe adsorbent hollow fibres with 1 l/min flow rate 1000 ppm concentration of n-butane, showing repeated breakthrough curve with dotted line

Table 5.6: Summary of the adsorption performance of the tri-lobe 13X/PESF hollow fibres with different air gap distances

Sample	TAHF 2	TAHF 6
13X/PESF/NMP mixture composition	82 wt% NMP: 18 wt% PESF 83 wt% 13X: 17 wt% PESF	
Bore fluid compositions	(50 wt% NMP: 50 wt% water)	
Bore fluid flow rate, ml/min	3	3
Air gap distance, cm	0	0.5
Regeneration Temperature,	200°C	200°C
t_b (h/g)	0.41	0.08
Breakthrough loading (%)	6.9	1.4
t_{eq} (h/g)	0.7	0.3
Equilibrium loading (%)	8.6	3.1

5.2.5.2 Scanning electron microscopy

The SEM morphologies in Figure 5.12 are the cross-sectional tri-lobe hollow fibres affected by air gap distance. Both tri-lobe hollow fibres have the same spinning conditions, except for the air gap distance. The porous structure decreases as the air gap distance increases, and that the macrovoids are reduced when the air gap distance reaches 0.5 cm. In addition, Figure 5.12(b) shows that 0.5cm air gap formed a thinner skin layer, while a 0cm air gap provided a thick skin layer, as shown in Figure 5.12(a). This can control the porosity of tri-lobe hollow fibre.

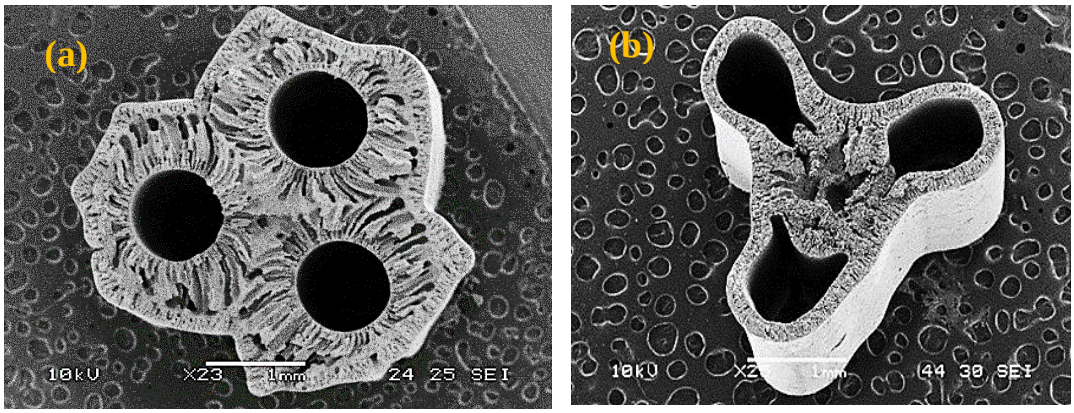

Figure 5.12. Scanning electron micrographs of tri-lobe hollow fibres (83 wt% 13X: 17 wt% PESF) at different air gap distance in the range of (a) 0 cm, x23 (b) 0.5 cm, x25.

Therefore, another conclusion that may be drawn is that, in addition to the critical 13X zeolite concentration and the flow rate of bore fluid, a critical air gap distance is another key parameter that influences the adsorption capacity and shape of tri-lobe hollow fibres.

5.2.6 Hydrophobic adsorbents for spinning tri-lobe hollow fibre

Tri-lobe adsorbent hollow fibres must operate effectively with high moisture. Therefore, HiSiv 1000 and HiSiv 3000 were used to fabricate hollow fibres with high moisture resistance. For these hydrophobic adsorbents, further NMP was added as needed to confirm that all the adsorbent could be suspended within the mixture of hollow fibres and its viscosity decreased to make spinning possible. Details of the parameters and spinning conditions used are shown in Table 5.7.

5.2.6.1 Adsorption performance testing

The dynamic adsorption challenge was performed using apparatus like that described in Chapter 3. N-butane was used as a model VOC to compare the dynamic adsorption capacity of tri-lobe adsorbent hollow fibres prepared from the commercial HiSiv 1000 and HiSiv 3000. The polymer ratio was kept at 83:17 during the preparation of the fibres. Figure 5.13 shows the breakthrough curves of tri-lobe adsorbent hollow fibres prepared from two different hydrophobic adsorbents (HiSiv 1000 and HiSiv 3000). As shown in Figure 5.13 and Table 5.7, the adsorption breakthrough time decreased from 0.22 to 0.21 hours/g of adsorbent as the adsorbent was changed from HiSiv 3000 to HiSiv 1000 under the same weight of adsorbent. The equilibrium loading of tri-lobe hollow fibres modules with HiSiv 3000 and HiSiv 1000 was calculated to be 4.6 and 5%, respectively. Furthermore, as can be seen in Figure 5.13, the breakthrough curves of tri-lobe HiSiv 3000 hollow fibre are sharp, and are clarified by a higher mass transfer rate and effective surface area to create access to adsorption sites. However, Figure 5.13 shows that the HiSiv 1000 tri-lobe hollow fibre fibres provides significantly broader breakthrough curves. This result can be explained by their lower effective surface area and higher diffusion resistance in the bore surface. This may prevent adsorbate molecules easily reaching the adsorption sites. To explain why the HiSiv 3000 tri-lobe fibres have higher mass transfer and effective surface area for n-butane adsorption under the same parameter conditions, SEMs were taken for HiSiv 1000 and HiSiv 3000 tri-lobe hollow fibre.

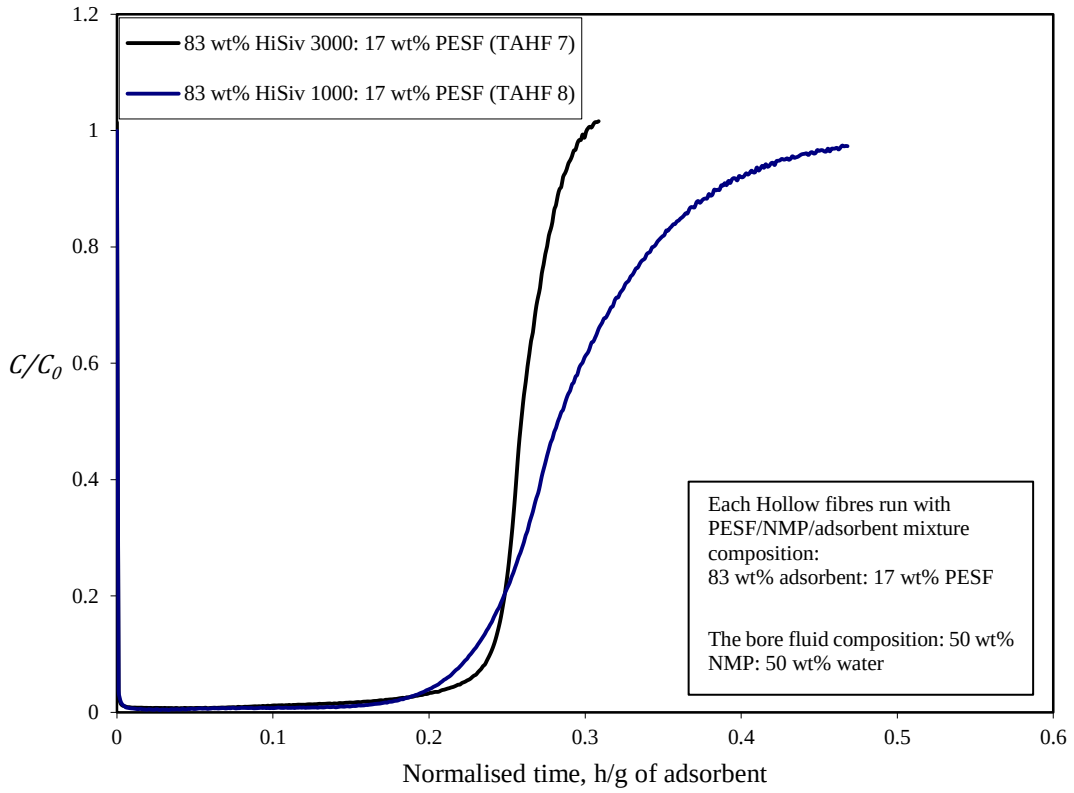

Figure 5.13. Comparison between the adsorption breakthrough curves of tri-lobe adsorbent hollow fibres with 1 l/min flow rate and 1000 ppm concentration of n-butane with different type of adsorbents

Table 5.7: Summary of the adsorption performance of the tri-lobe 13X/PESF hollow fibres with different type of adsorbents.

Sample	TAHF 7	TAHF 8
Adsorbent/PESF mixture composition	83 wt% HiSiv 3000: 17 wt% PESF	83 wt% HiSiv 1000: 17 wt% PESF
Bore fluid composition	(50 wt% NMP: 50 wt% water)	
Bore fluid flow rate, ml/min	3	3
Air gap distance, cm	0	0
Regeneration Temperature,	200°C	200°C
t_b (h/g)	0.22	0.21
Breakthrough loading (%)	3.8	3.5
t_{eq} (h/g)	0.31	0.47
Equilibrium loading (%)	4.6	5

5.2.6.2 Scanning electron microscopy

Figure 5.14(b) shows that the HiSiv 3000 fibre has a quite open macrostructure. However, the HiSiv 1000 tri-lobe fibre has a dense macrostructure (as shown in Figure 5.14(b) which could prevent the n-butane molecules to reach the adsorption sites easily. However, the macrovoidal structure of the HiSiv 3000 hollow fibre, as seen in

the low magnification image in Figure 5.14(d), suggests that they must show quick adsorption kinetics. This was observed for n-butane.

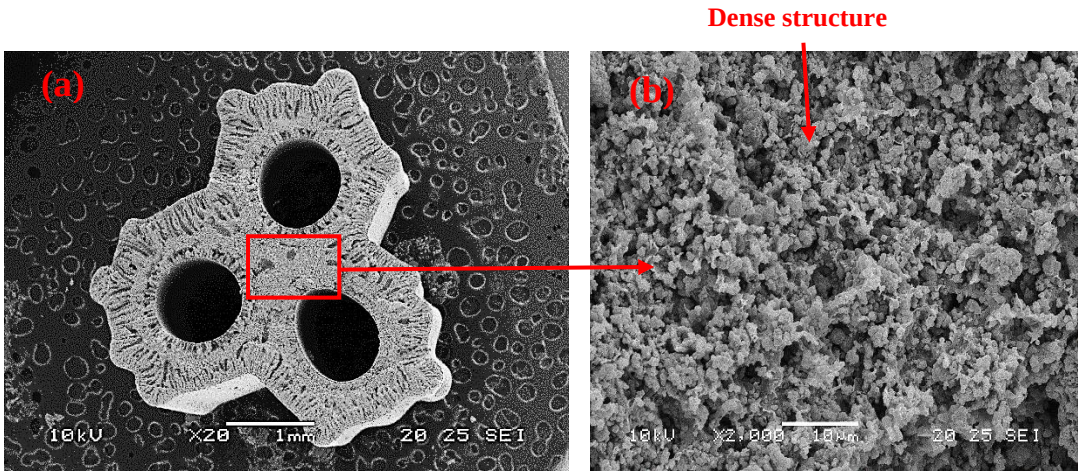

Cross-section of 83 wt% HiSiv 1000 tri-lobe hollow fibre (TAHF 8), x20 and x2000

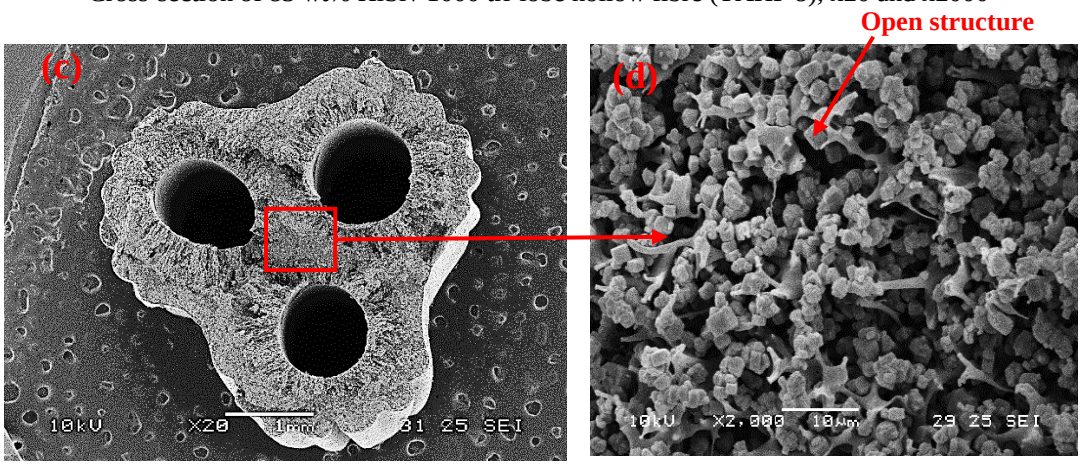

Cross-section of 83 wt% HiSiv 3000 tri-lobe hollow fibre (TAHF 7), x20 and x2000

Figure 5.14. Scanning electron micrographs of tri-lobe hollow fibres using different adsorbent of the following types (a) 83 wt% HiSiv 1000: 17 wt% PESF and (c) 83 wt% HiSiv 3000: 17 wt% PESF.

5.2.7 Hexagonal seven bore adsorbent hollow fibre

In this section, additional novel hexagonal hollow fibres containing seven bores were successfully fabricated from 13X zeolite and PESF using a special design of spinneret at the University of Bath. The spinneret design and dynamic adsorption challenge were performed using apparatus described in Chapter 3. Initially, mixtures were prepared using a ratio of 82 wt% NMP: 18 wt% PESF and 83 wt% 13X: 17 wt% PESF. The hexagonal hollow fibres were spun under different air gap distances.

5.2.7.1 Adsorption performance testing

Figure 5.15 and Table 5.8 show the parameter conditions and results of the dynamic breakthrough challenge of all hexagonal hollow fibres. As shown in Figure 5.15, the highest n-butane breakthrough times and equilibrium loadings were achieved with an 0mm air gap distance hexagonal hollow fibre, (0.17 hours/g of adsorbent and 3.5%wt). The 5mm air gap hexagonal fibre has the lowest equilibrium loading (2.2%wt). The breakthrough curves of these three samples are sharp. This means that these fibres clearly have a good kinetic performance which give good an accessibility for the n-butane molecules to reach the adsorption sites.

A key trend observed in breakthrough and equilibrium times was that hexagonal fibre with a 0mm air gap has greater n-butane breakthrough and equilibrium loading than fibres with other values. This is because a certain air gap value can lose a substructure of the porous layer. To describe why the 0mm air gap hexagonal hollow fibre has a higher breakthrough time and equilibrium loading for n-butane adsorption under the same parameter conditions, SEMs and nitrogen isotherms were taken for all samples.

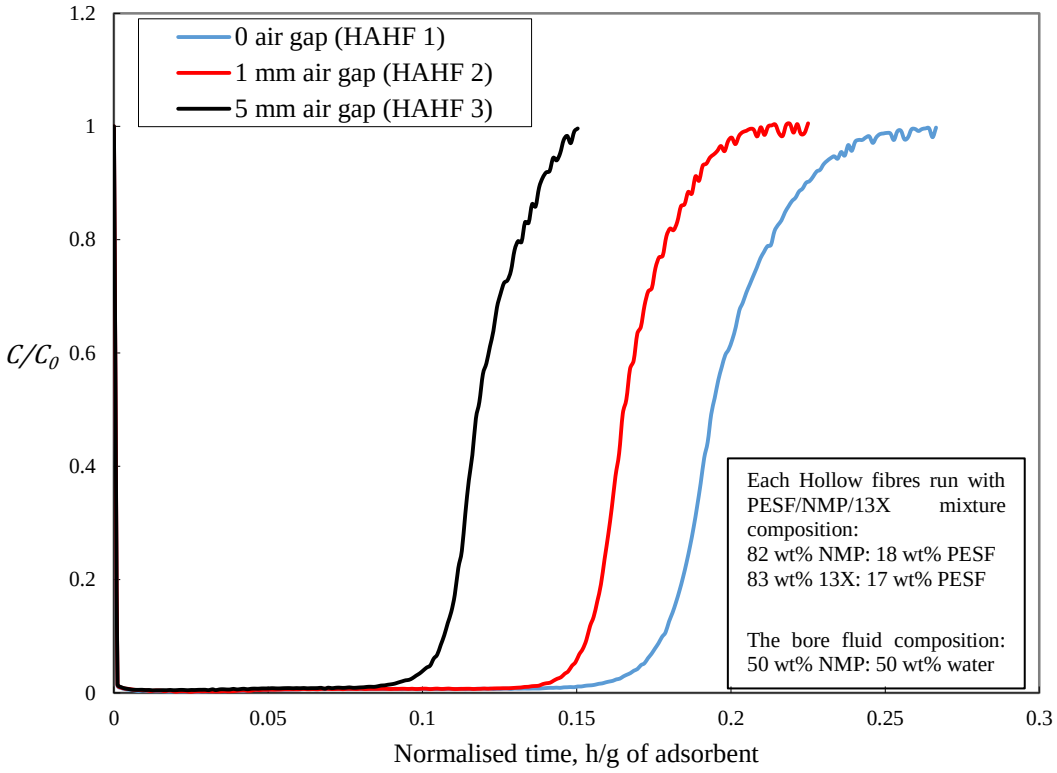

Figure 5.15. The effect of air gap length on the adsorption breakthrough curves of hexagonal adsorbent hollow fibres with 1 l/min flow rate and 1000 ppm concentration of n-butane.

Table 5.8: Summary of the adsorption performance of the hexagonal 13X/PESF hollow fibres with different air gap distances

Sample	hexagonal hollow fibres (HAHF 1)	hexagonal hollow fibres (HAHF 2)	hexagonal hollow fibres (HAHF 3)
13X/PESF/NMP mixture composition	82 wt% NMP: 18 wt% PESF 83 wt% 13X: 17 wt% PESF		
Bore fluid compositions	(50 wt% NMP: 50 wt% water)		
Bore fluid flow rate, ml/min	3	3	3
Air gap distance, mm	0	1	5
Regeneration Temperature,	200°C	200°C	200°C
t_b (h/g)	0.17	0.14	0.1
Breakthrough loading (%)	3	2.5	1.9
t_{eq} (h/g)	0.27	0.21	0.15
Equilibrium loading (%)	3.5	2.8	2.2

5.2.7.2 Scanning electron microscopy

Figure 5.16 shows the shape and porous structure transitions between hexagonal adsorbent hollow fibres with different air gap distances. The differences between the shapes of hollow fibres could be a result of the elongation-induced polymer chain orientation that takes place when the air gap distance has a certain value. The outer layer of the hexagonal fibre is exposed to tap water in the spinning bath. As the concentration between tap water and the adsorbent/solvent/polymer mixture is very steep, NMP is quickly drawn from the outside of the hollow fibre, causing it to coagulate rapidly and more densely. This process has an impact on the shape of hollow fibres, considering the state of polymer molecules during the coagulating process. As shown in Figure 5.16(a), with no air gap distance, the hexagonal fibre is expected to coagulate before the die swell is completed. However, with a longer air gap distance, die swell may be counteracted by gravitational effects, as shown in Figure 5.16(c) and 5.16(e). It can also be observed that the hexagonal hollow fibre with a 0mm air gap has a higher loading of 13X zeolite (Figure 5.16(b)), while the 1mm and 5mm air gap hollow fibres has a slightly lower 13X zeolite loading (Figure 5.16(d) and Figure 5.16(f)), which can lead to poor kinetics for adsorption.

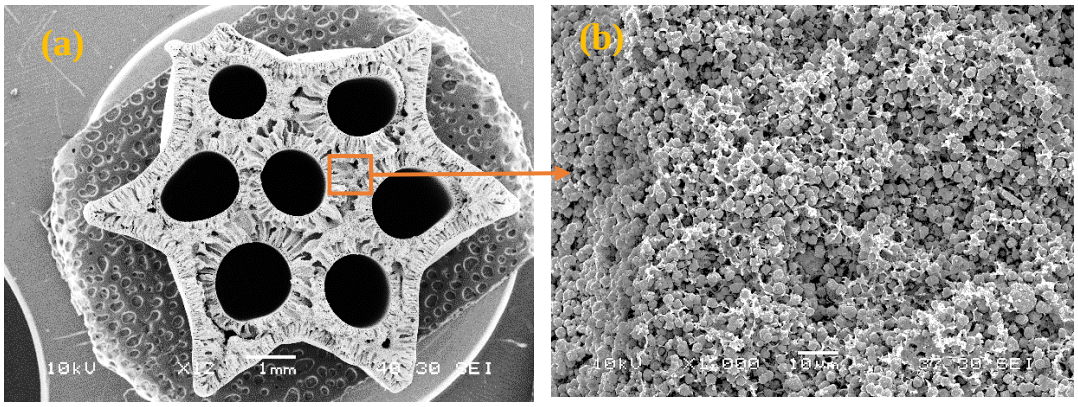

(a) Cross-section of 83 wt% 13X hexagonal hollow fibre (HAHF 1), x12 and x1000

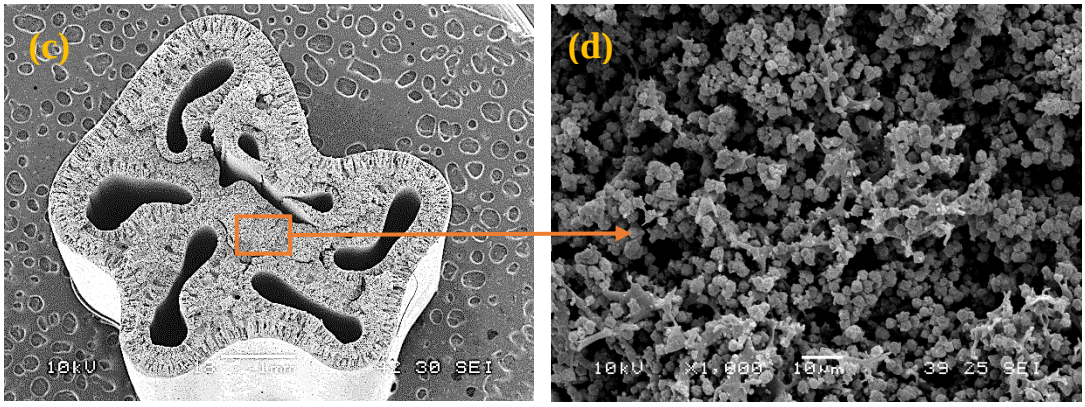

(b) Cross-section of 83 wt% 13X hexagonal hollow fibre (HAHF 2), x18 and x1000

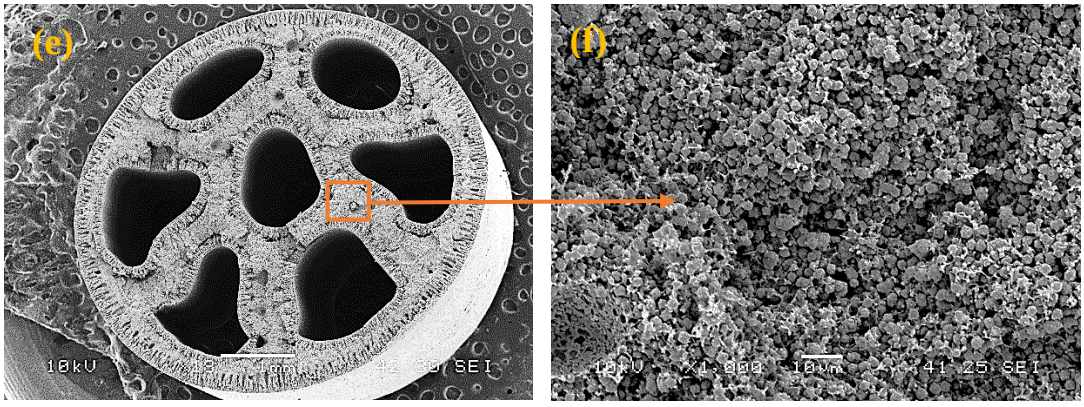

(c) Cross-section of 83 wt% 13X hexagonal hollow fibre (HAHF 3), x18 and x1000

Figure 5.16. Scanning electron micrographs of hexagonal hollow fibres (83 wt% 13X: 17 wt% PESF) at different air gap distances in the range of (a) 0mm (b) 1mm and (c) 5mm.

5.2.7.3 Nitrogen adsorption isotherm

To confirm the observations from the dynamic breakthrough challenge and scanning electron microscopy, nitrogen adsorption isotherms at 77K were determined for different air gap hexagonal adsorbent hollow fibres. Figure 5.17 shows the higher

nitrogen uptake by 0mm air gap fibre compared to 1mm and 5mm air gap fibres. In addition, it was determined that the BET surface areas for 0mm, 1mm and 5mm air gap hexagonal hollow fibres were approximately 449.7, 405.8 and 319.5 and m^2/g, respectively. Therefore, the lower porosity for the 5mm air gap hexagonal fibre suggests that the fibre spinning process reduces the accessibility of adoption sites. This was confirmed by the dynamic breakthrough study and SEM.

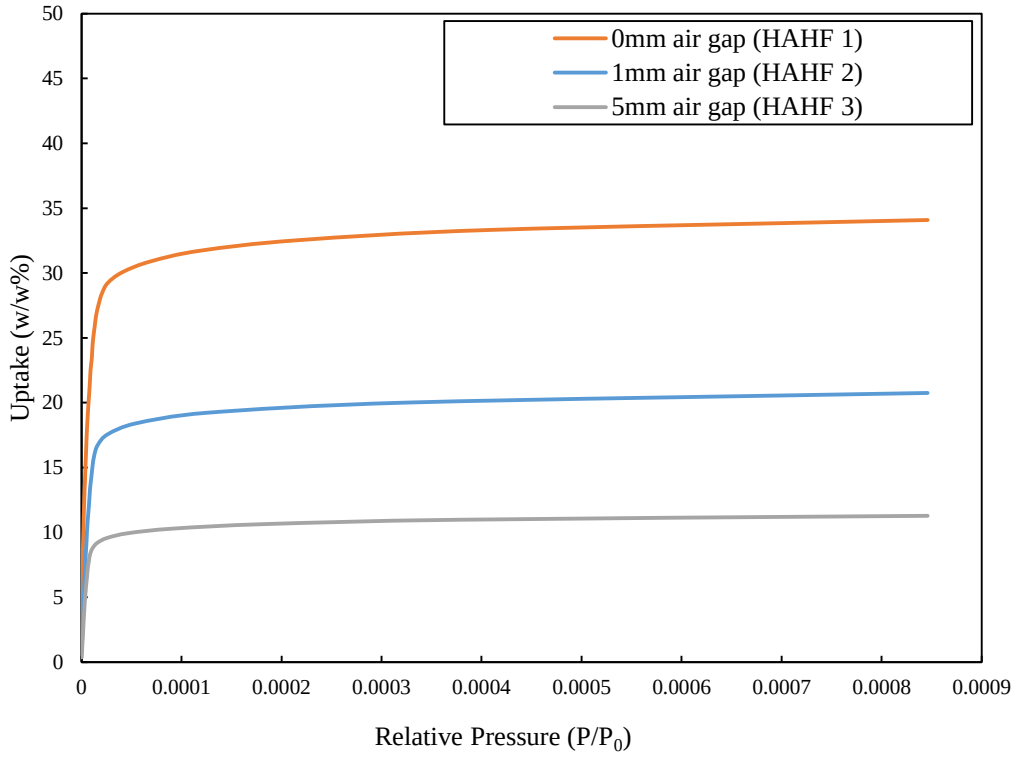

Figure 5.17. N_2 adsorption isotherms at 77K for hexagonal adsorbent hollow fibres (83 wt% 13X: 17 wt% PESF) at different ranges of air gap distances.

5.2 Summary

Novel tri-lobe multi-channel adsorbent hollow fibres have been manufactured successfully. Adsorption of N_2 and scanning electron microscopy both confirm the highly porous structure of 13X zeolite with a higher surface area of about 560.5 m^2/g for tri-lobe fibres compared to single adsorbent hollow fibres using the same PESF/13X/NMP mixture compositions. This is in line with physical reasoning, which predicts that higher adsorbent loading causes an effective surface area, creating good access to adsorption sites. In addition, it was found that adsorption capacity reached 10.9% in the breakthrough study for tri-lobe three-bore hollow fibres, compared to the

adsorption capacity of single hollow fibres (6.2%) of equivalent weight under adsorbent and experimental conditions. A further important point is that the pressure drop for tri-lobe adsorbent hollow fibres is much lower than for single adsorbent hollow fibre. Moreover, it was found that the tri-lobe hollow fibres showed improved mechanical properties compared to single adsorbent hollow fibres. This study has therefore confirmed that tri-lobe three-bore adsorbent hollow fibres would act as promising novel hollow fibres for the removal of toxic gases.

From these results, general optimisations of the adsorption capacity and shapes of tri-lobe hollow fibres can be made. The adsorption breakthrough loading increases with an increase in the concentration of 13X zeolite. However, considering the results for different mechanical properties and the adsorption capacity for the tri-lobe hollow fibres, the sample with 83 wt% 13X is a good tri-lobe hollow fibre to use in any additional examination of the dynamic adsorption of VOCs. In addition, the breakthrough time and equilibrium loading of the tri-lobe hollow fibres have been shown to decrease as the bore fluid flow rate increases; the bore fluid with a 6 ml/min flow rate passes through the bores very quickly without allowing the required time to create a porous structure.

The adsorption experiments of n-butane with hydrophobic tri-lobe hollow fibres show that HiSiv 1000 and HiSiv 3000 have good adsorption affinity for the hydrocarbon. It is concluded that both hydrophobics are potential adsorbents for the removal of VOCs.

Hexagonal 13X/PESF composite hollow fibres containing 83 wt% 13X zeolite were successful produced using a wet/wet spinning process. A novel hexagonal hollow fibre consisting of seven bores has been proposed to recover VOC molecules from gas streams. Adsorptions of n-butane reveals that hexagonal hollow fibres have good adsorption performance for small hydrocarbons (n-butane). Comparing the breakthrough curves, SEMs and nitrogen isotherms of different air gap hexagonal hollow fibres, it may be concluded that the higher equilibrium loading of 0cm air gap hexagonal hollow fibre indicates a superior kinetic performance due to a higher surface area (449.7 m^2/g) compared to the other hexagonal hollow fibres.

Therefore, it is concluded that the addition of channel (bores) in adsorbent hollow fibres for gas separation is an effective way of improving adsorption performance, kinetic performance and mechanical properties in a cost-effective manner.

Chapter 6: Modelling and Simulation of Adsorbent Hollow Fibres

Computational fluid dynamics (CFD) can be used to model, analyse complex systems involving mass transfer and fluid flow. Here, CFD is employed to solve the momentum and mass conservation equations described by partial differential equations (PDEs). CFD can reduce production time and costs in comparison with experiments and offers the ability to make predictions and study a range of complex flow problems where the analytical method is lacking (Tu *et al.*, 2012). Several studies have used CFD to predict experimental results in hollow fibre membranes (Barati *et al.*, 2014; Miramini *et al.*, 2013; Razavi *et al.*, 2013). Although CFD has been widely used in the simulation and modelling of several applications.

In this work, the fluid flow and mass transfer characterises of adsorbent hollow fibres have been simulated using a computational modelling package, COMSOL Multiphysics ver. 5.2. The simulation studies attempted to uncover the effect of hollow fibre geometries in order to predict their adsorption capacity and mass transfer mechanism. This study also examined some hollow fibres parameters as a result of the lack of readily available information, such as effective diffusivity, diffusivity and adsorption rate coefficient in order to improve the hollow fibre designs. The CFD technique is useful for predicting the mass transfer mechanisms of hollow fibres. It was not easily compared between computational and experimental findings. However, some of the simulation results showed the same trends of experimental results in the breakthrough curves.

6.1 Setting up the CFD model

COMSOL software was used to solve mass transfer and momentum equations. Figure 6.1 shows the steps taken in the modelling.

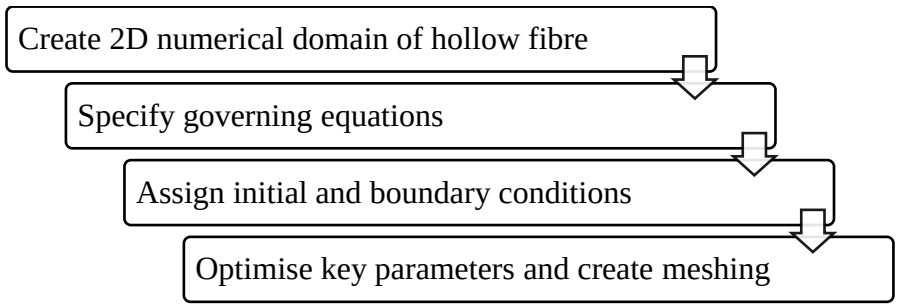

Figure 6.1. Flow chart of CFD steps

6.1.1 Numerical domain

The computational domain refers to simplified form of the physics geometry both in terms of geometrical representation and boundary condition imposition. In the adsorbent hollow fibre, the flow domain was divided into two domains, which can be seen in Figure 6.2. Domain 1 defined the mass transfer of fluid flow and the rate of change of the gas (n-butane) concentration through the bores (lumen) of hollow fibres. The type of fluid flow in domain 1 was assumed laminar flow effects throughout. In this domain, mass transfer of the fluid flow was dependent on convective and diffusive. In domain 2, the mass transfer through the porous media was dependent on both diffusive and adsorptive, due to the non-existence of fluid flow. Figure 6.2 also shows the governing equations solved in both domains.

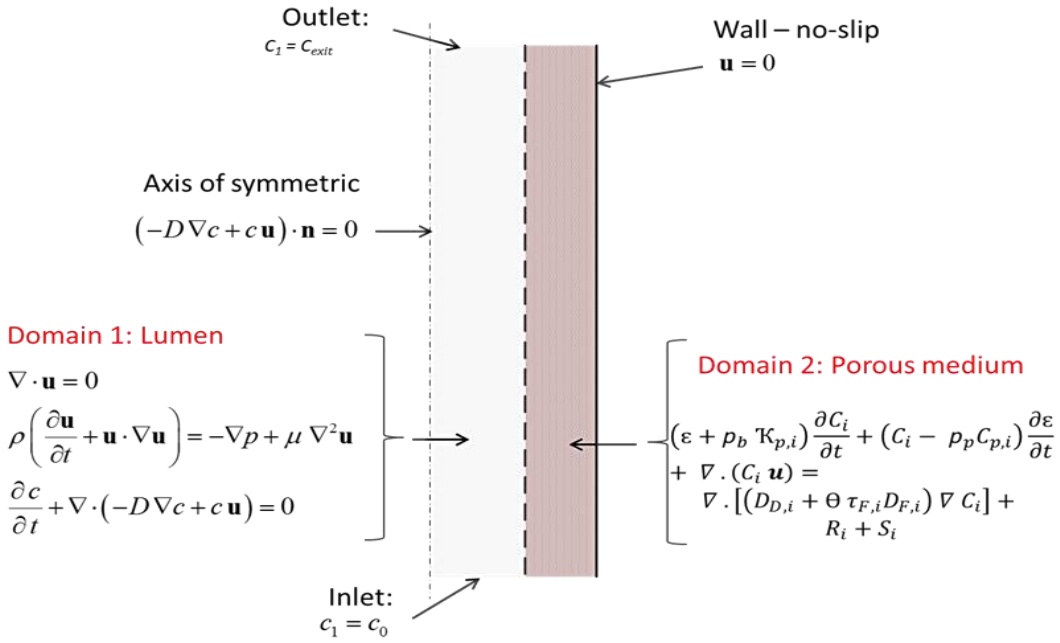

Figure 6.2. 2D representation of the computational domain and governing equations of single adsorbent hollow fibre module. Domain 1: lumen media; Domain 2: porous media.

6.1.2 Governing equations

CFD was used to solve the governing equations using COMSOL Multiphysics. These equations can be used to describe VOC adsorption using hollow fibres in both domains. Mass transfer occurs in three main steps according to the fluid-transport mechanism in adsorbent hollow fibres, specifically:

1. convection of the gas in the lumen of the hollow fibre
2. diffusion into the lumen and through the porous media
3. adsorption from the interface to the pore of the porous material.

- Gas flow into the bore of the hollow fibre (domain 1)

The continuity equation was solved to simulate the gas flow through the bore (domain 1) of the hollow fibre. This equation can be written as:

$$\frac{\partial \rho}{\partial t} + \nabla . (\rho \mathbf{u}) = 0 \qquad (6.1)$$

where ρ is fluid density and $\mathbf{u}$ is velocity vector. Assume ρ =constant, since pressure used is moderate.

To describe the momentum transfer of fluid, the Navier-Stokes equation was solved using two dimensions. The gravitational term is negligible, since the flow is pressure driven. The Navier-Stokes equation is given as follows:

$$\rho \frac{Du}{Dt} = \rho \left(\frac{\partial u}{\partial t} + u . \nabla u \right) = -\nabla p + \mu \nabla^2 u + \rho g \qquad (6.2)$$

where u is the fluid velocity p is pressure, μ is fluid viscosity and g is acceleration due to gravity.

The species transport equation can be written as follows:

$$\frac{DC}{Dt} = \frac{\partial C}{\partial t} + u . \nabla C - D \nabla^2 C = R \qquad (6.3)$$

where; C is the VOC concentration, R is the fluid phase concentration source term and D is the diffusion coefficient

- Gas flow through porous media

The species transport in porous media equation is used to investigate adsorption and diffusion in porous media. It is also known as the mobile (VOC gas) – immobile (porous material) equation. It involves adsorption, convection, dispersion, diffusion, reaction and source terms. This equation can be written as

$$\left(\varepsilon + \rho_b\, k_{p,i}\right)\frac{\partial c_i}{\partial t} + \left(c_i - \rho_p\, c_{p,i}\right)\frac{\partial \varepsilon}{\partial t} + \nabla . (c_i\, \mathbf{u}) = \nabla . \left[\left(D_{D,i} + \Theta\, \tau_{F,i}\, D_{eff,i}\right)\nabla\, c_i\right] + R_i + S_i \qquad (6.4)$$

where; ε is the porosity, ρ_b is the bulk density $k_{p,i}$ is constant which equal to k_a/k_d , c_i is the concentration of VOC, $D_{D,i}$ is the dispersion tensor, Θ is the volume fraction, is $\tau_{F,i}$ is the tortuosity factor, $D_{eff,i}$ is the effective diffusion, R_i is the reaction term and S_i is the source term.

On the left hand side of equation 6.4, the last term ($\nabla . (c_i\, \mathbf{u})$) introduces the convection which describes the movement of a gas in lumen media, whereas the first and second terms ($\left(\varepsilon + \rho_b\, k_{p,i}\right)\frac{\partial c_i}{\partial t} + \left(c_i - \rho_p\, c_{p,i}\right)\frac{\partial \varepsilon}{\partial t}$) describe the adsorption where the gases travel through the porous matrix. On the right hand side, the first term ($\nabla . \left[\left(D_{D,i} + \Theta\, \tau_{F,i}\, D_{F,i}\right)\nabla\, c_i\right]$) describes the spreading of mass, as gas travel through porous matrix, as well as the diffusion effective in porous media. R_i introduces the reaction rate which can account for reactions in gas or solid phase. S_i corresponds source term due to sink or fluid flow.

6.1.3 Boundary conditions

Table 6.1 shows the boundary conditions of adsorbent hollow fibre modules. These boundary conditions were applied in all simulations.

Table 6.1: Boundary conditions of the adsorbent hollow fibre model.

Initial conditions, at t = 0	C_0= 0 (Concentration of species (mol/m^3) in domain 1) u = 0 (Parabolic velocity (m/s)) C= 0 (Concentration of species (mol/m3) in domain 2)
Inlet conditions	C_0= 1000 ppm = 0.0428 mol/m^3
• Assumed 2-D axisymmetric, so only half of a single hollow fibre has been considered. • Axisymmetric – assumes that no materials or fluid flow through the boundary and no slip through wall.	

6.1.4 Mesh testing

Domain 1 and domain 2 were provided by a finite element grid (mesh). The points where these elements meet are called nodes. COMSOL software solves partial differential equations (PDEs) between these nodes. The accuracy of mixtures depends

on the number of mesh points, whereby an increase in mesh points leads to a more accurate mixture. Therefore, it was necessary to optimise certain parameters that would affect the accuracy of the numerical mixture. Mesh size and mesh shape are examples of these parameters. At this stage, the mesh shape was tested as a free triangular and quadrilateral, while the size of the mesh was tested, both fine and extra fine mesh sizes.

The mesh shape affected the breakthrough and equilibrium time of the breakthrough curve. Figure 6.3 shows the triangular mesh and quadrilateral mesh of the single adsorbent hollow fibre model using the same key parameters. It was found that the number of elements in triangular shape was greater. However, the breakthrough time and equilibrium time in the model with a quadrilateral mesh shape was almost the same as the model with a triangular mesh shape, as shown in Figure 6.4. This means that the difference between the two mesh shapes is negligible in breakthrough study within the model. Therefore, the triangular mesh shape was selected for this study due to the higher number of elements.

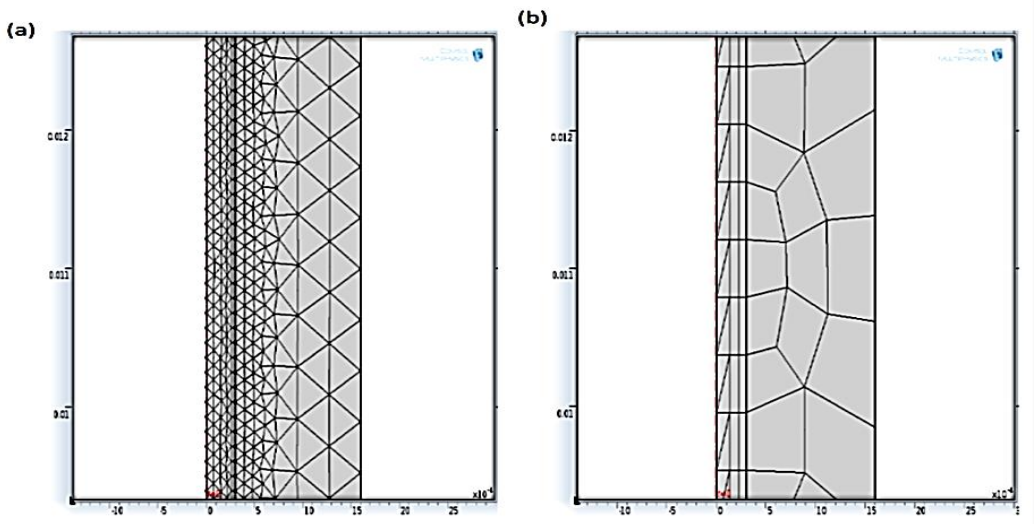

Figure 6.3. Single adsorbent hollow fibre model with (a) triangular mesh shape and (b) quadrilateral mesh shape.

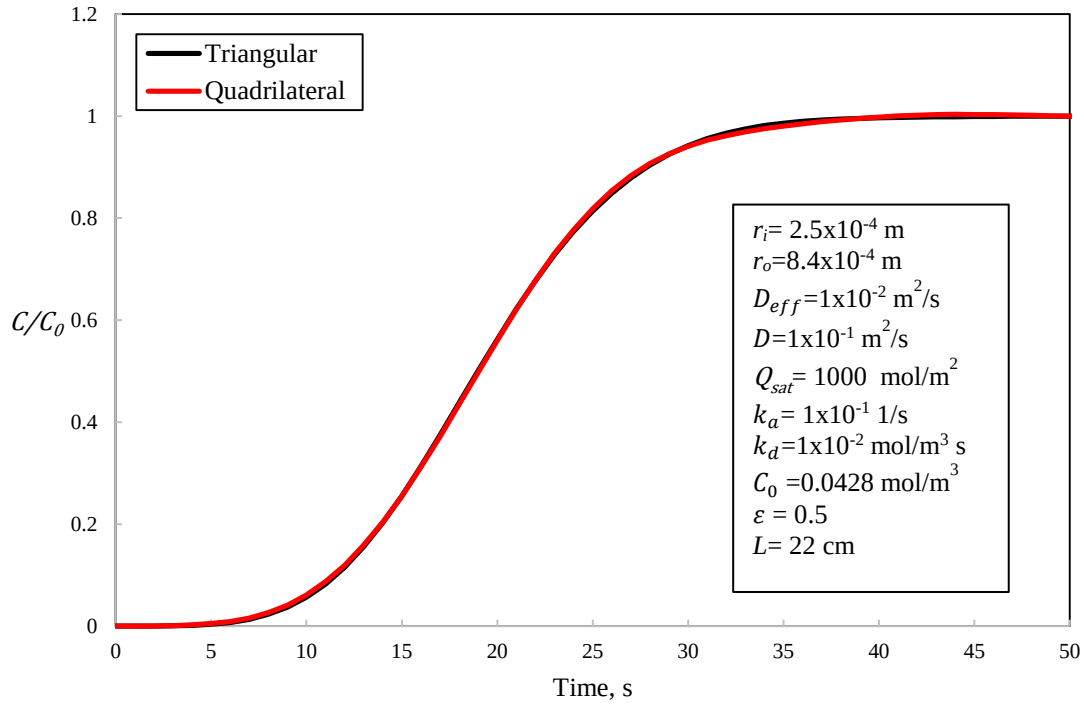

Figure 6.4. Breakthrough curves of single adsorbent hollow fibre models as a function of mesh shapes.

It was also discovered that changing the size of the mesh significantly affected the computed equilibrium time and breakthrough time. The four mesh size mentioned below (normal, fine, extra fine and extremely fine) were tested. The different mesh sizes fitted to the single adsorbent hollow fibre model are shown in Figure 6.5.

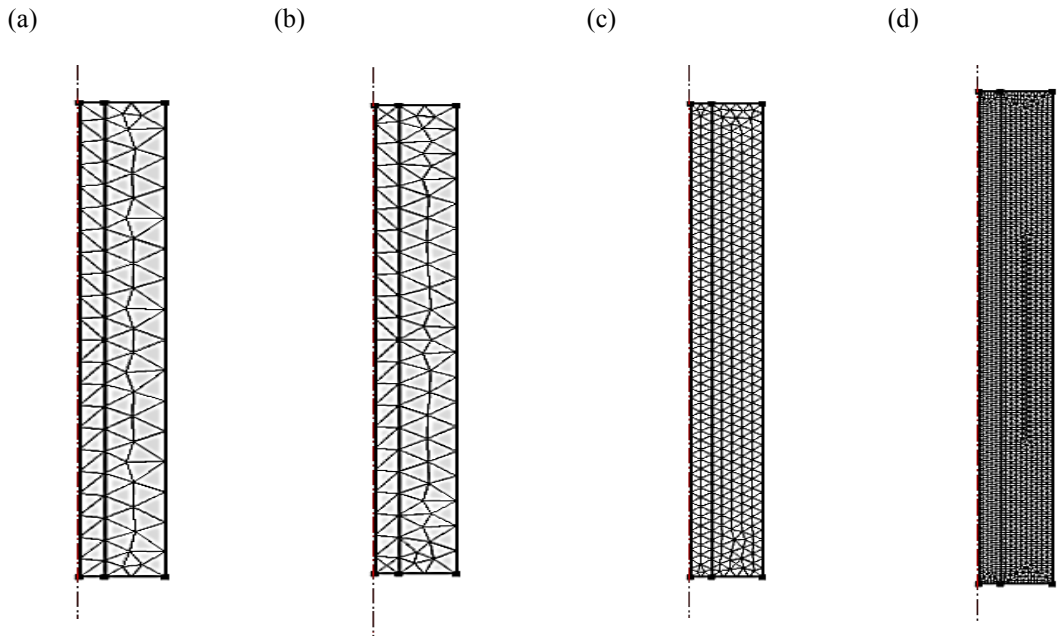

Figure 6.5. (a) Normal triangular mesh size for hollow fibre model, (b) Fine triangular mesh, (c) Extra fine and (d) extremely fine triangular mesh size.

Figure 6.6 shows that with the normal and fine mesh size the equilibrium time and breakthrough time are computed to be larger than the extra and extremely fine mesh size range. It was computed that for the extremely fine mesh size, the breakthrough and equilibrium times were 2 s and 6 s respectively. This was faster than the breakthrough time and equilibrium time for other mesh sizes. However, only 89 elements were solved with the normal mesh size, whereas 1672 elements were solved with the extremely fine mesh size, which can enhance the accuracy of numerical solutions. Therefore, although the time required to compute the extremely fine mesh size was much greater than that required to compute the normal mesh, an extremely fine mesh was accepted for use in this research.

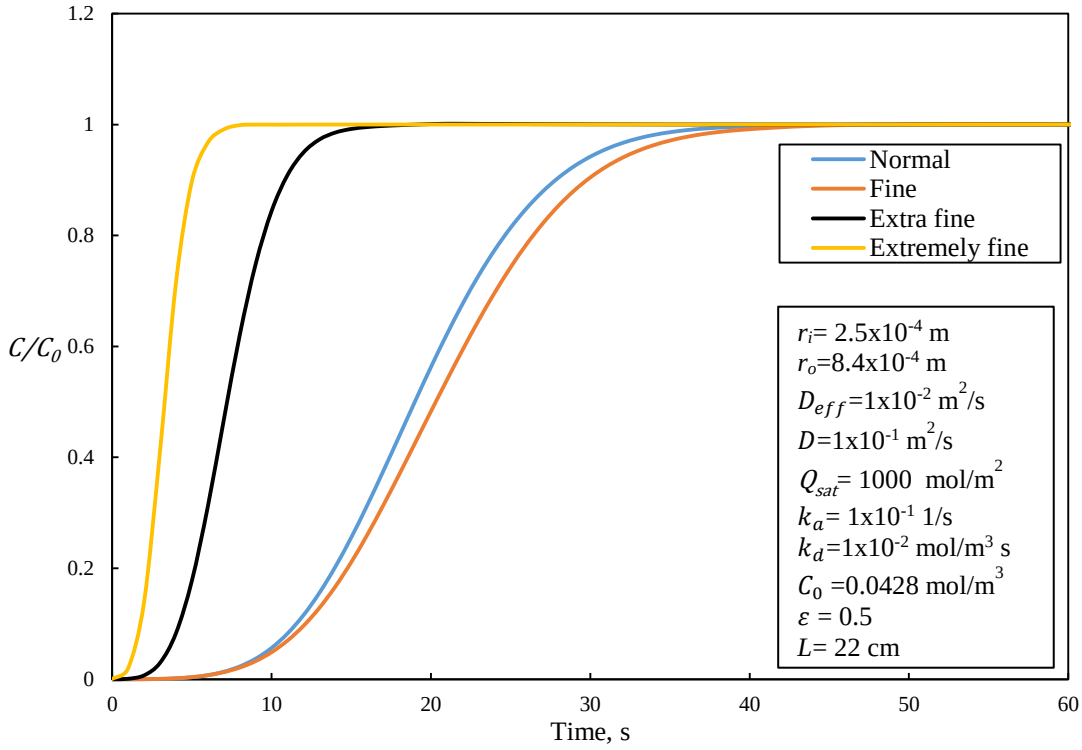

Figure 6.6. Breakthrough curves of single adsorbent hollow fibre models as a function of mesh size.

6.2 Testing of key parameters

In this research, each model that was created was run under isothermal conditions at 293.15 K, with a reference pressure of 101.3kPa. For the initial hollow fibre models, the dimensions of the fibres were obtained from work carried out in the laboratory. One of the aims of developing the model was to compare the results obtained from experimental data, as a method of validating the model. Ideally, this would have meant inputting mass transfer and kinetic parameter values obtained from adsorbent hollow

fibre analysis, and comparing the model's concentration profiles and breakthrough curves with those obtained experimentally. However, there was very limited data available that was specific to adsorbent hollow fibres, particularly kinetic constants and mass transfer parameters. It was thus difficult to determine these parameters at this stage of the research; however, breakthrough curves and isotherms have been determined, and so it was decided that the model would be tested over a range of values.

The key parameters were: adsorption capacity, diffusivity, effective diffusivity, desorption rate coefficient, and adsorption rate coefficient. These parameters were selected as they have a significant influence on the breakthrough curves, which are associated with kinetic and mass transfer considerations. Diameters of adsorbent hollow fibre, length, porosity, volumetric flow rate, and initial concentration of gas were assumed constant when testing the model. Each key parameter was tested over a range of values in order to observe breakthrough and equilibrium times. Table 6.2 lists the range of values tested for all of the parameters.

Table 6.2: Computational Parameters of single Adsorbent Hollow Fibre model used for mesh testing

Parameter	Unit	Values
Adsorption Rate Coefficient, K_a	1/s	$1x10^{-1}$, 1, 10
Desorption Rate Coefficient, K_d	mol/m^3 s	1, $1x10^{-2}$, $1x10^{-3}$
Adsorption Capacity, Q_{sat}	mol/m^2	500, 1000, 1500
Diffusivity, D	m^2/s	1, $1x10^{-1}$, $1x10^{-2}$
Effective Diffusivity, D_{eff}	m^2/s	$1x10^{-2}$, $1x10^{-3}$, $1x10^{-4}$

6.2.1 Adsorption rate coefficient

From observing the trend in adsorption rate coefficient test data points, as shown in Figure 6.7, it was found that the breakthrough time and equilibrium time increased as the adsorption rate coefficient increased. One explanation for this result could be that this was a result of the different values having an influence on the accuracy of the modelling solutions. On the other hand, if the difference was a result of the physics of the model then this could be because the adsorption rate was balanced with the desorption rate, producing breakthrough curves with maximum breakthrough times. Therefore, it was decided that the best adsorption rate coefficient value to obtain an

optimal breakthrough curve was 1x10^{-1} 1/s where there was a sharp breakthrough curve with low mass transfer resistance.

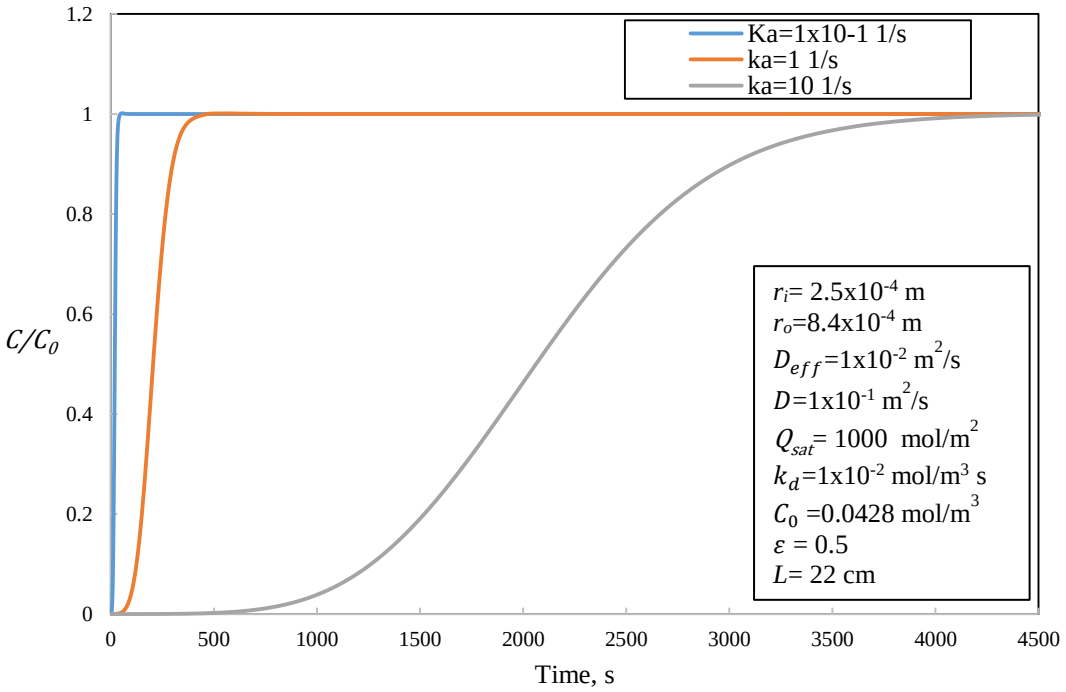

Figure 6.7. Breakthrough curves of single adsorbent hollow fibre models as a function of adsorption rate coefficient in the range of 1x10^{-1}, 1 and 10 mol/m^3 s.

6.2.2 Desorption rate coefficient

Since the desorption rate coefficient values are related to the adsorption rate coefficient values, the maximum breakthrough time obtained should have been specific to the corresponding adsorption rate coefficient values. Figure 6.8 shows that the breakthrough time and equilibrium time increased as desorption rate coefficient decreased; this trend was expected, since a decreasing desorption rate for a constant adsorption rate would cause faster desorption and so later breakthrough. This could be also due to the desorption rate dominating the kinetics, which means that fast desorption may cause less mass transfer and breakthrough taking place much faster.

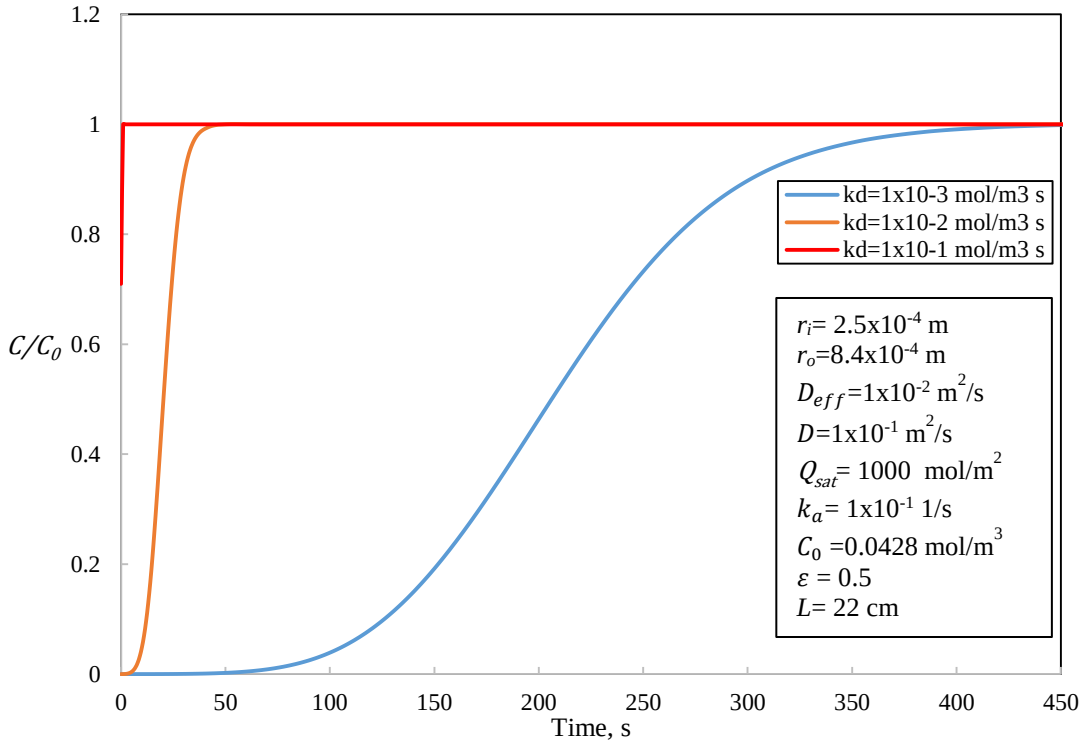

Figure 6.8. Breakthrough curves of single adsorbent hollow fibre models as a function of desorption rate coefficient in the range of 1x10^{-3}, 1x10^{-2} and 1x10^{-1} 1/s.

6.2.3 Adsorption capacity

As the adsorption capacity was increased, it was found that the equilibrium time and breakthrough time increased, which can be observed in Figure 6.9. There was clearly no optimal value for the adsorption capacity. Generally, a large adsorption capacity was required in the adsorbent hollow fibres. However, a very large adsorption capacity may have a negative influence on the system and cause difficulty with regard to the regeneration of the hollow fibre.

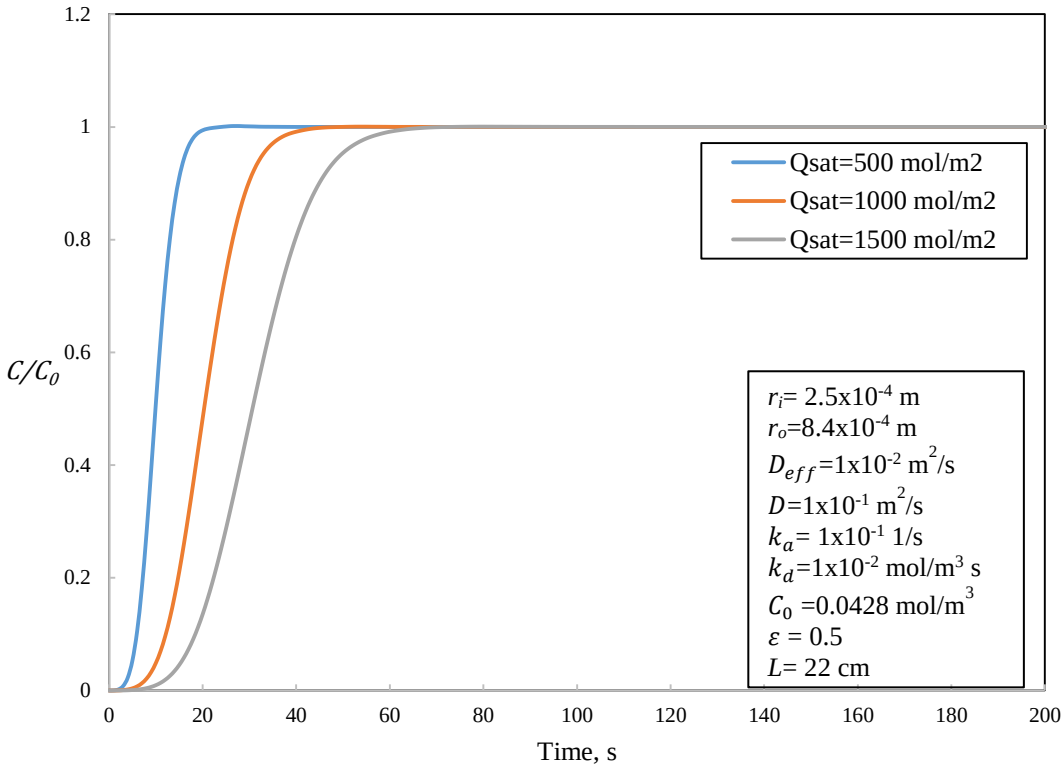

Figure 6.9. Breakthrough curves of single adsorbent hollow fibre models as a function of adsorption capacity in the range of 500, 1000 and 1500 mol/m^2.

6.2.4 Diffusivity

It was found that the diffusivity value has a similar effect on the breakthrough curve to the adsorbent hollow fibre when the values were equal to 1x10^{-1} and 1x10^{-2} m^2/s, which can be clearly seen in Figure 6.10. However, it can also be seen that for diffusivity values lower than 1x10^{-2} m^2/s, the breakthrough curve lost its normal 'S' shape. Therefore, it was decided that the diffusivity value should be equal to or higher than 1x10^{-2} m^2/s.

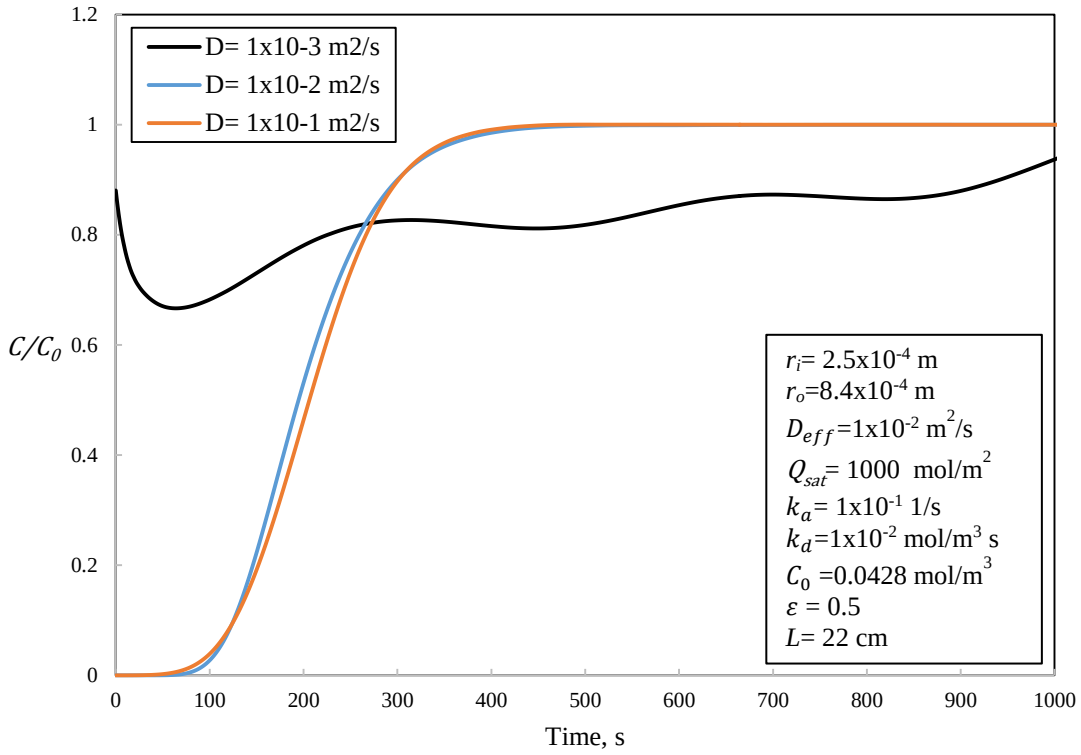

Figure 6.10. Breakthrough curves of single hollow fibre models as a function of diffusivity in the lumen media in the range of $1x10^{-3}$, $1x10^{-2}$ and $1x10^{-1}$ m^2/s.

6.2.5 Effective diffusivity

In this testing, all breakthrough curves have a similar shape due to the similar breakthrough time and equilibrium time, according to the results plotted in Figure 6.11. However, it was the fact that the value of effective diffusivity should be smaller than the value of diffusivity to allow the diffusion process occurs on the simulation. Therefore, the value of effective diffusivity should be smaller than the value of diffusivity.

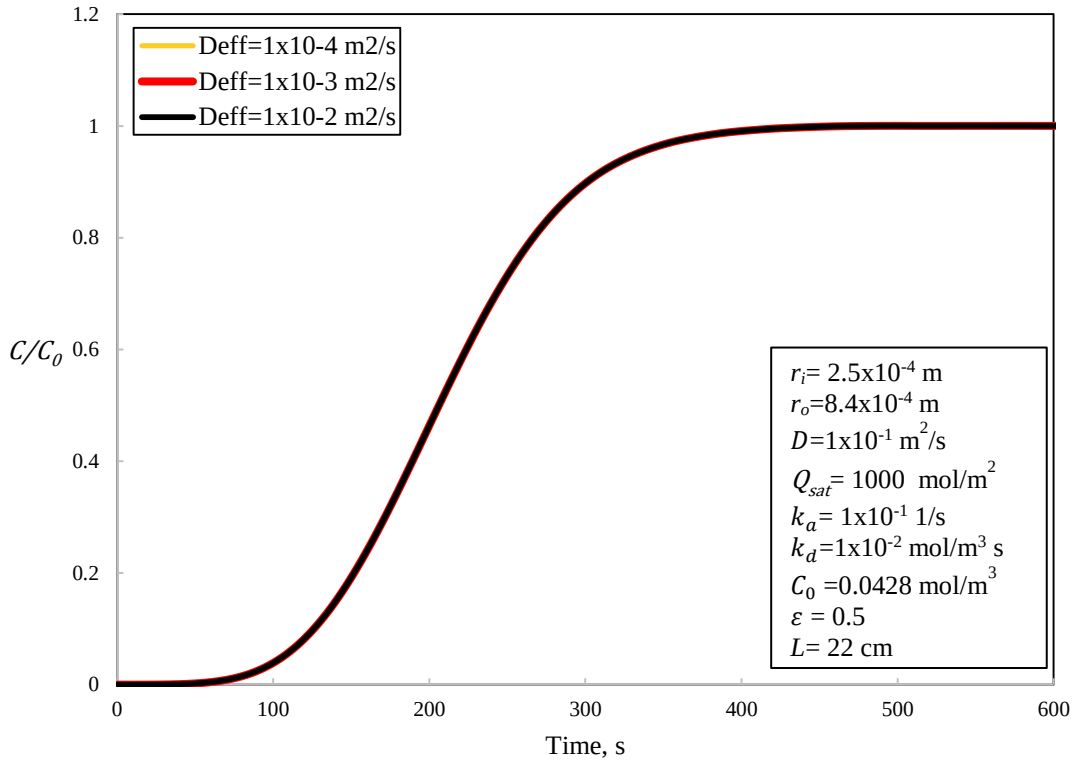

Figure 6.11. Breakthrough curves of single adsorbent hollow fibre models as a function of effective diffusivity in the porous media in the range of 1x10^{-2}, 1x10^{-3} and 1x10^{-4} (m^2/s).

From the testing study, therefore, it was decided that the key parameters of single adsorbent hollow fibre are shown in Table 6.3. The values of these key parameters will be used in the next sections.

Table 6.3: Computational Parameters of single Adsorbent Hollow Fibre model.

Parameter	Symbol	Unit	Value
Outer radius	r_o	m	1.60 x10^{-3}
Inner radius	r_i	m	3.00 x10^{-4}
Length	L	cm	22
Temperature	T	298.15	298.15
Pressure	P	atm	1
Density of n-butane	ρ	kg/m^3	2.48
Dynamic viscosity OF n-butane	μ	Kg/m.s	6.7x10^{-6}
Volumetric Flow Rate	Q	l/min	1
Initial Concentration	C_0	mol/m^3	0.0428
Adsorption Rate Coefficient	k_a	1/s	1.00 x10^{-1}
Desorption Rate Coefficient	k_d	mol/m^3 s	1.00 x10^{-2}
Adsorption Capacity	Q_{sat}	mol/m^2	1000
Diffusivity	D	m^2/s	1x10^{-1}
Effective Diffusivity	D_{eff}	m^2/s	1x10^{-2}

6.3 Simulation 1: Comparison of the adsorption performance of various values of inner radius of circular hollow fibre

This simulation was carried out to assess how the inner radius of single adsorbent hollow fibre affected adsorption performance.

6.3.1 Description

This simulation was used to predict the effect of inner radius on adsorption performance. The domains that were used in the simulation are shown in Figure 6.1.

The stationary parameters were used in this simulation are shown in Table 6.3 excluding the values of the inner and the outer radius.

It should be noted that the outer radius was calculated using Equation 6.5, as the volume of the porous matrix should be maintained. Table 6.5 shows the varied parameters used in this simulation. The Reynolds Number (Re) can be calculated using

Equation 6.6. The governing equations and boundary conditions used to solve this simulation are described in Sections 6.2.2 and 6.2.3 respectively.

$$\text{Volume of porous matrix} = \pi L(r_o^2 - r_i^2) \qquad (6.5)$$

$$Re = \frac{\rho u d}{\mu} = \frac{4\rho Q}{\pi \mu d} \qquad (6.6)$$

Table 6.4: Varied parameters of single adsorbent hollow fibres.

Inner radius (m)	**Outer radius (m)**	**Perimeter (m)**	**Volume of porous matrix (m^3)**	**Volume of bore (m^3)**	***Re***
0.0004	0.0016	0.0025	$1.6x10^{-6}$	$1.1x10^{-7}$	9843
0.0006	0.001663	0.0037	$1.6x10^{-6}$	$2.5x10^{-7}$	6562
0.0008	0.001745	0.0050	$1.6x10^{-6}$	$4.4x10^{-7}$	4921
0.001	0.001845	0.0062	$1.6x10^{-6}$	$6.9x10^{-7}$	3937
0.0012	0.00196	0.0075	$1.6x10^{-6}$	$9.9x10^{-7}$	3281

6.3.2 Results and discussions

The difference in the single adsorbent hollow fibre radius has a significant effect on the mass transfer coefficient, the pressure drop through the length of the geometry, and average fluid velocity. Figures 6.11 and 6.12 show the breakthrough times and the pressure drop across all models.

Figures 6.12 and 6.13 show that the breakthrough time reduced as the inner radius increased. This could be as a result of reducing the surface area where mass transfer could take place. Therefore, a lower rate of mass transfer can decrease breakthrough time. The Reynolds Number can be used to describe this effect. For a constant value of Q, ρ, L and μ, if the inner radius increases, the gas velocity through the bore decreases, and the Re decreases. Therefore, because of this model test, the most interesting finding was that two mechanisms affected the breakthrough time and mass transfer. The first mechanism was the result of the effect of the increased fluid velocity as the radius decreased. The second mechanism took place in the small inner radius, which influences the surface area. At the large inner radius, the gas velocity through the bore of adsorbent hollow fibre determined the rate of mass transfer by reducing the residence time of mass transfer from the lumen to the interface, which was not fast enough. Thus, it can reduce the breakthrough time.

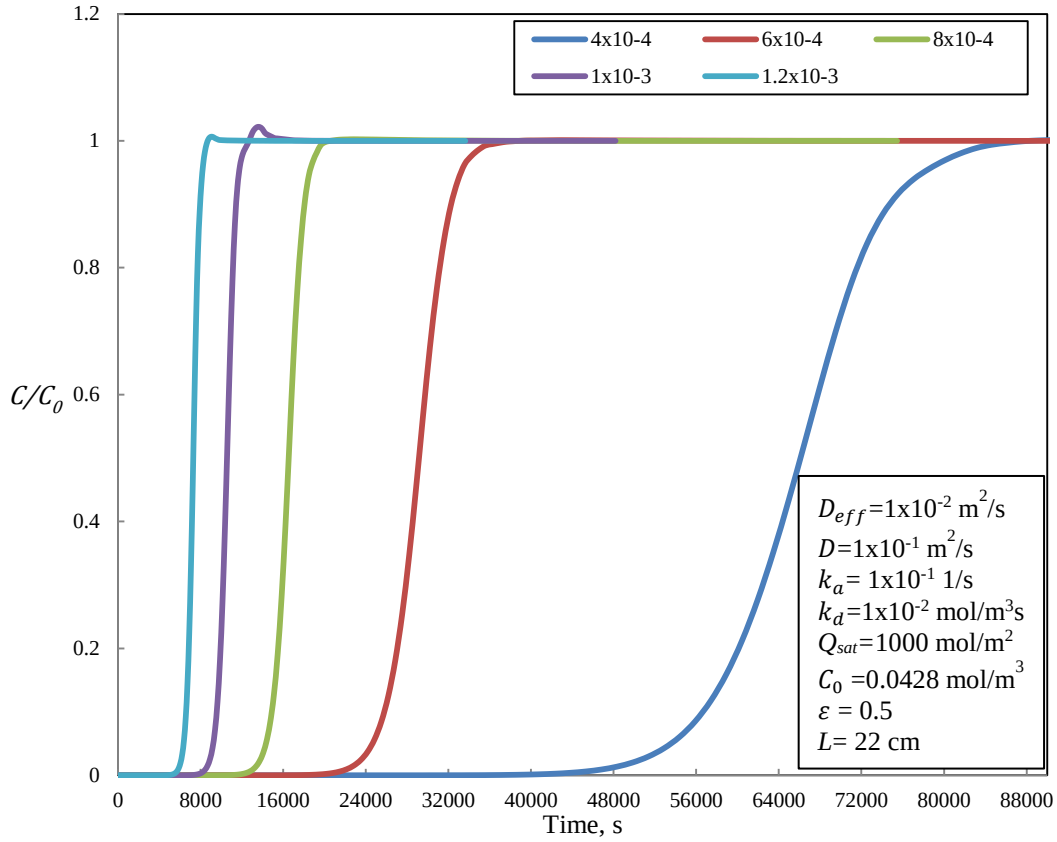

Figure 6.12. Breakthrough time for various values of inner radius between 4x10^{-4} and 1.2x10^{-3} m.

Figure 6.13 also shows that the pressure drop decreased as the bore radius increased. For this result, the Hagen-Poiseuille Equation (Equation 2.15) was used to determine the pressure gradient. It was found that the pressure drop was reduced as the inner radius of hollow fibre increased; between 4 x10-4 and 7.00 x10-4 m, the pressure drop decreased rapidly but between 8.00 x10^{-4} and 1.2 x10^{-4} m, it decreased gradually. This could be as a result of non-laminar velocity profiles creating high fluid velocities and a small inner radius, which comes to be more laminar as the inner radius increases. The current study found that the pressure drops through the adsorbent hollow fibre reduce, in correlation with any increase in the inner radius of the hollow fibre. It is assumed that as a result of non-laminar flow taking place within a small inner radius, the velocity became large.

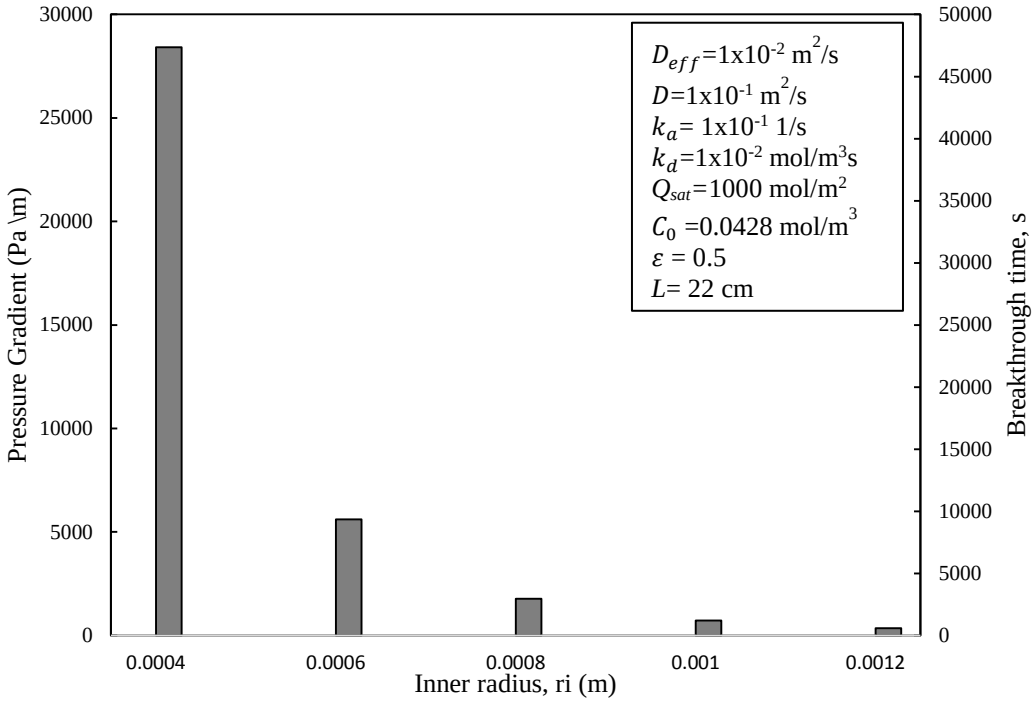

Figure 6.13. Pressure drop in adsorbent hollow fibres and Breakthrough time as a function of the inner radius between 4x10^{-4} to 1.2x10^{-3} m.

The breakthrough curve for the adsorption process in SAHF is shown in Figure 6.14. The n-butane was passed through the hollow fibre, where its concentration was changed by adsorption. These diagrams reveal that the adsorption of n-butane is achieved through modules, as indicated by the changing colours (mass transfer zone) with different heights at different times.

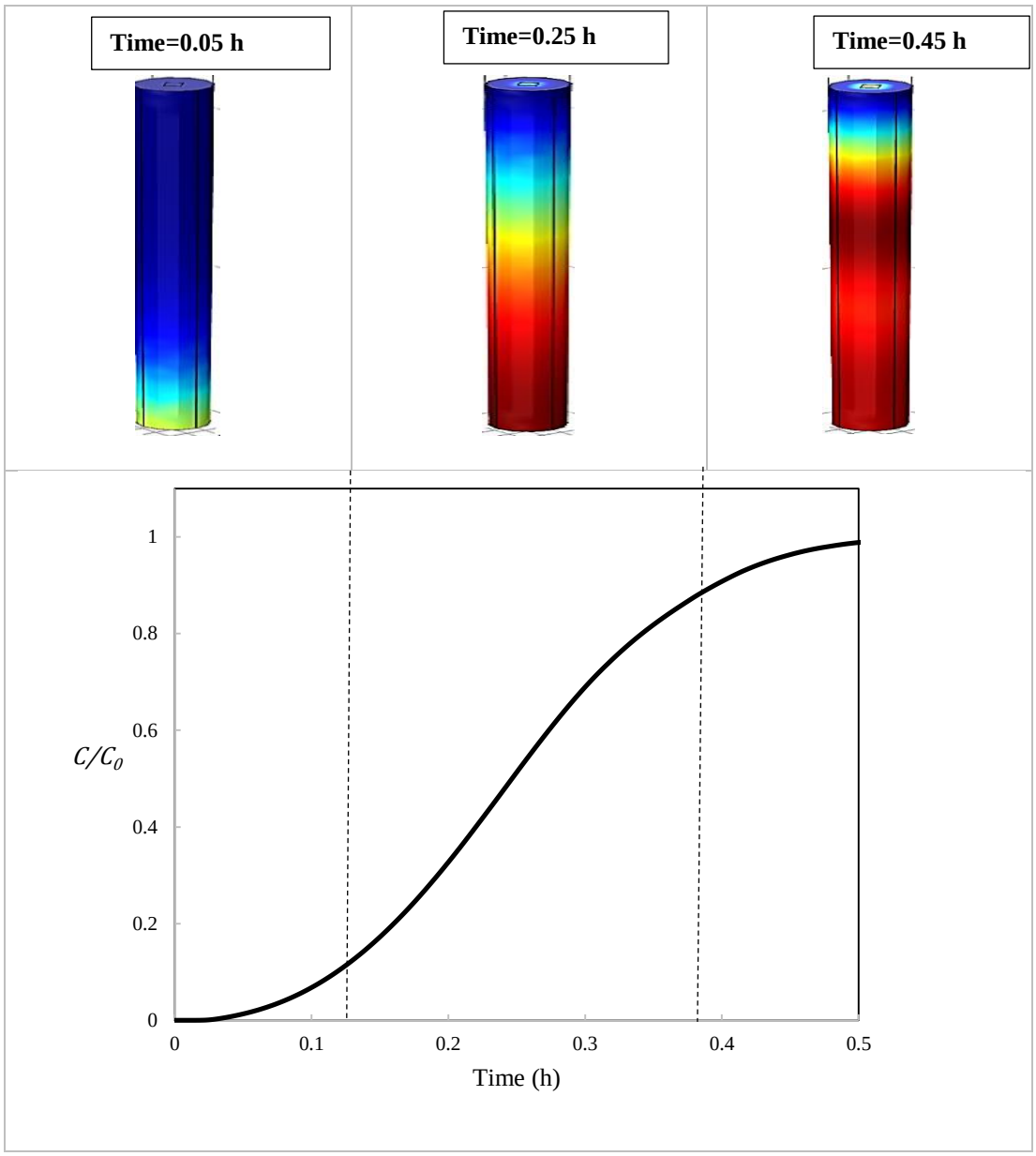

Figure 6.14. Breakthrough curve for single hollow fibre module viewing the movement of the mass transfer zone according to the time.

6.4 Simulation 2: Comparison of the adsorption performance of several adsorbent hollow fibre bore shapes

This simulation was proposed for gas adsorption through several adsorbent hollow fibre bore shapes. The parabolic velocity distribution was assumed for the gas flow in the bores of adsorbent hollow fibres. The feed gas was n-butane, and the porous matrix was a mix between the polymer and 13X zeolite. The procedure used to simulate the models is presented in the sections 6.4.1 and 6.4.2.

6.4.1 Description

All models were developed based on the following assumptions:

- The mass transport through the bore is laminar flow, isotherm Newtonian incompressible and steady state.
- The boundary condition of the wall is no slip.
- To compare with other bore shapes of adsorbent hollow fibres, the following parameters should be maintained:
    1. Volume of porous matrix
    2. Hydraulic diameter
    3. Density of gas
    4. Dynamic viscosity of gas
    5. Average velocity

In this study, the governing equations in the bore (Equation (6.1), Equation (6.2) and Equation (6.3)) as well as in the porous media (Equation 6.4)) were discretised based on the finite element method. For this purpose, COMSOL (5.2) was used to solve the governing equations and to identify the breakthrough time from breakthrough curves. Triangular shape meshes were generated by COMSOL.

The model domain of all models is shown in Table 6.5. As is shown, all models are divided into two sections: lumen (bore) and porous media. The feed gas was passed through the bore and diffused to the porous media. The equation for calculating the hydraulic diameter of each bore shape is also shown in Table 6.5.

Table 6.5 Computational domain and hydraulic diameter of different bore shape of adsorbent hollow fibre models.

Bore shape	2D computational domain of Adsorbent Hollow fibres	Hydraulic diameter
Circle	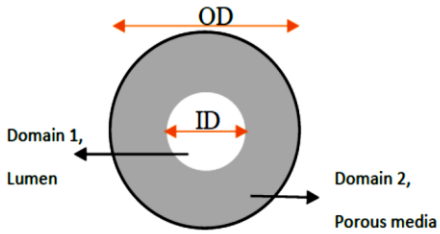	$D_h = \mathrm{ID}$
Cross	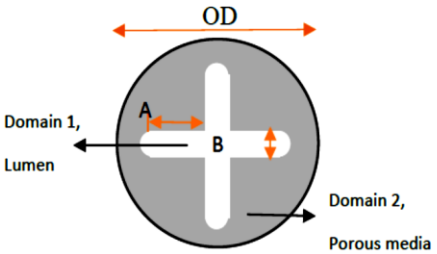	$D_h = \frac{4(4AB + B^2 + \frac{\pi}{2}B^2)}{2\pi B + 8A}$
Tri-lobe	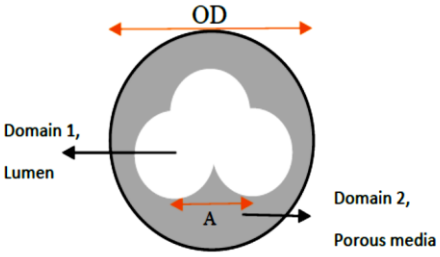	$D_h = \frac{4(\frac{1}{2}A^2 + \frac{\pi}{8}A^2 + \frac{3\pi}{16}A^2)}{\frac{6}{4}\pi A + \frac{\pi}{2}A}$

Since modelling was conducted for n-butane removal, the physical parameters used for the simulations were the same as those in Section 6.3.1. In order to achieve the same volume of the porous matrix for each model, the parameter dimensions were calculated, as shown in Table 6.6.

Table 6.6: Dimension and computational parameters of different bore shape of adsorbent hollow fibre models.

Shape	Circle	Cross	Tri-lobe
Inner Diameter (m)	0.0016	----	----
Outer diameter (m)	0.0035	0.004	0.004
Cross-sectional Area (m^2)	$2x10^{-6}$	$4.9x10^{-6}$	$4.3x10^{-6}$
Perimeter (m)	0.005	0.012	0.011
Hydraulic Diameter (m)	0.0016	0.0016	0.0016
Total Volume (m^3)	$2.1x10^{-6}$	$2.7x10^{-6}$	$2.6x10^{-6}$
Volume of shape (m^3)	$4.4x10^{-7}$	$1.1x10^{-6}$	$9.4x10^{-7}$
Volume of porous matrix (m^3)	$1.7x10^{-6}$	$1.7x10^{-6}$	$1.7x10^{-6}$
Effective Diffusivity (m^2/s)	$1x10^{-2}$	$1x10^{-2}$	$1x10^{-2}$
Diffusivity (m^2/s)	$1x10^{-1}$	$1x10^{-1}$	$1x10^{-1}$
Adsorption capacity (mol/m^2)	1000	1000	1000
Adsorption rate coefficient (1/s)	$1x10^{-2}$	$1x10^{-2}$	$1x10^{-2}$
Desorption rate coefficient (mol/m^3 s)	$1x10^{-1}$	$1x10^{-1}$	$1x10^{-1}$
Initial concentration (mol/m^3)	0.0428	0.0428	0.0428
Porosity	0.5	0.5	0.5
Length of fibre (cm)	22	22	22

6.4.2 Results and discussions

The breakthrough curves generated for the set of model equations from the mass balance through the different bore shape adsorbent hollow fibre modules are solved using COMSOL 5.2, as shown in Figure 6.15. The breakthrough times were greater in the case of the cross bore adsorbent hollow fibre modules (t_b= 7554 s) than in the case of tri-lobe (t_b= 1122 s) and circular (t_b= 3777 s) bore hollow fibre modules at the same volume of the porous matrix. Therefore, in light of this result, it may be concluded that the adsorption capacity of the cross bore hollow fibre module is greater than that of the other modules. This may be due to an increased surface area in the cross bore on which for mass transfer to occur, meaning that the breakthrough time increased as a result of the higher rate of mass transfer.

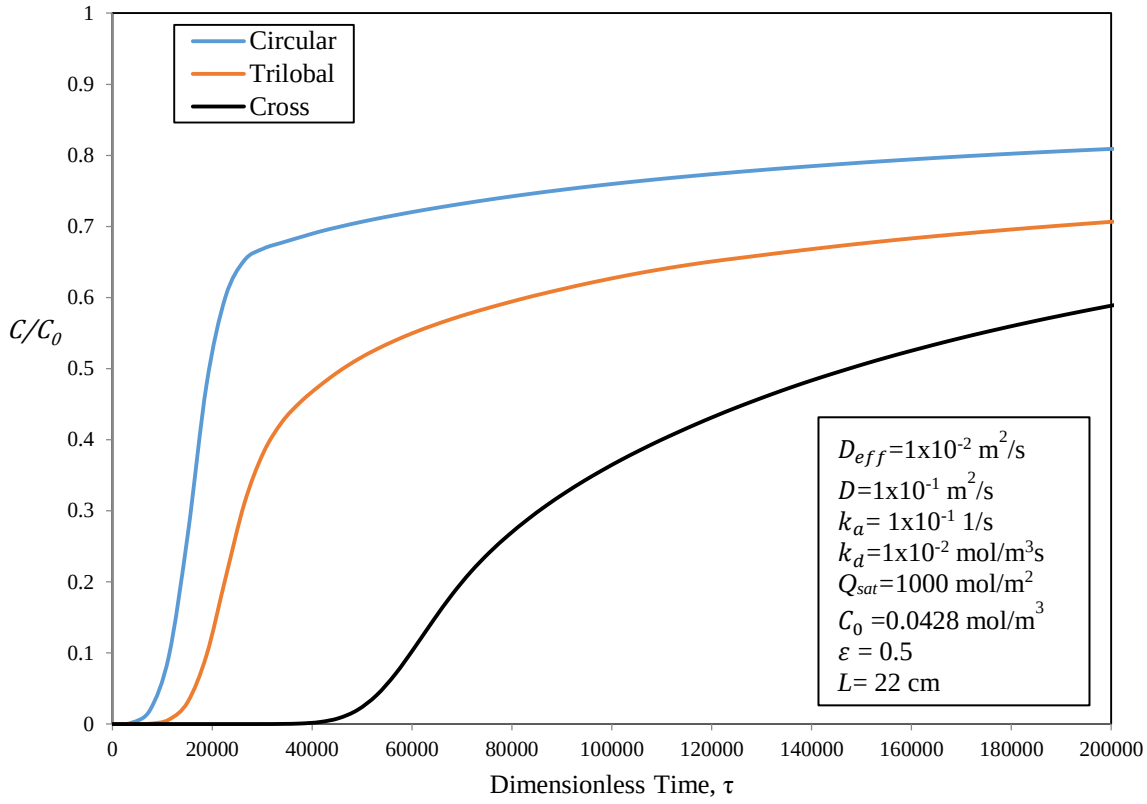

Figure 6.15. Breakthrough time for several bore shapes of adsorbent hollow fibres models.

The distribution concentration of n-butane in the lumen and the porous media of adsorbent hollow fibre modules is shown in Figure 6.16. The diagram shows that the bores of all adsorbent hollow fibre modules have the highest concentration of n-butane. In addition, the concentration changes along the hollow fibres are significant. It is clearly revealed that as the n-butane phase flows through the bores (lumen), n-butane is transferred from the gas bulk towards the porous media, as a result of the concentration gradient between the lumen and the porous media.

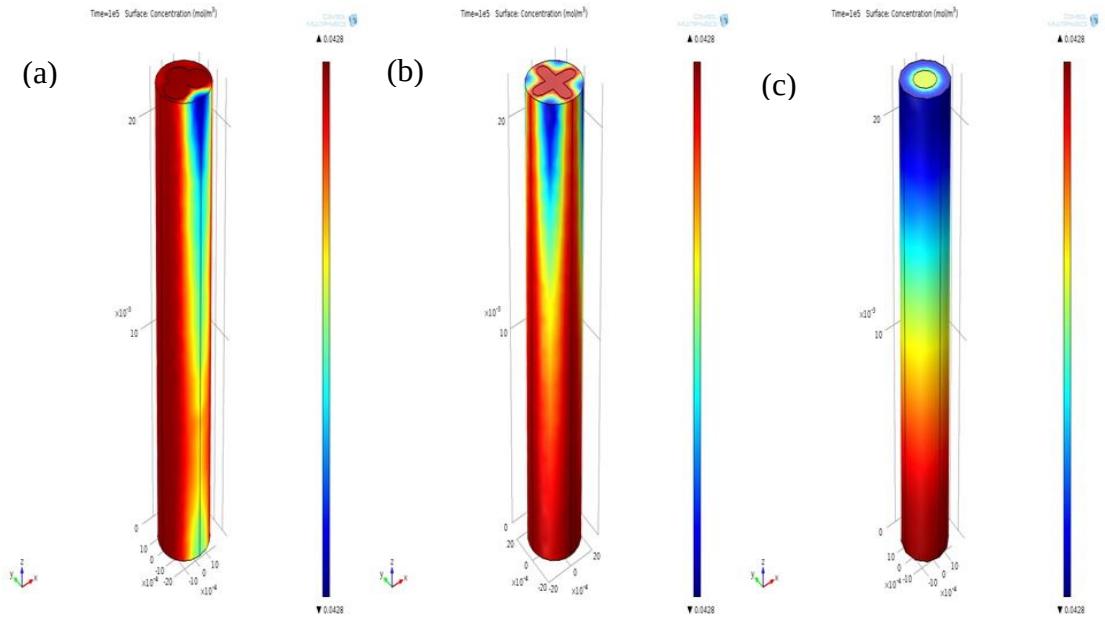

Figure 6.16. Comparison of concentration profiles in several bore shapes of adsorbent hollow fibre models at t= 28 hours; (a) Tri-lobe, (b) Cross and (c) circular. Blue colour= low concentration of gas whereas red colour= high concentration of gas.

6.5 Simulation 3: Comparison of the adsorption performance between single adsorbent hollow fibre and tri-lobe adsorbent hollow fibre

2D mathematical model is proposed for transport of n-butane through single and tri-lobe three bore adsorbent hollow fibre modules. It can be said that the simulation was carried out in nearly the same conditions as experimental works. The procedure used to simulate the models is presented in the sections 6.5.1.

6.5.1 Description

In order to present the modelling for the transportation of n-butane in the single and tri-lobe three bore adsorbent hollow fibre modules, a model domain is required to simulate the adsorption process. Figure 6.17 shows the model domain and triangular mesh elements of this simulation; this was developed for a hollow fibre divided into two parts (lumen and porous media). It can be seen that size of the mesh element between domain 1 and domain 2 is smaller than in other zones of hollow fibres. This is because the concentration changes are higher in this zone.

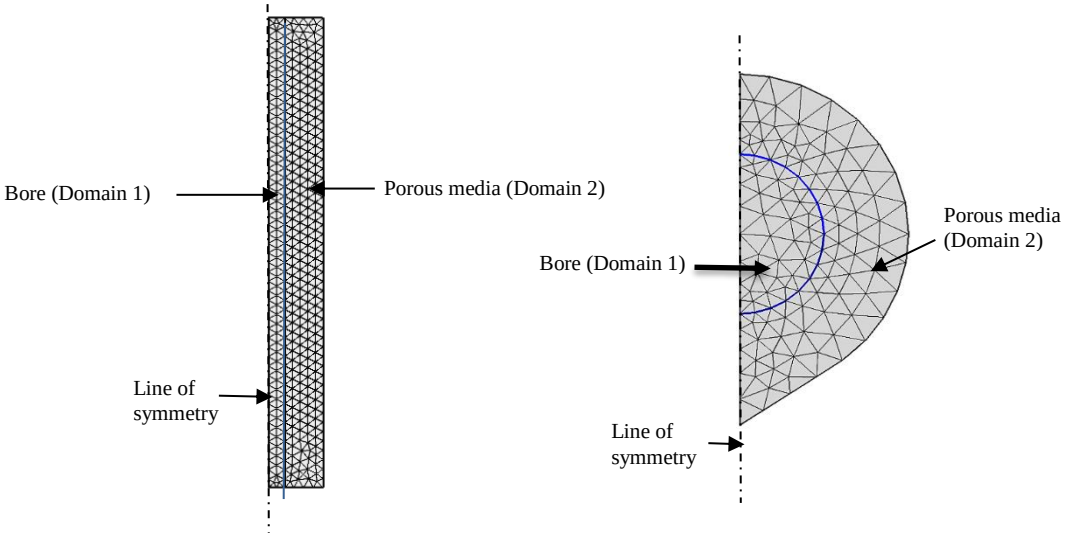

½ Single adsorbent hollow fibre **1/6th Segment tri-lobe adsorbent hollow fibre**

Figure 6.17. 2D computational domain and triangular mesh of single and tri-lobe adsorbent hollow fibres modules.

In this simulation, the following assumptions were considered:

- The mass transport through the bore is laminar flow, isotherm Newtonian incompressible and steady state.
- The boundary condition of the wall is no slip.
- In both hollow fibre modules, the volume of porous media is the same.

The governing equations for the description of n-butane transport from the lumen to porous media are described in Section 6.2.2. The dimensions and physical parameters used for the modules are shown in Table 6.7.

Table 6.7: The parameters of single and tri-lobe three bores adsorbent hollow fibre modules.

Parameter Name	SAHF	TAHF
Outer Fibre Radius, r_o (m)	$0.84x10^{-3}$	---
Inner Fibre Radius, r_i (m)	$0.25x10^{-3}$	$0.5x10^{-3}$
Fibre length, L (m)	0.22	0.22
Temperature, T (K)	293.15	293.15
Initial Pressure, P_0 (barg)	0	0
Volumetric Flow Rate, Q (m^3/s)	$1.67x10^{-5}$	$1.67x10^{-5}$
Initial Concentration, C_0 (mol/m^3)	0.0428	0.0428
Volume of porous media (m^3)	$4.4x10^{-7}$	$4.4x10^{-7}$
Adsorption Rate Coefficient, k_a (1/s)	$1x10^{-1}$	$1x10^{-1}$
Desorption Rate Coefficient, k_d (mol/m^3 s)	$1x10^{-2}$	$1x10^{-2}$
Saturation Capacity, Q_{sat} (mol/m^3)	4125	4125
Diffusivity, D (m^2/s)	$1x10^{-1}$	$1x10^{-1}$
Effective Diffusivity, D_{eff} (m^2/s)	$1x10^{-2}$	$1x10^{-2}$
Reynolds Number, Re	295.47	86.9

6.5.2 Results and discussions

The breakthrough curves created for the set of governing equations produced from the mass transport through the adsorbent hollow fibre modules were solved using the commercial package COMSOL Multiphysics 5.2. This is shown in Figure 6.18, which also presents a comparison between single and tri-lobe three-bore adsorbent hollow fibre module breakthrough curves using the same porous media volume, effective diffusivity, diffusivity, adsorption and desorption rate coefficient, temperature, and initial concentration and adsorption saturation capacity. The results reveal that the breakthrough time for the tri-lobe hollow fibre module is higher than that for the single hollow fibre module. This result emphasises the higher mass transfer rate in the tri-lobe hollow fibre module in comparison with the single hollow fibre module.

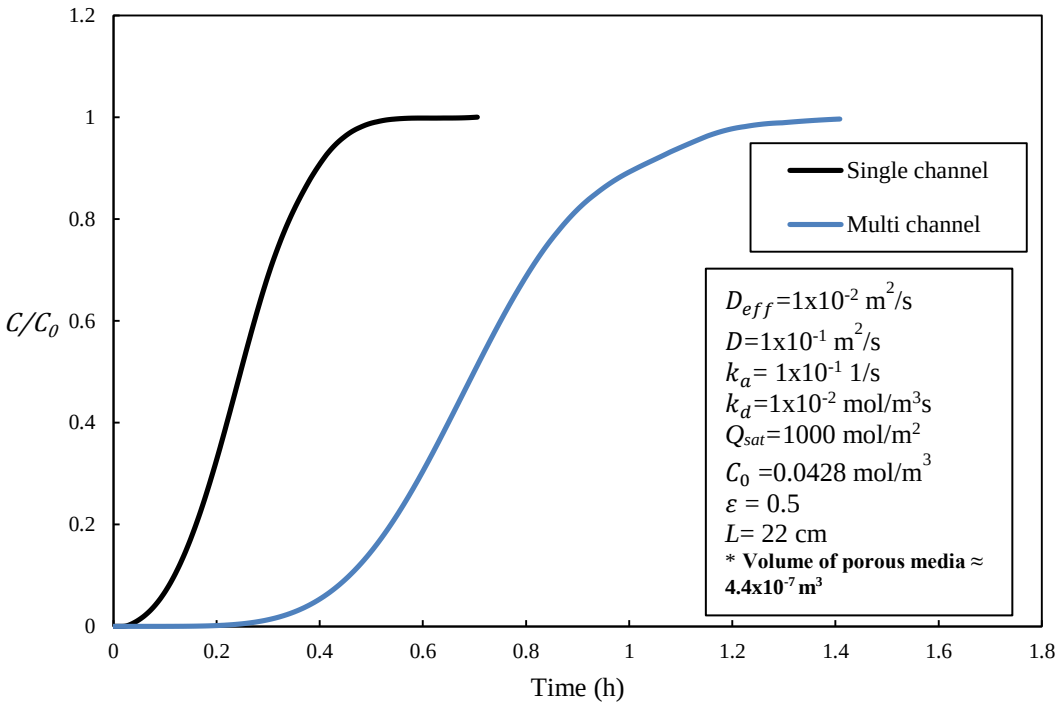

Figure 6.18. Breakthrough curves of single and tri-lobe three bores adsorbent hollow fibre modules.

6.5.3 Model validation

Experiments were performed for single adsorbent hollow fibre and tri-lobe adsorbent hollow fibre for removal of n-butane at least three times. Valid results were identified by comparing breakthrough curves. To validate the simulation of adsorbent hollow fibre for the adsorption of n-butane from the air, the simulation breakthrough curves were compared with experimental results, as shown in Figure 6.19. Both data sets relate to the removal of n-butane from air using adsorbent hollow fibres with the same geometry and dimensional parameters, excluding mass transfer constants (diffusivity and effective diffusivity) and kinetic constants (adsorption and desorption rate coefficient). It was not possible to determine these parameters in this research but, by identifying the higher breakthrough time and equilibrium time. Figure 6.18 from simulation study shows that single adsorbent hollow fibre has lower breakthrough time and equilibrium time than tri-lobe hollow fibre of equivalent weight of the adsorbent. Also, Figure 6.19 from experimental work shows the similar trend of the equivalent volume of the porous matrix.

Therefore, it could be ascertained that the simulation breakthrough curves of hollow fibres are in good agreement with the experimental breakthrough curves. This confirms

that the modelling procedures and governing equations used in this simulation were appropriate and can be used for further work.

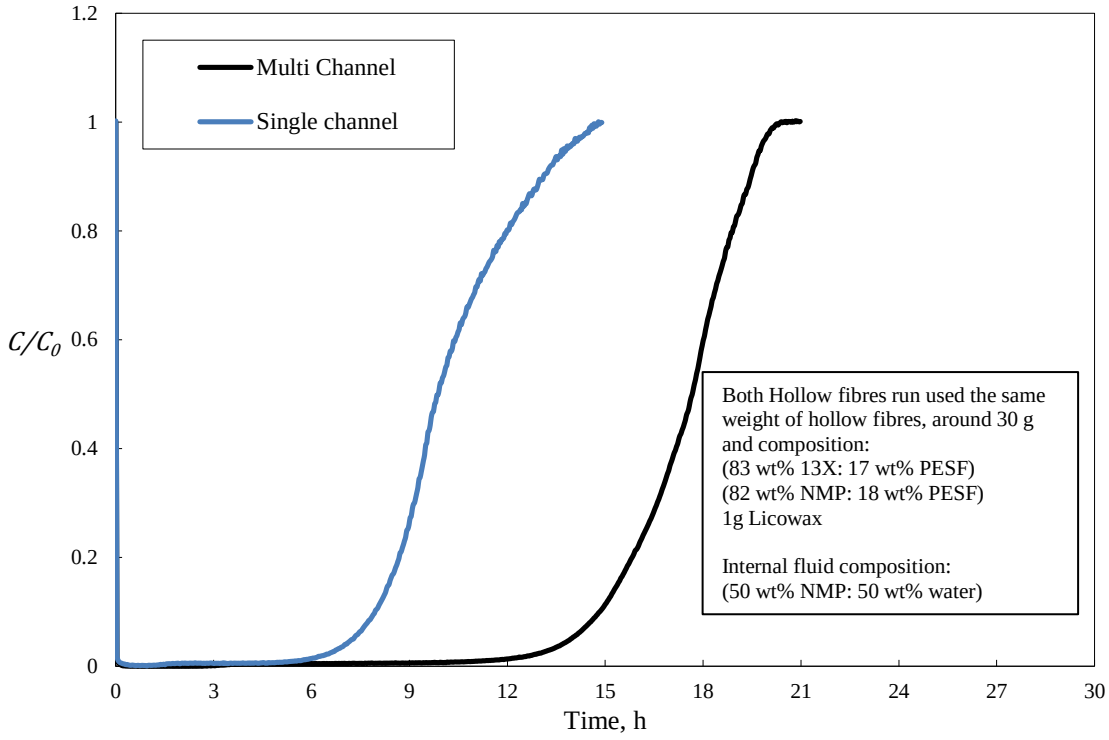

Figure 6.19. Comparison between the adsorption breakthrough curves of single and tri-lobe three bores adsorbent hollow fibres with 1 l/min flow rate 1000 ppm concentration of n-butane.

6.6 Summary

The adsorbent hollow fibre was modelled successfully via computational fluid dynamics using COMSOL Multiphysics 5.2. Separation of n-butane as a model of an adsorbent hollow fibre module was theoretically studied in this research. The simulations were based on numerical mass transfer solutions for species in the adsorbent hollow fibre module. The finite element method was utilised to solve the governing equations. The use of the hollow fibre model does not incorporate some physical properties, such as diffusivity, effective diffusivity, adsorption rate coefficient and adsorption capacity. The limitation of these necessary properties could affect the accuracy of simulation results. By testing the key parameters of hollow fibre models, it was possible to achieve a good solution that could be used for all simulations in this research. Following the testing of key parameters, it was found that:

1. Because of the increased adsorption capacity, the breakthrough and equilibrium times also rose.

2. In effective diffusivity testing, all breakthrough curves have similar shape, as a result of the similar breakthrough time and equilibrium time.
3. The breakthrough time and equilibrium time increased as the adsorption rate and desorption rate increased, because the adsorption rate was balanced by the desorption rate, producing breakthrough curves with maximum breakthrough times.
4. The diffusivity value has a similar effect on the breakthrough curve for the adsorbent hollow fibre when the value was equal to $1x10^{-1}$ and $1x10^{-2}$ m^2/s, whereas if it was lower than $1x10^{-2}$ m^2/s, the breakthrough curve lost its normal 'S' shape.

The main findings from all simulation modelling in this research are as follows:

1. Looking at the simulation results from model tests on the inner radius of the single adsorbent hollow fibre, it becomes apparent that the breakthrough time reduced as the inner radius increased upon exposure to the same porous matrix volume, due to reduced surface area on which for mass transfer to occur, and the effect of the increased fluid velocity as the inner radius decreased. In addition, the pressure drop through the adsorbent hollow fibre decreased as the inner radius of the hollow fibre increased, due to the non-laminar taking place at the small inner radius, where the velocity rose. In this simulation, the experimental results and model prediction were in strong agreement with model prediction.

2. The simulation of the adsorption performance of several adsorbent hollow fibre bore shapes showed that the breakthrough time is greater in the case of a cross-bore adsorbent hollow fibre module than in the case of tri-lobe and circular bore hollow fibre modules. This is possibly due to an increased surface area in cross-bore on which for mass transfer to occur, meaning that the breakthrough time increased in response to the higher rate of mass transfer.
3. The simulation results of single adsorbent hollow fibre and tri-lobe three-bore adsorbent hollow fibre for adsorption of n-butane revealed that the breakthrough time for the tri-lobe hollow fibre module is higher than for the

single hollow fibre module. This could be due to the higher mass-transfer rate in the tri-lobe hollow fibre module when compared to the single hollow fibre module. This result was validated through a comparison with the experimental result for adsorption of n-butane. It could thus be determined that the simulation breakthrough curves of hollow fibres are in sufficient agreement with the experimental breakthrough curves.

Chapter 7: Conclusion and Recommendations for Future Work

This thesis focused on the development of highly novel multi-channel adsorbent hollow fibres which can be applied to the recovery and removal of VOC. To the researcher's best knowledge this research would be the first study of the development of multi-channel adsorbent hollow fibres with low pressure drop and high adsorbent composition. Multi-channel adsorbent hollow fibres have been successfully fabricated by wet/wet spinning, followed by a phase inversion technique using a polymer/adsorbent/solvent mixture. To optimise the adsorption performance of single adsorbent hollow fibres, it has been found that the parameters affecting this fibre structure are the adsorbent concentration, the heat treatment temperature, the adding of pore former, and the bore fluid compositions.

The aim of this study has been met by achieving each of the objectives described below:

1. The improved single adsorbent hollow fibres incorporating 13X zeolite (that is those having good BET surface porosity, good mechanical properties, good adsorption capacity and good kinetic performance) were made with the 13X zeolite, PESF polymer, NMP solvent and Licowax C pore former. The best combination and recipe for spinning of the 13X single hollow fibre was double-layer spinning with a composition of 83 wt% 13X zeolite powder to 17 wt% PESF polymer. Also, the best composition of bore fluid mixture was 50 wt% NMP to 50 wt% water. The most effective heat treatment temperature of this single adsorbent hollow fibres was found to be 200°C.

2. With the single adsorbent hollow fibres the characterisation studies revealed that reasonable pre-treatment temperature (at 200°C) can allow 13X zeolite particles to be released from the PESF structure and to create better access to the adsorption sites.
3. The single adsorbent hollow fibres, prepared from the adsorbent/solvent/polymer mixture with pore former (Licowax PM) showed a much better kinetic performance for the adsorption of n-butane than its single adsorbent hollow fibre without pore former. The adsorption equilibrium loading calculated from breakthrough studies showed that the hollow fibres

with pore former provided better adsorption performance due to enhancing the porosity of the fibre structure. This result confirms the data found when using a nitrogen adsorption isotherm. However, the increase in the porosity can affect the mechanical properties of hollow fibres.

4. The optimum composition of bore fluid for the preparation of the adsorbent hollow fibres was found to be 50 wt% NMP and 50 wt% water. In this composition, delayed phase inversion in the bore wall appeared to allow plenty time to create a porous structure during the diffusion process.
5. Comparison of the adsorption performance of different concentration of 13X in hollow fibres has shown that 85 wt% 13X has a higher adsorption equilibrium loading due to the greater surface area which attracts n-butane molecules to adsorption sites, but much poorer mechanical properties compared with 83 wt% and 84 wt% 13X zeolite.
6. The n-butane adsorption capacity at equilibrium of the optimised single adsorbent hollow fibres (83 wt% 13X, 17 wt% PESF and 1g Licowax PM) and BET surface area 475.6 m^2/g was found to be 6.2%.
7. Novel multi-channel tri-lobe adsorbent hollow fibres with a high BET surface area of 560.5 m^2/g have been successfully manufactured with three bores by wet/wet spinning, followed by a phase inversion technique. Adsorption breakthrough studies have shown that multi-channel adsorbent hollow fibres perform better than single adsorbent hollow fibres prepared from the same compositions of adsorbent/solvent/polymer mixture at same adsorbent weight for the adsorption of n-butane. This is because the 13X zeolite particles in tri-lobe hollow fibre are densely packed within the fibre structure. The pressure drop for tri-lobe adsorbent hollow fibres is much lower than it in the single adsorbent hollow fibre. The mechanical properties of tri-lobe hollow fibre also are better than it in the single hollow fibre.
8. The n-butane adsorption loadings (at the equilibrium point) of tri-lobe hollow fibres (83 wt% 13X, 17 wt% PESF and 1g Licowax PM) was found to be 10.9%.
9. The nitrogen adsorption isotherm of the tri-lobe hollow fibres is nearly coincident with that of 13X zeolite powder. However, the nitrogen adsorption isotherm of the single adsorbent hollow fibre with the same compositions is somewhat poorer. This confirms that the microporous surfaces of the tri-lobe

hollow fibres provide higher access to adsorption sites compared to single hollow fibre, and most significantly, displays that the polymer does not cover the adsorption sites.

10. The adsorption experiments of n-butane on hydrophobic tri-lobe hollow fibres show that HiSiv 1000 and HiSiv 3000 have good adsorption affinity for the hydrocarbon. It is concluded that both hydrophobic are potential adsorbents for the removal of VOCs.
11. The breakthrough time and equilibrium loading of the tri-lobe adsorbent hollow fibres were shown to decrease with increasing flowrate of bore fluid. The breakthrough time of 6 ml/min tri-lobe hollow fibres are lower than those of the 3 ml/min fibres. This is because the bore fluid with 6 ml/min flow rate passes very fast through the bores without allowing required time for creating a porous structure.
12. Novel hexagonal seven bore adsorbent hollow fibres prepared from 83 wt% 13X zeolite and 17 wt% PESF have also been successfully manufactured using a special spinneret at University of Bath. Adsorption breakthrough studies at different air gap length have shown that 0 cm hexagonal hollow fibre carry out better adsorption capacity than with other hexagonal fibres with 0.5 and 1 cm air gap length due to the higher value of BET surface area. The breakthrough curve for this type of hollow fibre is the sharpest of the all samples in this research. This allows n-butane molecules easily reaching the adsorption sites.
13. Adsorbent hollow fibres have been successfully modelled using computational fluid dynamics via COMSOL Multiphysics 5.2. It was found that direct comparison between experimental and computational results was not possible due to the lack of information on the adsorption and desorption properties. However, the results of two experiments show similar trends with modelling results.

It is possible to summarise that the combined effects of a reasonable polymer/adsorbent/solvent mixture composition, a suitable bore fluid flowrate and composition a suitable pre-treatment temperature can produce adsorbent hollow fibres which have greater qualities over 13X zeolite hollow fibres.

In conclusion, this research showed the capability of preparing the novel multi-channel adsorbent hollow fibres for future hollow fibre structured adsorbent. Many advantages

are accrued with the novel multi-channel adsorbent hollow fibre for gas separation. It has a higher surface area per unit volume, lower pressure drop, higher adsorbent loading, better mechanical properties, lower mass-transfer resistance and better adsorption capacity. This research intended to demonstrate the approach for a novel generation of energy efficient multi-channel adsorbent hollow fibre for the recovery and separation of volatile organic compounds.

The further optimisation of novel multi-channel adsorbent hollow fibres is suggested to improve their adsorption performance, shape and flexibility for chemical applications. Also, it is important to measure the kinetic constant and mass transfer properties of adsorbent hollow fibres for using in simulation studies. Therefore, future works are suggested to be concentrated on the following areas:

1. To spin multi-channel adsorbent hollow fibres with good mechanically flexible. This may be achieved by increasing the polymer content.
2. To study the dynamic adsorption with a broader range of toxic gases.
3. To manufacture tri-lobe and hexagonal adsorbent hollow fibres with regular shapes. This may be achieved by increasing the extrusion pressure of mixture during spinning experiment or changing the composition of the mixture.
4. To simulate adsorbent hollow fibre for gas separation with a high agreement with experimental results. This may be achieved by measuring the mass transfer properties and kinetics constant such as effective diffusivity, diffusivity and adsorption rate coefficient.
5. To study the separation and adsorption of multi-component VOC mixtures without and with moisture. The emissions of valuable materials from chemical processes commonly contain complex mixtures in humid streams. Additional experiments should be carried out to study the recovery of complex mixtures with a range of relative humidity.

Bibliography

Akhtar, F., Andersson, L., Ogunwumi, S., Hedin, N. & Bergström, L., 2014. Structuring adsorbents and catalysts by processing of porous powders. *Journal of the European Ceramic Society,* 34(7), pp. 1643-1666.

Altinkok, C., Kiskan, B. & Yagci, Y., 2011. Synthesis and characterization of sulfone containing main chain oligobenzoxazine precursors. *Journal of Polymer Science Part A: Polymer Chemistry,* 49(11), pp. 2445-2450.

Baker, R., 2012. *Membrane technology and applications.* John Wiley & Sons.

Barati, F., Ghadiri, M., Ghasemi, R. & Nobari, H.M., 2014. CFD Simulation and Modeling of Membrane-Assisted Separation of Organic Compounds from Wastewater. *Chemical Engineering & Technology,* 37(1), pp. 81-86.

Barth, C., Goncalves, M., Pires, A., Roeder, J. & Wolf, B., 2000. Asymmetric polysulfone and polyethersulfone membranes: effects of thermodynamic conditions during formation on their performance. *Journal of Membrane Science,* 169(2), pp. 287-299.

Brenner, H., 2013. *Adsorption Calculations and Modelling.* Elsevier.

Brunazzi, E., Paglianti, A. & Petarca, L., 1996. Design of absorption columns equipped with structured packings. *La Chimica e l'industria,* 78(4), pp. 459-467.

Crittenden, B., Patton, A., Jouin, C., Perera, S., Tennison, S. & Echevarria, J.A.B., 2005. Carbon monoliths: a comparison with granular materials. *Adsorption,* 11(1), pp. 537-541.

Dai, Y., Johnson, J., Karvan, O., Sholl, D.S. & Koros, W., 2012. Ultem®/ZIF-8 mixed matrix hollow fiber membranes for CO 2/N 2 separations. *Journal of Membrane Science,* 401, pp. 76-82.

Department for Environment, F.R.A., 2014. *Emissions of air pollutants in the UK, 1970 to 2013* [Online]. Available from: https://www.gov.uk/government/uploads/system/uploads/attachment_data/file/388195/Emissions_of_air_pollutants_statistical_release_2014.pdf [Accessed].

Díaz, E., Ordóñez, S., Vega, A. & Coca, J., 2004. Adsorption characterisation of different volatile organic compounds over alumina, zeolites and activated carbon using inverse gas chromatography. *Journal of chromatography A,* 1049(1), pp. 139-146.

Dick, E., 2009. Introduction to finite element methods in computational fluid dynamics. *Computational Fluid Dynamics.* Springer, pp. 235-274.

Dou, B., Hu, Q., Li, J., Qiao, S. & Hao, Z., 2011. Adsorption performance of VOCs in ordered mesoporous silicas with different pore structures and surface chemistry. *Journal of hazardous materials,* 186(2), pp. 1615-1624.

Du, N., Park, H.B., Dal-Cin, M.M. & Guiver, M.D., 2012. Advances in high permeability polymeric membrane materials for CO 2 separations. *Energy & Environmental Science,* 5(6), pp. 7306-7322.

Dwivedi, P., Gaur, V., Sharma, A. & Verma, N., 2004. Comparative study of removal of volatile organic compounds by cryogenic condensation and adsorption by activated carbon fiber. *Separation and Purification Technology,* 39(1), pp. 23-37.

Ergun, S., 1952. Fluid flow through packed columns. *Chem. Eng. Prog.,* 48, pp. 89-94.

Feng, X., Pan, C.Y., McMinis, C.W., Ivory, J. & Ghosh, D., 1998. Hollow-fiber-based adsorbers for gas separation by pressure-swing adsorption. *AIChE journal,* 44(7), pp. 1555-1562.

Flanigen, E.M., Jansen, J. & van Bekkum, H., 1991. *Introduction to Zeolite Science and Practice.* Elsevier.

Forati, T., Atai, M., Rashidi, A., Imani, M. & Behnamghader, A., 2014. Physical and mechanical properties of graphene oxide/polyethersulfone nanocomposites. *Polymers for Advanced Technologies,* 25(3), pp. 322-328.

Golden, C.M.A., Golden, T.C. & Battavio, P.J., 2005. Multilayered adsorbent system for gas separations by pressure swing adsorption. Google Patents.

Guan, R., Zou, H., Lu, D., Gong, C. & Liu, Y., 2005. Polyethersulfone sulfonated by chlorosulfonic acid and its membrane characteristics. *European Polymer Journal,* 41(7), pp. 1554-1560.

Gupta, V.K. & Verma, N., 2002. Removal of volatile organic compounds by cryogenic condensation followed by adsorption. *Chemical Engineering Science,* 57(14), pp. 2679-2696.

Hasbullah, H., Kumbharkar, S., Ismail, A.F. & Li, K., 2011. Preparation of polyaniline asymmetric hollow fiber membranes and investigation towards gas separation performance. *Journal of membrane science,* 366(1), pp. 116-124.

Henley, E.J., Seader, J.D. & Roper, D.K., 2011. *Separation process principles.* Wiley.

Hess, J.L. & Smith, A., 1962. *Calculation of non-lifting potential flow about arbitrary three-dimensional bodies.*

Huang, X., Feng, F. & Cao, L., Year. The competitive adsorption of multi-component VOCs on activated carbon. In: Electric Technology and Civil Engineering (ICETCE), 2011 International Conference on, 2011. IEEE, pp. 1669-1672.

Husain, S. & Koros, W.J., 2007. Mixed matrix hollow fiber membranes made with modified HSSZ-13 zeolite in polyetherimide polymer matrix for gas separation. *Journal of Membrane Science,* 288(1), pp. 195-207.

İnel, O., Topaloğlu, D., Aşkın, A. & Tümsek, F., 2002. Evaluation of the thermodynamic parameters for the adsorption of some hydrocarbons on 4A and 13X zeolites by inverse gas chromatography. *Chemical engineering journal,* 88(1), pp. 255-262.

Jeffs, C.A., 2015. *Removal of toxic industrial chemicals using novel adsorbent hollow fibres.* University of Bath.

Kapantaidakis, G. & Koops, G., 2002. High flux polyethersulfone–polyimide blend hollow fiber membranes for gas separation. *Journal of membrane science,* 204(1), pp. 153-171.

Khalilpour, R., Abbas, A., Lai, Z. & Pinnau, I., 2013. Analysis of hollow fibre membrane systems for multicomponent gas separation. *Chemical Engineering Research and Design,* 91(2), pp. 332-347.

Khan, F.I. & Kr Ghoshal, A., 2000. Removal of volatile organic compounds from polluted air. *Journal of loss prevention in the process industries,* 13(6), pp. 527-545.

Kim, H.J., Nah, S.S. & Min, B.R., 2002. A new technique for preparation of PDMS pervaporation membrane for VOC removal. *Advances in Environmental Research,* 6(3), pp. 255-264.

Kim, K.-J. & Ahn, H.-G., 2012. The effect of pore structure of zeolite on the adsorption of VOCs and their desorption properties by microwave heating. *Microporous and Mesoporous Materials,* 152, pp. 78-83.

Kuboňová, L., Obalová, L., Skovranek, L. & Troppová, I., 2013. The balancing of VOC concentration fluctuations by adsorption/desorption process on activated carbon. *Adsorption,* 19(2-4), pp. 667-673.

Lasseuguette, E., Rouch, J.-C. & Remigy, J.-C., 2013. Hollow-fiber coating: application to preparation of composite hollow-fiber membrane for gas separation. *Industrial & Engineering Chemistry Research,* 52(36), pp. 13146-13158.

Li, G., Singh, R., Li, D., Zhao, C., Liu, L. & Webley, P.A., 2009. Synthesis of biomorphic zeolite honeycomb monoliths with 16000 cells per square inch. *Journal of Materials Chemistry,* 19(44), pp. 8372-8377.

Li, T., Pan, Y., Peinemann, K.-V. & Lai, Z., 2013. Carbon dioxide selective mixed matrix composite membrane containing ZIF-7 nano-fillers. *Journal of membrane science,* 425, pp. 235-242.

Liu, Y., Koops, G. & Strathmann, H., 2003. Characterization of morphology controlled polyethersulfone hollow fiber membranes by the addition of polyethylene glycol to the dope and bore liquid solution. *Journal of membrane science,* 223(1), pp. 187-199.

Loh, C.H. & Wang, R., 2012. Effects of Additives and Coagulant Temperature on Fabrication of High Performance PVDF/Pluronic F127 Blend Hollow Fiber

Membranes< i> via</i> Nonsolvent Induced Phase Separation. *Chinese Journal of Chemical Engineering,* 20(1), pp. 71-79.

Mao, Z., Jie, X., Cao, Y., Wang, L., Li, M. & Yuan, Q., 2011. Preparation of dual-layer cellulose/polysulfone hollow fiber membrane and its performance for isopropanol dehydration and CO 2 separation. *Separation and purification technology,* 77(1), pp. 179-184.

McCabe, W.L., Smith, J.C. & Harriott, P., 1993. *Unit operations of chemical engineering.* McGraw-Hill New York.

Micromeritics.com, 2016. *3 Flex Chemisorption | Micromeritics* [Online]. Available from: http://www.micromeritics.com/3Flex-Chemisorption.aspx [Accessed 14 Sep. 2016].

Miramini, S.A., Razavi, S., Ghadiri, M., Mahdavi, S. & Moradi, S., 2013. CFD simulation of acetone separation from an aqueous solution using supercritical fluid in a hollow-fiber membrane contactor. *Chemical Engineering and Processing: Process Intensification,* 72, pp. 130-136.

Moreno-Castilla, C. & Pérez-Cadenas, A.F., 2010. Carbon-based honeycomb monoliths for environmental gas-phase applications. *Materials,* 3(2), pp. 1203-1227.

Mulder, M., 1996. *Basic Principles of Membrane Technology Second Edition.* Kluwer Academic Pub.

Nijhuis, T., Kreutzer, M., Romijn, A., Kapteijn, F. & Moulijn, J., 2001. Monolithic catalysts as efficient three-phase reactors. *Chemical Engineering Science,* 56(3), pp. 823-829.

Ozturk, B. & Yilmaz, D., 2006. Absorptive removal of volatile organic compounds from flue gas streams. *Process Safety and environmental protection,* 84(5), pp. 391-398.

Pan, C., 1986. Gas separation by high-flux, asymmetric hollow-fiber membrane. *AIChE Journal,* 32(12), pp. 2020-2027.

Pan, C.Y. & McMinis, C.W., 1992. Hollow fiber bundle element. Google Patents.

Peng, N., 2009. *FUNDAMENTALS OF HOLLOW FIBER FORMATION FOR GAS SEPARATION.* NATIONAL UNIVERSITY OF SINGAPORE.

Peng, N. & Chung, T.S., 2008. The effects of spinneret dimension and hollow fiber dimension on gas separation performance of ultra-thin defect-free Torlon< sup>®</sup> hollow fiber membranes. *Journal of Membrane Science,* 310(1), pp. 455-465.

Perera, S.P. & Tai, C.C., 2009. Hollow fibres. Google Patents.

Rahbari-Sisakht, M., Ismail, A. & Matsuura, T., 2012. Development of asymmetric polysulfone hollow fiber membrane contactor for CO< sub> 2</sub> absorption. *Separation and Purification Technology,* 86, pp. 215-220.

Razavi, S.M.R., Razavi, S.M.J., Miri, T. & Shirazian, S., 2013. CFD simulation of CO 2 capture from gas mixtures in nanoporous membranes by solution of 2-amino-2-methyl-1-propanol and piperazine. *International Journal of Greenhouse Gas Control,* 15, pp. 142-149.

Ren, X.H., Stapf, S. & Blümich, B., 2005. Magnetic resonance visualisation of flow and pore structure in packed beds with low aspect ratio. *Chemical engineering & technology,* 28(2), pp. 219-225.

Rezaei, F. & Webley, P., 2010. Structured adsorbents in gas separation processes. *Separation and Purification Technology,* 70(3), pp. 243-256.

Ruthven, D., 2000. Adsorption fundamentals. Kirk–Othmer encyclopedia of chemical technology. New York: Wiley.

Sarkar, T. & Mulchandani, A., 2015. Volatile Organic Compounds. In: L.M. Moretto & K. Kalcher, eds. *Environmental Analysis by Electrochemical Sensors and Biosensors.* Springer New York, pp. 1023-1046.

Schweitzer, P.A., 1988. *Handbook of separation techniques for chemical engineers.* McGraw-Hill New York etc.

Seader, J.D. & Henley, E.J., 2011. Separation process principles.

Shirzadeh-Gharacheh, A. & Rahbari-Sisakht, M., 2016. Polyvinylidene fluoride hollow fiber mixed matrix membrane contactor incorporating modified ZSM-5 zeolite for carbon dioxide absorption. *RSC Advances,* 6(82), pp. 78865-78874.

Song, W., Tondeur, D., Luo, L. & Li, J., 2005. VOC adsorption in circulating gas fluidized bed. *Adsorption,* 11(1), pp. 853-858.

Subrenat, A.S. & Le Cloirec, P.A., 2006. Volatile organic compound (VOC) removal by adsorption onto activated carbon fiber cloth and electrothermal desorption: an industrial application. *Chemical Engineering Communications,* 193(4), pp. 478-486.

Tai, C.-C. & Wang, Y.-H., 2013. Development of adsorbent hollow fibres for environmental applications. *Adsorption Science & Technology,* 31(1), pp. 85-98.

Tai, C.C., 2007. *Novel adsorbent hollow fibres.* PhD Thesis, University of Bath.

Thundyil, M.J. & Koros, W.J., 1997. Mathematical modeling of gas separation permeators—for radial crossflow, countercurrent, and cocurrent hollow fiber membrane modules. *Journal of Membrane Science,* 125(2), pp. 275-291.

Tu, J., Yeoh, G.H. & Liu, C., 2012. *Computational fluid dynamics: a practical approach.* Butterworth-Heinemann.

UOP, H., 2006. *HiSivTM 3000 Adsorbent* [Online]. Available from: http://www.antibakteria.ch/upload/files/pdf/gb%20industrie/1446/PD_HiSiv3000.pdf [Accessed 2017].

Vivek Kumar, 2012. *Adsorption Equilibria and Regeneration* [Online]. Available from: http://www.slideshare.net/VivekKumar36/adsorption-regenerationvivek-kumarneeri [Accessed 2016].

Watson, J., 1999. *Separation methods for waste and environmental applications.* CRC Press.

Weller, S. & Steiner, W.A., 1950. Engineering aspects of separation of gases. Fractional permeation through membranes. *Chem. Eng. Progress,* 46.

Wendt, J. & Anderson, J., 2009. Basic philosophy of CFD. *Computational fluid dynamics: An introduction*, pp. 5-8.

Williams, J.L., 2001. Monolith structures, materials, properties and uses. *Catalysis Today,* 69(1), pp. 3-9.

Wypych, G., 2001. *Handbook of solvents.* ChemTec Publishing.

Xu, Z.-L. & Qusay, F.A., 2004. Polyethersulfone (PES) hollow fiber ultrafiltration membranes prepared by PES/non-solvent/NMP solution. *Journal of Membrane Science,* 233(1), pp. 101-111.

Yang, R.T., 1986. Gas separation by adsorption processes.

Yang, R.T., 2013. *Gas separation by adsorption processes.* Butterworth-Heinemann.

Zhao, L., Chen, Y., Wang, B., Sun, C., Chakraborty, S., Ramasubramanian, K., Dutta, P.K. & Ho, W.W., 2016. Multilayer polymer/zeolite Y composite membrane structure for CO 2 capture from flue gas. *Journal of Membrane Science,* 498, pp. 1-13.

Zhao, X., Ma, Q. & Lu, G., 1998. VOC removal: comparison of MCM-41 with hydrophobic zeolites and activated carbon. *Energy & Fuels,* 12(6), pp. 1051-1054.

Zulhairun, A., Ng, B., Ismail, A., Murali, R.S. & Abdullah, M., 2014. Production of mixed matrix hollow fiber membrane for CO 2/CH 4 separation. *Separation and Purification Technology,* 137, pp. 1-12.

Conference presentations

1. A. Alsharif, Y. M. J. Chew, and S. P. Perera. (2014) *Multi-channel Adsorbent Hollow Fibres for Removal of VOCs* [Presentation]. Exhibited at *the organised Emerging Separation Technologies event*, IChemE, London
2. A. Alsharif, Y. M. J. Chew, and S. P. Perera. (2015) *Development and Optimisation of 13X Zeolite Adsorbent Hollow Fibre for Environmental Pollution Control* [Poster]. Exhibited at *the 8th Saudi Students Conference*, Imperial College and KAUST, London
3. A. Alsharif, Y. M. J. Chew, and S. P. Perera. (2016) *The Influence of Various Parameters on Porous Structure of 13X Zeolite Adsorbent Hollow Fibres* [Poster]. Exhibited at *the 9th Saudi Student Conference*, University of Birmingham, Birmingham.
4. A. Alsharif, Y. M. J. Chew, and S. P. Perera. (2016) *CFD Simulation of N-Butane/Carbon Dioxide Separation from Air Using Composite Hollow Fibre Membrane* [Poster]. Exhibited at *the Emerging and Hybrid Membrane Technology Conference*, University of Swansea and IChemE, Swansea.
5. A. Alsharif, Y. M. J. Chew, and S. P. Perera. (2016) *Enhanced Volatile Organic Compounds Adsorption Performance Using Novel Multi-Channel Adsorbent Hollow Fibre* [Poster]. Exhibited at *the ChemEngdayUK conference*, University of Bath and IChemE, Bath.
6. A. Alsharif, Y. M. J. Chew, and S. P. Perera. (2016) *Enhanced Volatile Organic Compounds Adsorption Performance Using Novel Multi-Channel Adsorbent Hollow Fibre* [Poster]. Exhibited at *the Centre for Advanced Separations Engineering Showcase*, University of Bath, Bath.
7. A. Alsharif, Y. M. J. Chew, and S. P. Perera. (2017) *Development and Simulation of Tri-lobe Adsorbent hollow Fibres for Recovery of Volatile Organic Compounds* [Manuscript research paper]. Exhibited *at Adsorption Journal.*

Appendix I

The calculation of equilibrium loading of high adsorbent hollow fibre (10 wt% PESF, 90 wt% 13x zeolite).

Feed condition: $\boldsymbol{C_0} =$ 0.1% (1000 ppmv) n-butane and $\boldsymbol{Q}$ =1L/min.

Dry mass: 50 g

n-butane molecular weight (MW): 58 g/mol.

P 1 atm

n 1 mol

T 293 K

R 0.0821 L.atm/mol

$$v = \frac{(n * R * T)}{P} = \frac{1 * 0.0821 * 293}{1} = 24.05 \frac{L}{mol}$$

Adsorption breakthrough curve:

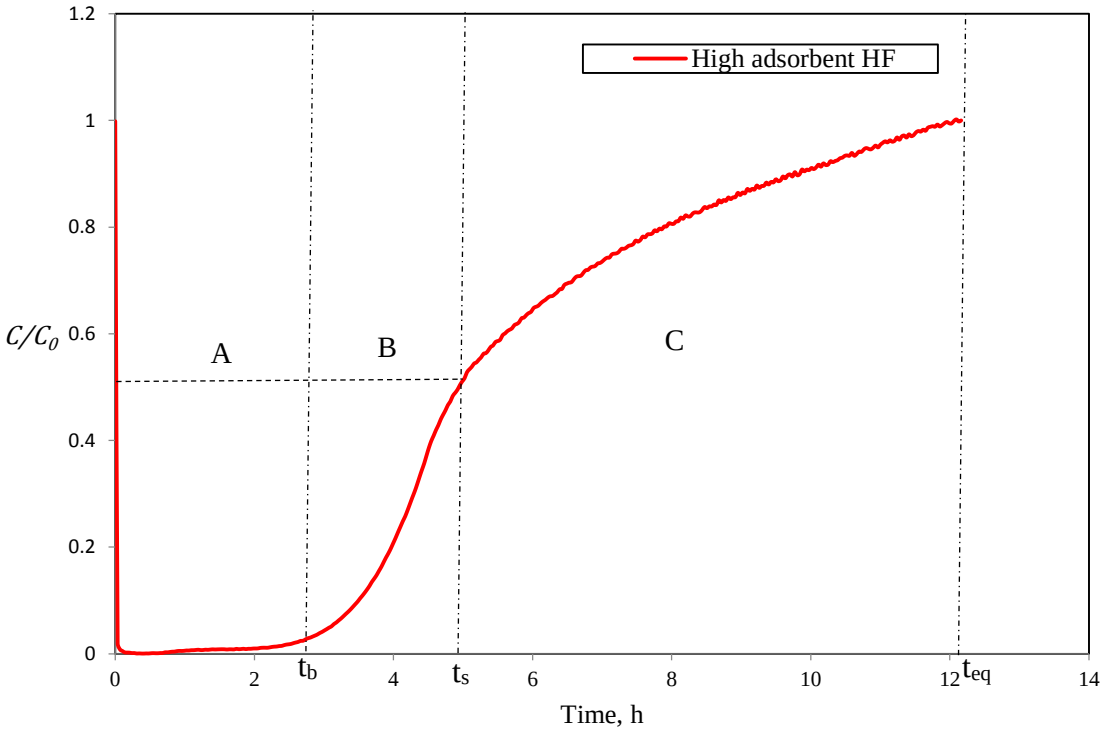

From the figure:

Breakthrough time = 133.254 min.

Equilibrium time $t_{eq=}$ 729.78 min.

$$\text{Breakthrough loading (\%)} = \frac{Q * C_0 * t_b * MW}{V * Dry\ mass} = \frac{1 * 1001.72 * 133.254 * 58}{24.05 * 50}$$

$$= 0.64\%$$

Equilibrium loading equation:

$$mass\ adsorbate = \frac{MW\left(\frac{g}{mol}\right) * Q\left(\frac{l}{min}\right) * \text{P}(atm) * C_0(ppm)}{10e6 * R\left(\frac{atm}{mol * K}\right) * T(K)} t_f(\text{min}) - \frac{MW * Q * p * C_0}{10e6 * R * T} * \int_0^{t_f} \frac{C}{C_0} dt$$

Mass adsorbate = A-B*C

$$A = \frac{58 * 1 * 1 * 1000 * 729.78}{10^6 * 0.0821 * 293} = 1.75$$

$$B = \frac{58 * 1 * 1 * 1000}{10^6 * 0.082 * 298} = 0.0024$$

$$C = \int_0^{t_{eq}} \frac{C}{C_0}\, dt = 6.37\ hours = 382.2\ min.$$

Equilibrium loading = A-BC = 1.75-(0.0024*382.2) = 0.83 g of n-butane

$$Equilibrium\ loading = \left(\frac{0.83}{50}\right) * 100 = 1.6\ \%$$

Appendix II

Providing the calculation of the mechanical properties of single adsorbent hollow fibre:

Equations used to calculate the stress, strain and Young`s modulus of elasticity of hollow fibre at breaking point is detailed below. An example calculation is given using data from sample SAHF4 (83 wt% 13X: 17 wt% PESF). The stress, strain and Young`s modulus of elasticity, were calculated from the following equations:

$$Ultimate\ tensile\ strength\ (Stress) = \frac{\text{Maximum load (Force)}}{\text{Original cross sectional area}} = \frac{4.49}{0.062}$$

$$= 0.72\ \text{MPa}$$

$$\text{Strain} = \frac{Extension}{Length} = \frac{0.39\ mm}{90\ mm} = 0.0044$$

$$\text{Young`s modulus of elasticity} = \frac{Stress}{Strain} = \frac{0.72\ MPa}{0.0044} = 163.6\ GPa$$

Appendix III

Figure 1 shows a certain range of PESF concentration within which the slope of the viscosity curve suddenly becomes sharper. The concentration of mixture at the crossed point of extrapolation lines of the two linear parts of the viscosity curve is shown to be the critical concentration of mixture. The identification of the critical concentration of PESF/13X is very important for fabrication the adsorbent hollow fibre which is the edge to form macrovoid-free. When the PESF concentration exceeds the critical value, the macrovoids and porosity of adsorbent hollow fibre could be probably eliminated. It can be seen that the critical concentration of PESF is 21%. In this concentration, the viscosity of mixture equal to 15 Pa.s.

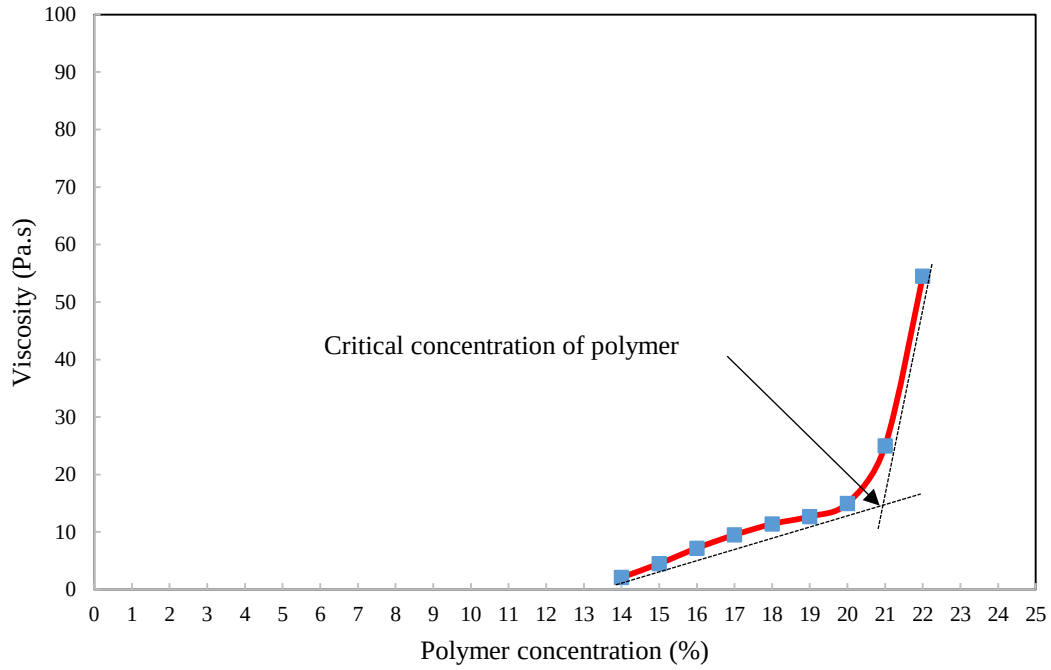

Figure 1. The critical concentration of PESF/NMP mixture.